

UNDERSTANDING RESISTANCE AND SENSITIVITY TO IMPROVE CANCER TREATMENT

Živa Pogačar

UNDERSTANDING RESISTANCE AND SENSITIVITY TO IMPROVE CANCER TREATMENT

Živa Pogačar

ISBN: 978-94-6419-608-5

Cover: Ilse Modder, www.ilsemodder.nl

Lay-out: Ilse Modder, www.ilsemodder.nl

Printing: Gildeprint, www.gildeprint.nl

Copyright © Ziva Pogacar 2022. All rights reserved. No part of this thesis may be reproduced in any form without written permission from the author or, when appropriate, of the publishers of the publications.

About the cover: The process of science relies on countless small experiments whose impact becomes clearer when we look at them together. This cover is a mosaic showing a microscopy image of senescent A549 lung cancer cells. Each dot is a well of cells stained by crystal violet in a colony formation assay performed during my PhD. First, a database of wells with different amounts of surviving cells and thus different intensity of color was assembled. Next, a computer algorithm by Hadi Gharibi replaces each pixel of the original image with a well of similar intensity, creating a custom mosaic from scanned colony formation assay plates.

Understanding resistance and sensitivity to improve cancer treatment

Hoe het begrijpen van de (on)gevoeligheid van kanker leidt tot betere behandeling

(met een samenvatting in het Nederlands)

Proefschrift

ter verkrijging van de graad van doctor aan de
Universiteit Utrecht
op gezag van de
rector magnificus, prof.dr. H.R.B.M. Kummeling,
ingevolge het besluit van het college voor promoties
in het openbaar te verdedigen op dinsdag 15 november 2022 des ochtends te 10.15 uur

door

Živa Pogačar

geboren op 2 januari 1992
te Ljubljana, Slovenië

Promotor:

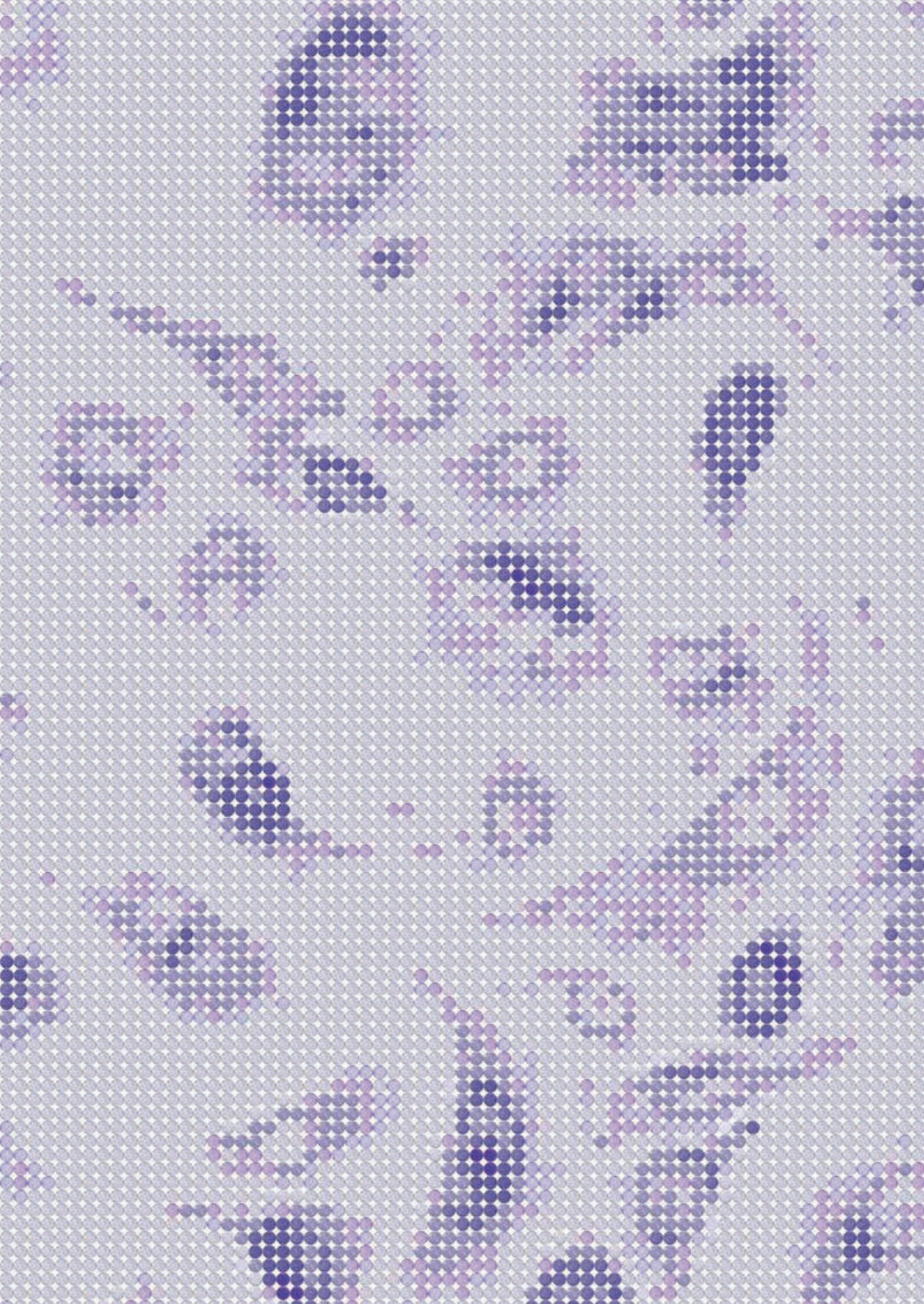
Prof. dr. R. Bernards

Copromotor:

Dr. R. Leite de Oliveira

TABLE OF CONTENTS

Chapter 1	General introduction and thesis outline	9
Chapter 2	Genetic and compound screens uncover factors modulating cancer cell response to indisulam	29
Chapter 3	Indisulam synergizes with palbociclib to induce senescence through inhibition of CDK2 kinase activity	65
Chapter 4	Using functional genetic screens to understand cancer immune evasion	101
Chapter 5	General discussion	125
Appendix	Nederlandse samenvatting	138
	Povzetek v slovenščini	140
	Curriculum Vitae	142
	Publication list	143
	Acknowledgements	144



Chapter 1

General introduction

Adapted from:

The importance of genetic screens in precision oncology (ESMO Open, 2019)

ADVANTAGES AND LIMITATIONS OF PRECISION ONCOLOGY

Precision medicine is defined as administering the right medicine at the right dose at the right time to the right patient. Despite being used in different medical fields, it is most commonly applied to oncology. Prasad and Gale analyzed the use of precision oncology in the biomedical literature by classifying 50 articles over three time intervals¹. Between 2005 and 2010, the term precision oncology was mainly used to describe the use of targeted therapies such as epidermal growth factor receptor (EGFR) inhibitors or BCR/ABL1 inhibitors like gefitinib/erlotinib and imatinib. In 2013, precision oncology was used to describe the use of therapies based on specific biomarkers, like the administration of crizotinib for lung cancer patients whose tumor had an EML-ALK rearrangement. By 2016, the definition of precision oncology referred to the use of next generation sequencing to guide the treatment choice. Regardless of this evolution in terminology, precision oncology has always been referred to the use of a certain drug based on molecular aberrations carried by the tumor. Historically, treatment decisions were made based on the histology of the tumor while nowadays are also based on mutation analysis². Genomic projects like The Cancer Genome Atlas (TCGA)³, have identified the main drivers of most solid and hematological malignancies, thus improving the diagnostic and the classification process, as well as the therapeutic approaches (Table 1).

Table 1. List of current approved molecular-driven treatments.

Disease	Gene	Drug
CML*	ABL	Imatinib
Resistant CML	mutant ABL	Dasatinib
HES**	PDGGRa	Imatinib
CMML***	PDGFRb	Imatinib
Myelofibrosis	JAK2	Ruxolitinib
AML****	FLT3	Quizartinib
Gastrointestinal stomal tumor	KIT	Imatinib
Lung cancer	EGFR	Erlotinib, Gefitinib
Kidney cancer	VEGFR	Sunitinib, Sorafenib
Breast cancer	HER2	Trastuzumab/Pertuzumab
Lung cancer	ALK	Crizotinib
Melanoma	BRAF	Vemurafenib/Trametinib
Ovarian cancer	BRCA	Olaparib
Gastric cancer	HER2	Trastuzumab

*Chronic myeloid leukemia, **Hypereosinophilic syndrome; ***Chronic myelomonocytic leukemia, **** acute myeloid leukemia.

The observation that many genomic aberrations are recurrent across multiple cancer types has led to the design of both basket and umbrella trials. The inhibition of HER2

in breast, gastric and colon cancer is, in this context, a successful example⁴⁻⁶ Molecular profiling of tumors has clearly shown to be beneficial for treatment decision making. Indeed, several trials have shown that an individualized approach based on the molecular profiling of the tumor, can result in a better progression free survival (PFS) when compared to the PFS of the previous regimen received by the patients⁷⁻⁹. This benefit has been observed in adult as well as in pediatric cohorts^{10,11}. Nevertheless, in spite of these encouraging results, none of these trials were randomized. The SHIVA trial, which is the only completed randomized phase II basket trial for precision oncology, showed that the use of molecularly targeted agents outside their indications did not improve the clinical outcome of heavily pre-treated patients as compared to the treatment according to clinician's choice¹². However, the effect of targeted anticancer drugs outside their approved indications is still under evaluation in big international precision oncology initiatives like the Target Agent and Profiling Utilization Registry (TAPUR), the Molecular Analysis of Therapy Choice (MATCH) and the Secured Access to Innovative Therapies (AcSé) Programme¹³⁻¹⁵.

There are several other limitations that interfere with a broader success of precision oncology. For example, from the DNA sequencing data, we have learned that fewer than 10% of advanced cancer patients have a simple actionable mutation^{16,17}. Moreover, although some targets might appear to be interesting, the activity of drugs that inhibit them can be limited. Davis et al¹⁸ clearly showed that most drugs that entered the market in the period between 2009 and 2013 did not show a benefit in overall survival (OS) or in quality of life after three years follow up.

Furthermore, we know from basket trials that the histological context can be an important determinant of response to targeted agents¹⁹⁻²¹. This means that we cannot completely ignore the histology of the tumor nor the molecular context in which the mutation has been detected. Secondly, even if the tumor depends on that aberration, meaning that we can block the tumor growth specifically, mechanisms of acquired resistance might still emerge^{22,23}, which again may be tissue-specific. Finally, the use of gene expression profiling is not yet a clinical standard, drugs targeting a specific aberration might not be effective, combinatorial approaches might be toxic to the patient and tumors are heterogeneous in space and time.

One way to overcome these limitations is to further dissect the biology of cancer aberrations by using synthetic lethal interaction approaches. In this review, we will describe the different approaches using functional genetic screens and their applications in precision medicine. We will summarize the current evidence showing that synthetic lethality can help to understand some of the limitations and lead to improve the success rate of precision oncology. Most importantly, we will also highlight the limitations of such approaches and the difficulties to translate preclinical findings into clinical practice.

SYNTHETIC LETHALITY AND GENETIC SCREENS

The understanding of cancer biology as well as advances in precision oncology heavily relies on preclinical research. Approaches that exploit synthetic lethality can help understand cancer vulnerabilities, mechanisms of primary and secondary resistance to treatment, the role of specific aberrations (mutations, amplifications, gene silencing) and their dependence on the tissue context.

Synthetic lethality is described as a phenomenon where a deficiency of two genes leads to cell death, but the deficiency of either one does not impair cell viability^{24,25} (Figure 1). The deficiency can be due to a loss-of-function mutation, epigenetic silencing or pharmacological inhibition of the protein.

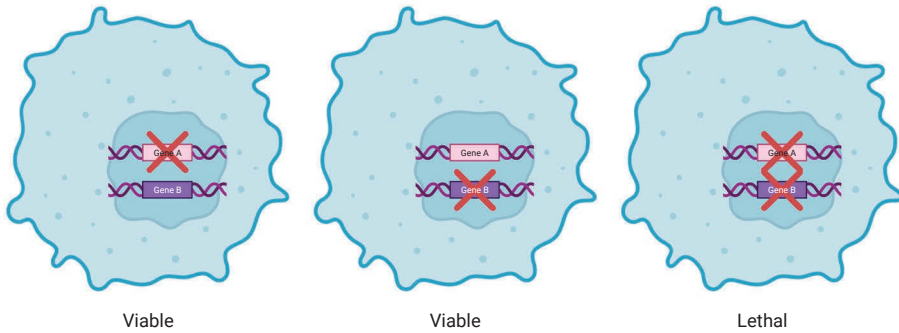


Figure 1: Synthetic lethality is defined as a phenomenon where a loss of either gene A or gene B is tolerated by the cell, but the loss of A and B is lethal. The figure was generated using Biorender.

The first clinically relevant example of a synthetic lethal interaction in cancer was the one between mutations in the genes encoding BRCA 1 and 2 and inhibition of the enzymes of the Poly (ADP-ribose) polymerase (PARP) family of enzymes. Its discovery came from the observation that *Parp* null mice are viable, but rely heavily on BRCA-mediated homologous recombination to repair the DNA damage. This led to the hypothesis that the inverse was true as well, meaning that BRCA deficient cells would depend more on PARP. This hypothesis-driven approach of predicting a synthetic lethal interaction turned out to be true. Actually, tumors that harbor BRCA1 or 2 loss of function mutations are especially sensitive to PARP inhibitors^{26,27}. These results were followed by the investigation and approval of PARP inhibitors for the treatment of patients with a germline BRCA1/2 mutated ovarian and breast cancer.

This interaction is an example of genotype-specific synthetic lethality, where a mutation in a tumor cell causes dependency on another pathway in order to maintain viability.

When the compensatory pathway is inhibited, either genetically or pharmacologically, viability is impaired. Those types of interactions are of great importance for cancer treatment, since they offer selective targeting of mutated cancer cells over normal cells. In addition, drug-specific synthetic lethality can be exploited to identify rational combinational treatment. In this case, a combination of two drugs can be more effective than each of the drugs alone²⁸.

A valuable tool to discover novel synthetic lethal interactions are functional genetic screens. Screens can offer an unbiased insight into complex biological processes, identify cancer vulnerabilities and biomarkers of resistance and sensitivity to the specific treatment. A genetic screen can be performed only with the help of techniques that allow large-scale gene perturbations, for example RNA interference (RNAi), clustered regularly interspaced palindromic repeats (CRISPR) or transposons.

The first breakthrough technology that allowed for a systematic screening of multiple thousands of genes was RNAi using small interfering RNA (siRNA) to degrade selected transcripts^{29,30}. Although revolutionary at the time, the biggest drawback of this technology was the transient and unstable silencing. A significant improvement was achieved by the introduction of the short hairpin (shRNA) technologies, that was characterized not only by a more stable and durable knockdown, but also by the possibility to pool the shRNAs which simplified the screening procedure³¹⁻³³. Despite the success of shRNA based genetic screens, also this technology had its drawbacks, mainly off-target effects³⁴.

Lastly, CRISPR technology got adapted for precise genome editing in mammalian cells. The CRISPR-Cas9 system, which was originally discovered in bacteria as a form of primitive immune system to protect against viral infections³⁵, consists of two parts: an endonuclease Cas9 and a single guide RNA (sgRNA) molecule. When they are both present in the cell, they form a complex, which is guided to the target genomic DNA location by the sgRNA. Next, Cas9 cuts the DNA resulting in a double strand break. As the cells try to repair the double strand break, small insertions and deletions (indels) can arise at the break site. These indels can lead to loss-of-function mutation in the targeted gene. Therefore, the knockout of the gene is a direct consequence of error-prone DNA-repair mechanisms and not due to the double strand break. By using a variety of sgRNAs that target any gene in the genome, we can create knockout mutations in every gene. In addition, the Cas9 protein has been modified, allowing to also perform transcriptional silencing known as CRISPR interference (CRISPRi) or activation (CRISPRa) screens^{36,37}. The main limitations of CRISPR screens include big difference in efficiency between sgRNAs leading to variable editing and mismatch tolerance, also producing some off-target effects³⁸. In comparison to shRNA, CRISPR shows better on-target activity and is nowadays widely used for screening³⁹.

In addition to RNAi and CRISPR, transposons can also be used to disrupt genes. Transposons have been modified to allow the performance of insertional mutagenesis screens. In this type of screens, the enzyme transposase randomly cuts and pastes the transposon sequences across the genome, thus disrupting genes. The most widely used transposon systems are PiggyBac and Sleeping Beauty systems⁴⁰. Even if this system is less effective for studying recessive phenotypes, the use of a haploid cell line HAP1, that contains only one copy of each gene⁴¹, can circumvent this limitation. Overview of their molecular mechanisms is depicted in Figure 2.

Independent of the technology used, genetic screens can answer a variety of biological questions by changing the setup and read-out of the screen. To identify novel synthetic lethal interactions with a certain gene alteration we can perform synthetic lethal or “drop-out” screens.

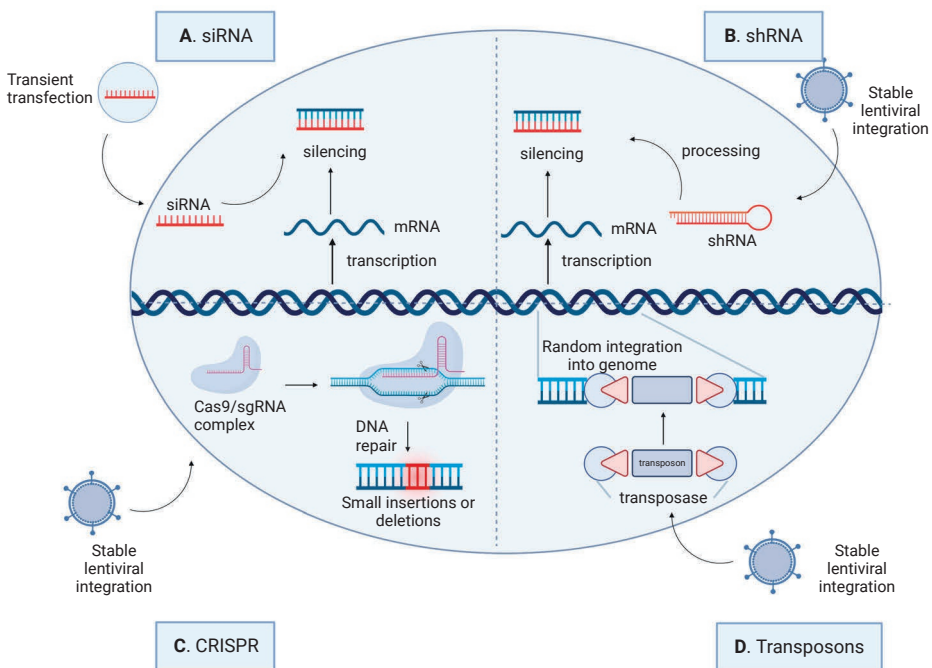


Figure 2: Molecular mechanisms of genetic perturbations (A) siRNA molecule is transiently transfected into the cell, where it binds and thus silences the target mRNA molecule. (B) shRNA is introduced in the cell through viral infection. Upon stable integration into the genomic DNA, it is processed into a siRNA that silences the target mRNA. (C) CRISPR system is generally introduced in the cell through viral infection. Upon stable integration into the genomic DNA, both Cas9 and the sgRNA are expressed. The endonuclease Cas9 and a sgRNA form therefore a complex causing a double strand DNA break at a target location. Mistakes during DNA repair can cause mutations at the break site. (D) Upon viral infection, transposon and transposase enzyme integrate into the genomic DNA and lead to random insertions in the genome, thus disrupting genes. The figure was generated using Biorender.

We can make use of isogenic cell line pairs or large panels of cell lines where one group carries the mutation while the other one does not⁴². In addition to loss-of-function mutations, those aberrations also include gain-of-function mutations, gene amplifications, overexpression, gene signatures and epigenetic changes⁴³⁻⁴⁶. Moreover, we can use drop-out screens to find genes whose loss can confer sensitivity to a certain drug treatment, thus uncovering mechanisms of primary resistance. The potential clinical utility of those screens lies in discovering new combinational treatment strategies that overcome primary resistance⁴⁷ or identification of predictive biomarkers of response that can be used to select the group of patients that is most likely to benefit from that treatment⁴⁸. In contrast to drop-out screens, positive selection screens or “enrichment screens” can be used to identify mechanisms of secondary resistance to a certain drug and identify which genes upon loss confer resistance to the specific treatment (Fig.3)⁴⁹. Besides genetic screens, other approaches can help in uncovering synthetic lethal interactions and finding new combinations of treatment, for example drug screens and computational approaches^{50,51}.

One of the major advantages of functional genetic screens is that they can be applied to any biological process. However, they do require an extensive *in vitro* and *in vivo* validation, as well as clinical trials before a novel finding can be translated into clinical practice.

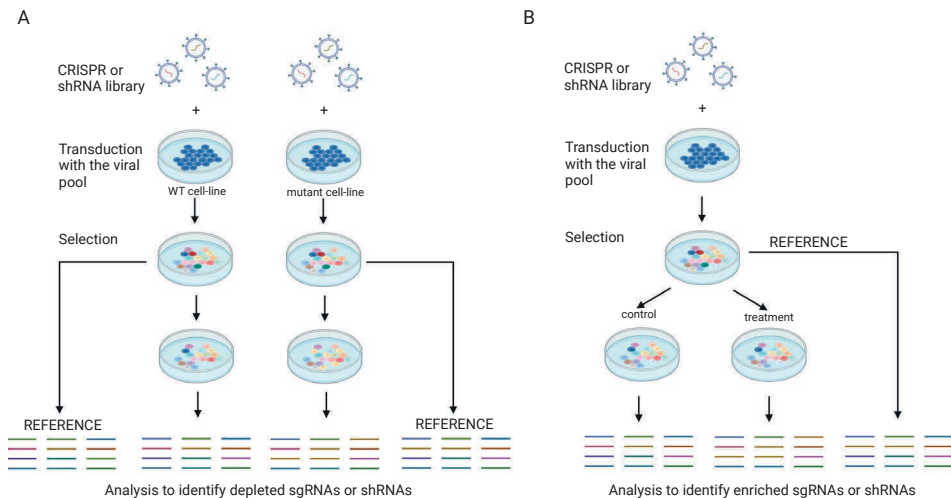


Figure 3: Functional genetic screens (A) Drop-out screen, an isogenic cell line pair infected with the CRISPR library, selected and cultured alongside. Next, gRNA or shRNA barcodes are recovered, and the abundance of barcodes between the cell lines and the reference samples is compared. (B) Resistance screen where a cell line that is sensitive to the test treatment is used. After infection and selection, the cell population is split to treated and control arm. Next, barcodes are recovered from remaining cells and compared between reference sample, treated and untreated samples. The figure was generated using Biorender.

Table 2. “From Bench to the Bed-Side”. Depicts preclinical findings followed by clinical trials and clinical practice implementation.

Preclinical findings	Clinical trials	Clinical practice changing
EGFR loss is synthetic lethal with BRAF(V600E) in CRC <i>in vivo</i> and <i>in vitro</i> models ⁴⁷	53-60	FDA breakthrough therapy designation[60]
BRAF-like CC are vulnerable to anti-mitotic agents ⁴⁶	66-68,99	Controversial data. Waiting for further studies
PTEN loss and PIK3CA mutations confer resistance to trastuzumab in HER2 amplified breast cancer cell lines ⁷⁰	73-77	Not yet
E-cadherin loss is synthetic lethal with ROS1 inhibitors in lobular breast cancer preclinical models ⁷⁸	79	Trial not yet recruiting
Loss of BCL-XL is synthetic lethal with MEK inhibition in KRAS mutant preclinical models ⁸⁰	81	Trial on going
Loss of PTPN2 synergizes with Immunotherapy in mouse transplantable tumor models ⁸⁵	No trials ongoing nor retrospective analysis of already closed trials	Not yet
Identification of biomarkers of response and resistance to Immunotherapy in a mouse melanoma model ^{86,87}	No trials ongoing nor retrospective analysis of already closed trials	Not yet
Identification of novel targets for Immunotherapy ⁸⁸	No trials ongoing nor retrospective analysis of already closed trials	Not yet

APPLYING GENETIC SCREENS TO PRECISION ONCOLOGY

Targeted therapies like Braf and MEK inhibitors revolutionized the treatment of BRAF(V600E) metastatic melanoma and have been shown to be active in other malignancies as well⁵². Paradoxically, although the same point mutation occurs in about 8-10% of colorectal cancer (CRCs), these tumors do not respond to the BRAF(V600E) inhibitor (vemurafenib) when used as single agent²⁰. The mechanism underlying this unresponsiveness has been elegantly uncovered using a synthetic lethal screen. In particular, Prahallad et al⁴⁷ performed a drop-out screen in BRAF(V600E) CRC cell lines looking for kinases that could sensitize cells to vemurafenib. With this approach, they discovered a feedback re-activation of EGFR upon Braf inhibition in BRAF(V600E) CRC cells as the driver of unresponsiveness to such treatment. These results led to the hypothesis that Braf inhibitors need to be administered in combination with EGFR inhibitors to effectively kill these tumors. This hypothesis has been extensively validated both *in vitro* and *in vivo*. Most importantly, the results of this preclinical work have led to the design of several clinical trials, where BRAF(V600E) metastatic CRC (mCRC) patients have been treated either with a dual combination of Braf and EGFR inhibitors or a triple combination of a BRAF, EGFR and MEK or PI3K inhibitors⁵³⁻⁵⁵. The results of

these studies have clearly shown that the dual and triple blockade improved response rates and outcome as compared to Braf inhibition alone. Simultaneously, a Phase 1b study and a phase II study, evaluated the combination of targeted therapies with chemotherapy in a three-drug regimen of vemurafenib, cetuximab and irinotecan^{56,57}. The addition of a Braf inhibitor showed an increase of response rate and PFS when compared to the standard combination of anti-EGFR treatment and chemotherapy. Finally, the BEACON CRC⁵⁸ is the first phase III trial that compares the triple combination (Braf, MEK and EGFR inhibitors) versus dual combination (Braf and EGFR inhibitor) versus a control arm (EGFR inhibitor and chemotherapy) as second or third line treatment for BRAF (V600E) mCRC patients. Recently, an update of the safety lead of the study confirmed the triple combination to be safe. Clinical activity was characterized by 48% of overall response rate (ORR) and efficacy by an improved PFS and OS as compared to standard of care⁵⁹. Based on these data, the U.S Food and Drug Administration (FDA) has granted breakthrough therapy designation of the triple combination as second or third line treatment to patients affected by BRAF (V600E) mCRC⁶⁰. Nevertheless, the responses and the outcome benefit were not observed in the entire cohort of patients enrolled and secondary resistance occurred. Recently, CRCs have been classified into four distinct consensus molecular subtypes (CMS): CMS1 characterized by microsatellite instability and immune infiltration (14%), CMS2, known as canonical with WNT and MYC signaling activation (37%), CMS3 harboring metabolic dysregulation (13%) and CMS4 with mesenchymal characteristics (23%)⁶¹. Notably, BRAF(V600E) mutations are present across all four different CRC molecular subtypes.

In addition, Oddo et al.⁶² described that mutation leading to reactivation of the MAPK pathway represent the major mechanisms of secondary resistance. Therefore, tumor heterogeneity and clonal evolution could partially explain the heterogeneous response to both, the dual and triple blockade, observed in those clinical trials.

Prior to the CMS classification⁶¹ two independent groups found BRAF(V600E) colon cancers (CCs) to be characterized by a distinct gene expression profile when compared to KRAS-mutant and KRAS-BRAF double wild type (WT2) CCs. These tumors were defined as BRAF-mutant like by a transcriptional signature^{63,64}. To note, this gene signature identified not only BRAF(V600E) CCs but also subsets of KRAS-mutant (30%) and WT2 (13%) CCs. The relevance of this transcriptional signature relies on the fact that the BRAF-mutant like tumors harbor similar poor prognosis regardless of the presence of BRAF(V600E) mutation^{63,64}. The signature has been further validated in a larger cohort of BRAF(V600E) CC patients⁶⁵ and its biological implication has been investigated by using a synthetic lethal screen. By performing a drop-out screen, Vecchione et al.⁴⁶, identified RANBP2 to be synthetic lethal with the BRAF-like signature in CC cell lines. Further investigation of the function of this protein in CC cell lines, led to the hypothesis that BRAF-like CC cells lines could be more vulnerable to antimetabolic agents. This concept

was extensively validated *in vitro* and *in vivo* models and is currently under investigation in the Motricolor consortium⁶⁶. Immediately after this finding, a prospective multicenter phase-II clinical study started, where chemorefractory BRAF(V600E) mCRC patients were treated with vinorelbine⁶⁷. A total of 20 patients were enrolled. Unfortunately, no responses were observed, with only one stable disease reported. In contrast, Masuishi et al.⁶⁸ reported tumor shrinkage in four BRAF (V600E) mCRC patients treated with eribulin as third and fifth line of treatment. Based on the results of these four cases, the BRAVERY study is now investigating the activity of eribulin as second line treatment in BRAF(V600E) mCRC⁶⁹. The hypothesis generated from Vecchione et al.⁴⁶, is still far from being applicable, highlighting how complex is to translate preclinical findings into clinical practice.

An example of enrichment screen performed by Berns et al.⁷⁰ identified loss of PTEN as well as activating mutations in PIK3CA to induce resistance to trastuzumab in HER2 amplified breast cancer cell lines. These findings were further validated in a small cohort of HER2 amplified breast cancer patients where both PIK3CA mutations and low PTEN expression correlated with poor prognosis after trastuzumab treatment. Moreover, similar preclinical results were obtained by other independent groups and with different HER2 inhibitors supporting the relevance of these discovery^{71,72}. Based on these results, the role of PIK3CA mutations and loss of PTEN in HER2 amplified breast cancer patients treated with anti-HER2 antibody has been investigated, both in neoadjuvant and metastatic setting. The combined analysis of the GeparQuattro, GeparQuinto and GeparSixto trials showed PIK3CA mutant HER2 amplified breast tumors to have reduced pathological complete response (pCR) when compared to PIK3CA WT tumors⁷³. Similarly, Majewsky et al.⁷⁴ found lower pCR rate upon trastuzumab and lapatinib monotherapy or in combination in PIK3CA mutant HER2 amplified early breast cancer patients versus PIK3CA WT tumors. Additionally, PIK3CA mutated HER2 positive metastatic breast cancer patients treated with capecitabine and lapatinib showed lower PFS compared to PIK3CA WT HER2 positive patients⁷⁵. To increase statistical power, Loibl et al.⁷⁶, performed a pooled analysis including approximately 1000 HER2 amplified breast cancer patients whose PIK3CA status was known and were treated with anti-HER2 antibody. They confirmed PIK3CA mutant tumors to have lower chances to achieve a pCR when treated with HER2 blockade. Interestingly, this is especially significant in hormone receptor (HR) positive group as compared to the HR negative group. Importantly, none of the studies observed differences in outcome between PIK3CA mutant and PIK3CA WT tumors. Finally, the biomarker analysis of the NeoSphere study⁷⁷ found only *PIK3CA* mutations in exon 9 to be associated with resistance to HER2 blockade. Overall, even if the results of the preclinical genetic screen are clear and robust, PIK3CA mutations are not used as predictive biomarker yet. Furthermore, other clinical variables might be considered to better understand its role in predicting resistance to HER2 blockade in breast cancer. More recently, a group of researchers discovered loss of E-Cadherin, a frequently

mutated gene in breast (>13%) and gastric cancer (>14%), to be synthetic lethal with ROS1 inhibitors, such as crizotinib. Authors used lobular breast cancer models for a perturbation-screen with a focused library and a compound-screen with drugs that are either approved in the clinic or that are being tested. As a result, E-cadherin loss became a potential biomarker for treatment with ROS1 inhibitors in a significant subset of patients with poor prognosis ⁷⁸. Currently, a phase-II clinical trial is testing crizotinib as a monotherapy in diffuse gastric cancer as well as crizotinib in combination with fulvestrant in lobular breast cancer ⁷⁹.

Another example of frequent genetic alteration that cannot be selectively targeted yet is KRAS mutations. The development of MEK inhibitors became a promising option for the treatment of these aggressive tumors. Lamentably, KRAS mutant tumors harbor different mechanisms of primary resistance to those inhibitors. In an attempt to identify genes whose loss could synergize with MEK inhibitors in KRAS mutant cancer cells, Corcoran et al. performed a loss of function genetic screen. They identified Bcl-XL, a member of BH-3 anti-apoptotic family, to be synthetic lethal with MEK inhibitors in KRAS mutant cell lines. These data were further validated in preclinical models by using a Bcl-XL inhibitor (Navitoclax) ⁸⁰. At present, a clinical trial is recruiting patients with advanced or metastatic solid tumors to test MEK inhibitor (trametinib) in combination with Navitoclax ⁸¹.

In the last few years, checkpoint inhibitors have shown encouraging results that have changed the therapeutic approach of certain tumors, like non-small cell lung cancer (NSCLC), melanoma and microsatellite instable (MSI) mCRC ⁸²⁻⁸⁴. In spite of this success, the efficacy and responsiveness to anti PD1, PD-L1 and CTLA-4 varies among different tumor types and across individual patients. Therefore, establishment of predictive biomarkers for checkpoint blockades as well as identification of novel targets for cancer immunotherapy are key to maximize therapeutic benefits. In this context, the use of genetic screens could be of great support. For example, by using a pooled loss-of-function *in vivo* genetic CRISPR-Cas9 screen to unravel genes responsible for sensitivity and resistance, Manguso et al. demonstrated that loss of PTPN2 in cancer cells enhances interferon- γ -mediated effects on antigen presentation and growth suppression, thus increasing the efficacy of immunotherapy in a mouse transplantable tumor model ⁸⁵. Similarly, another group performed an enrichment genome-scale CRISPR/Cas9 screen in co-culture with activated cytotoxic CD8+ T-lymphocytes seeking for genes whose loss evoke resistance to adaptive immune response. The authors identified the expression of five negative regulators of the MAPK pathway as responsible for resistance to immunotherapy⁸⁶. On the opposite, loss of genes belonging to the SWI/SNF complex, the nuclear factor κ B (NF- κ B) pathway and metabolic pathway were shown to confer sensitivity to immunotherapy in a mouse melanoma model. Patel et al.⁸⁷ confirmed that loss of genes with a role in antigen presentation pathway as well as in interferon- γ

signaling are responsible for immunotherapy resistance. Among the validated genes, they identified that loss of APLNR reduces the efficacy of adoptive cell transfer and checkpoint blockade by interacting with JAK1, thus, modulating interferon- γ responses. Finally, Mezzadra et al.⁸⁸ used an haploid genetic screen to seek for regulators of PD-L1 protein. They identified CMTM4 and CMTM6 as new potential target to block the PD-1 pathway. Altogether, these data highlight the importance of genetic screens to unveil mechanisms of responsiveness to immunotherapy as well as new potential targets to exploit therapeutically. Nevertheless, none of those results have been validated in the clinic yet. A schematic overview of the preclinical findings and the clinical studies reported above is depicted in Table 2.

FUTURE DIRECTIONS

Precision oncology is based on the molecular profile of cancer cells. Defining genetic alterations helps to establish a precise molecular diagnosis of the tumor and to predict the course of the disease. Moreover, it allows the administration of a tailored therapy in accordance to the genomic aberrations carried by that individual tumor. The development of targeted therapies requires several years of intense multidisciplinary effort, from understanding the cancer biology to testing a new drug in a phase III study. Nevertheless, large phase III clinical trials are often not feasible for rare tumor subtypes. In this context, a possible solution are basket trials, which can accelerate the translation into clinical practice. Moreover, several limitations need to be considered during this complex process, like unpredicted toxicity of combinatorial treatments, tumor evolution, cancer heterogeneity, context dependency and the tumor microenvironment. In addition, due to the ever increasing number of FDA approved cancer drugs, the number of possible drug combinations increases exponentially. This poses a conundrum that can only be solved by upfront selection of the most potent combinations. We have argued here that genetic screens can be a useful tool to identify such powerful drug combinations. A second potential clinical use regards the notion that not all patients treated with a specific drug will benefit from it. As we have discussed as well, genetic screens can help to identify biomarkers of response or resistance.

After almost two decades from the introduction of the RNAi technology in human cancer cells, we are starting to witness the benefits of the use of genetic screens. As a result, we see new therapies being implemented for some malignancies that were untreatable before. Indeed, some clinical trials are finding strong correlation in what has been described *in vitro*⁴⁷. In addition, organoids and *in vivo* screens are now being exploited as techniques to study the complex interplay between the tumor and its stroma. Although *in vivo* screens are technically a huge challenge, they have become a valuable tool, especially when looking for targets that are related with the immune system.

The technology that allows genome wide screens has become easily available, cheaper and relatively simple to implement. As a consequence, there has been an exponential increase in the number of screens performed. Even though there are indications that functional genetic screens can play a role in clinically relevant discoveries, there are a lot of hurdles to deal with, when translating the pre-clinical observation from a genetic screen into clinical practice.

Firstly, genetic screens are often long and complicated. It should also be remembered that complete removal of a protein from a cell is not necessarily the same as pharmacological inhibition of the protein, as proteins can also have scaffolding functions. Thus, nor CRISPR or shRNA technologies can simulate drug inhibition. On the one hand, shRNAs are prone to off-target effects. On the other hand, CRISPR screens have less off-target effects, however, drugs seldom inhibit a protein for the full 100%, which is the result of a CRISPR knockout. Moreover, even if a genetic screen unveils a new target, the development of small molecule inhibitors needed to clinically validate can often take years. Therefore, a great number of genetic screens with potential clinical utility still remain to be proven relevant for the patients.

Secondly, to overcome limitations like context dependency, heterogeneity and tumor evolution, the use of a comprehensive and integrated analysis can be of great help. Combining genetic approaches with cell line analysis and patient data, when available, could help to overcome these problems in order to focus on clinical relevant targets⁸⁹. As a result, we need to design smarter and better screens, to maximize the outcomes while minimizing the costs. Since screens can be adapted to answer a wide variety of questions, we can use them to investigate complex biological processes. We can use different reporter systems for phenotype selection⁹⁰, or knock-in of a selection marker to a target locus⁹¹. Now, we can design screens that are not focused only on cell death or proliferation. For example, a flow-cytometry based read-out allows separation of the population of cells based on any protein for which an antibody is available. Currently, CRISPR technology offers a diverse toolkit to modify gene expression. In addition, CRISPRa and CRISPRi, introduction of diverse point mutations or epigenetic reprogramming is possible. Subsequently, it is expected that screens adopting these technologies will offer novel insights into the complex biology of the cancer cell in the near future.

Another important aspect that applies to precision oncology is that the phenotype and behavior of a certain tumor might be the consequence of the activity of multiple genes. For example, it may not be the aberration in gene X that plays a role in that specific tumor context, but rather the combination with other gene aberrations. To better model this, we need to develop systems that allow perturbations of more than one gene at the time. In that respect, there have been significant improvements in the last years to develop screens that allow screening for interactions, both with shRNAs and

CRISPR⁹²⁻⁹⁴. Additionally, a dual system that combines activation of transcription with knockout has recently been developed, which can further expand our understanding of genetic interactions⁹⁵. Furthermore, we can couple pooled genetic screens with single cell RNA sequencing, for example Perturb-seq, which allows immediate transcriptional profiling of genetically diverse populations⁹⁶⁻⁹⁸.

In conclusion, genetic screens have already shown to be a relevant tool to find new therapeutic options and to predict treatment response. Nevertheless, it is an early technology that we are still improving. Therefore, optimizing and integrating this technology with other analysis would potentially bring us to the new era of precision oncology.

THESIS OUTLINE

Using functional genetic screens can uncover new factors mediating resistance and sensitivity to cancer treatment. In this thesis we use genetic screens to study resistance and sensitivity to targeted treatment and immunotherapy and propose new biomarkers and combination treatments. In **chapter 2** we identify new factors of resistance and sensitivity to molecular glue degrader - indisulam. We show that loss of SRPK1 sensitizes cancer cells to indisulam through accumulation of splicing errors. Furthermore, we show that loss of CAND1 leads to indisulam resistance. We also show that cancer cells acquire resistance to indisulam which can be circumvented by combining indisulam with BCL-xL inhibitors. In **chapter 3** we perform genetic screens to find enhancers of CDK4/6 inhibitor palbociclib. We validate CDK2 as a top hit that upon loss improves senescence induction by palbociclib. We then combine indisulam, an indirect CDK2 inhibitor with palbociclib and show induction of senescence in various cancer cell line models and reduction of tumor growth *in vivo*. In **chapter 4** we use molecular patient data of acquired resistance to immune checkpoint blockade to generate a custom CRISPR library and perform a genetic screen using a T-cell and melanoma co-culture *in vitro*. We validate loss of B2M as a resistance mechanism to immune checkpoint blockade and T-cell killing. Finally, in **chapter 5** we summarize the findings of the thesis and discuss them in the broader context of the field. We show multiple examples of genetic screens with the potential to impact the clinical practice.

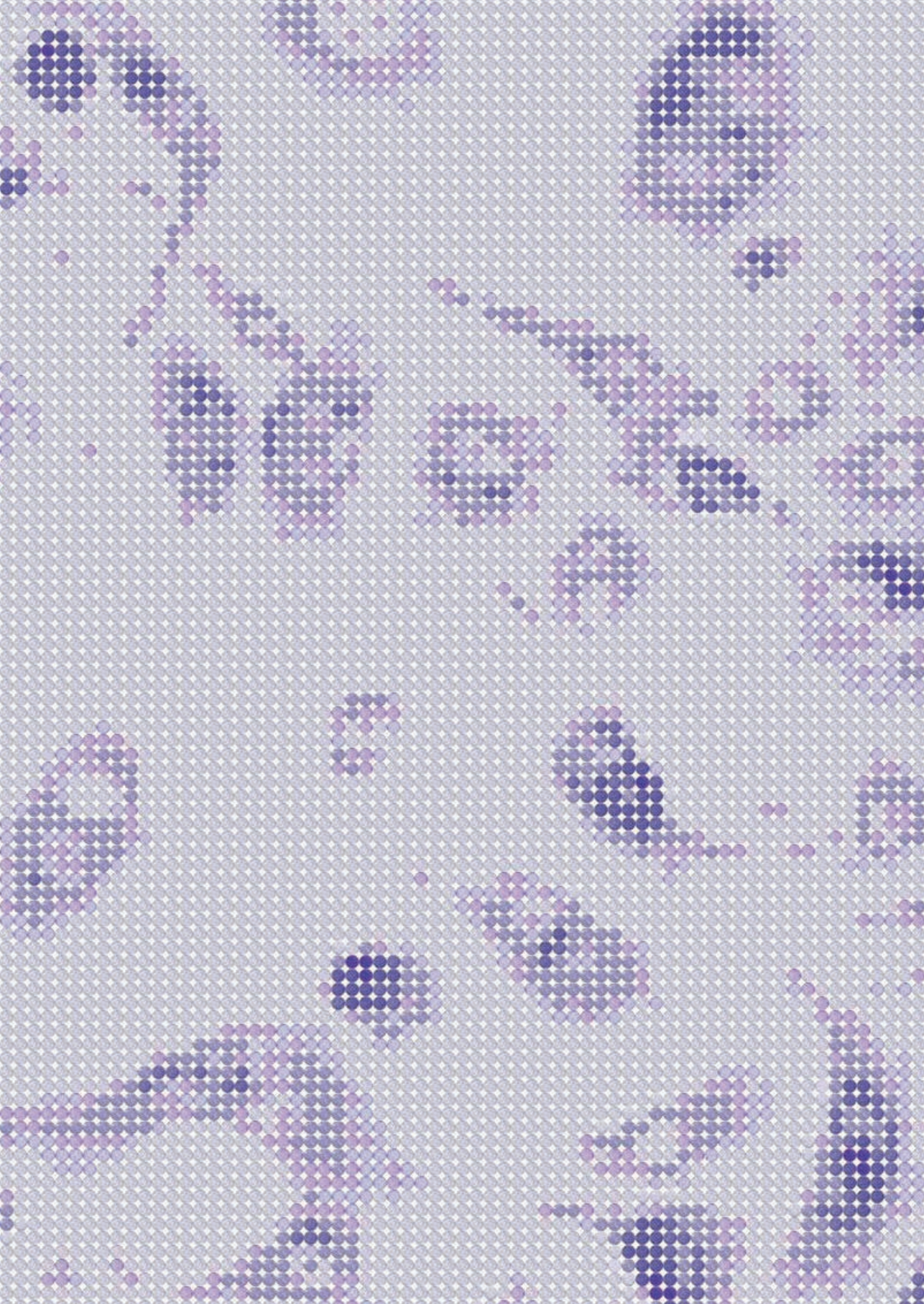
REFERENCES

1. Prasad, V. & Gale, R. P. What Precisely Is Precision Oncology—and Will It Work? *ASCO post* (2017).
2. Gerlinger, M. *et al.* Intratumor heterogeneity and branched evolution revealed by multiregion sequencing. *N. Engl. J. Med.* **366**, 883–892 (2012).
3. The Cancer Genome Atlas. <https://cancergenome.nih.gov/>.
4. Baselga, J., Perez, E. A., Pienkowski, T. & Bell, R. Adjuvant trastuzumab: a milestone in the treatment of HER-2-positive early breast cancer. *Oncologist* **11 Suppl 1**, 4–12 (2006).
5. Sartore-Bianchi, A. *et al.* Dual-targeted therapy with trastuzumab and lapatinib in treatment-refractory, KRAS codon 12/13 wild-type, HER2-positive metastatic colorectal cancer (HERACLES): a proof-of-concept, multicentre, open-label, phase 2 trial. *Lancet Oncol.* **17**, 738–746 (2016).
6. Bang, Y.-J. *et al.* Trastuzumab in combination with chemotherapy versus chemotherapy alone for treatment of HER2-positive advanced gastric or gastro-oesophageal junction cancer (ToGA): a phase 3, open-label, randomised controlled trial. *Lancet* **376**, 687–697 (2010).
7. Von Hoff, D. D. *et al.* Pilot study using molecular profiling of patients' tumors to find potential targets and select treatments for their refractory cancers. *J. Clin. Oncol.* **28**, 4877–4883 (2010).
8. Prager, G. W. *et al.* Results of the extended analysis for cancer treatment (EXACT) trial: a prospective translational study evaluating individualized treatment regimens in oncology.
9. Hoefflin, R. *et al.* Personalized Clinical Decision Making Through Implementation of a Molecular Tumor Board: A German Single-Center Experience. *JCO Precision Oncology* 1–16 (2018).
10. Kim, E. S. *et al.* The BATTLE trial: personalizing therapy for lung cancer. *Cancer Discov.* **1**, 44–53 (2011).
11. Harttrampf, A. C. *et al.* Molecular Screening for Cancer Treatment Optimization (MOSCATO-01) in Pediatric Patients: A Single-Institutional Prospective Molecular Stratification Trial. *Clin. Cancer Res.* **23**, 6101–6112 (2017).
12. Le Tourneau, C. *et al.* Molecularly targeted therapy based on tumour molecular profiling versus conventional therapy for advanced cancer (SHIVA): a multicentre, open-label, proof-of-concept, randomised, controlled phase 2 trial. *Lancet Oncol.* **16**, 1324–1334 (2015).
13. The Targeted Agent and Profiling Utilization Registry. *ASCO* <https://www.tapur.org/>.
14. NCI-MATCH Trial (Molecular Analysis for Therapy Choice). *National Cancer Institute* <https://www.cancer.gov/about-cancer/treatment/clinical-trials/nci-supported/nci-match>.
15. Buzyn, A. *et al.* Equal access to innovative therapies and precision cancer care. *Nat. Rev. Clin. Oncol.* **13**, 385–393 (2016).
16. Group, E.-A. C. R. & Others. Executive summary: interim analysis of the NCI-MATCH trial. *ECOG-ACRIN Cancer Research Group*.
17. Meric-Bernstam, F. *et al.* Feasibility of Large-Scale Genomic Testing to Facilitate Enrollment Onto Genomically Matched Clinical Trials. *J. Clin. Oncol.* **33**, 2753–2762 (2015).
18. Davis, C. *et al.* Availability of evidence of benefits on overall survival and quality of life of cancer drugs approved by European Medicines Agency: retrospective cohort study of drug approvals 2009–13. *BMJ* **359**, j4530 (2017).
19. Chapman, P. B. *et al.* Improved survival with vemurafenib in melanoma with BRAF V600E mutation. *N. Engl. J. Med.* **364**, 2507–2516 (2011).
20. Kopetz, S. *et al.* Phase II Pilot Study of Vemurafenib in Patients With Metastatic BRAF-Mutated Colorectal Cancer. *J. Clin. Oncol.* **33**, 4032–4038 (2015).
21. Hyman, D. M. *et al.* Vemurafenib in Multiple Nonmelanoma Cancers with BRAF V600 Mutations. *N. Engl. J. Med.* **373**, 726–736 (2015).
22. Wagle, N. *et al.* Dissecting therapeutic resistance to RAF inhibition in melanoma by tumor genomic profiling. *J. Clin. Oncol.* **29**, 3085–3096 (2011).
23. Morgillo, F., Della Corte, C. M., Fasano, M. & Ciardiello, F. Mechanisms of resistance to EGFR-targeted drugs: lung cancer. *ESMO Open* **1**, e000060 (2016).
24. Dobwansky, T. H. Genetics of Natural Populations: Recombination and Variability in Populations of *Drosophila Pseudoobscura*. *Genetics* (1946).
25. Nijman, S. M. B. Synthetic lethality: general principles, utility and detection using genetic screens in human cells. *FEBS Lett.* **585**, 1–6 (2011).
26. Farmer, H. *et al.* Targeting the DNA repair defect in BRCA mutant cells as a therapeutic strategy. *Nature* **434**, 917–921 (2005).
27. Bryant, H. E. *et al.* Specific killing of BRCA2-deficient tumours with inhibitors of poly(ADP-ribose) polymerase. *Nature* **434**, 913–917 (2005).
28. Brunen, D. & Bernards, R. Drug therapy: Exploiting synthetic lethality to improve cancer therapy. *Nat. Rev. Clin. Oncol.* **14**, 331–332 (2017).
29. Brummelkamp, T. R., Bernards, R. & Agami, R. A system for stable expression of short interfering RNAs in mammalian cells. *Science* **296**, 550–553 (2002).
30. Berns, K. *et al.* A large-scale RNAi screen in human cells identifies new components of the p53 pathway. *Nature* **428**, 431–437 (2004).
31. Burgess, D. J. *et al.* Topoisomerase levels determine chemotherapy response in vitro and

- in vivo. *PNAS* **105**, 9053–9058 (2008).
32. Silva, J. M. *et al.* Profiling essential genes in human mammary cells by multiplex RNAi screening. *Science* **319**, 617–620 (2008).
 33. Schlabach, M. R. *et al.* Cancer proliferation gene discovery through functional genomics. *Science* **319**, 620–624 (2008).
 34. Jackson, A. L. *et al.* Expression profiling reveals off-target gene regulation by RNAi. *Nat. Biotechnol.* **21**, 635–637 (2003).
 35. Makarova, K. S., Grishin, N. V., Shabalina, S. A., Wolf, Y. I. & Koonin, E. V. A putative RNA-interference-based immune system in prokaryotes: computational analysis of the predicted enzymatic machinery, functional analogies with eukaryotic RNAi, and hypothetical mechanisms of action. *Biol. Direct* **1**, 7 (2006).
 36. Gilbert, L. A. *et al.* Genome-Scale CRISPR-Mediated Control of Gene Repression and Activation. *Cell* **159**, 647–661 (2014).
 37. Konermann, S. *et al.* Genome-scale transcriptional activation by an engineered CRISPR-Cas9 complex. *Nature* **517**, 583–588 (2015).
 38. Fortin, J.-P. *et al.* Multiple-gene targeting and mismatch tolerance can confound analysis of genome-wide pooled CRISPR screens. *Genome Biol.* **20**, 21 (2019).
 39. Evers, B. *et al.* CRISPR knockout screening outperforms shRNA and CRISPRi in identifying essential genes. *Nat. Biotechnol.* **34**, 631–633 (2016).
 40. O'Donnell, K. A. Advances in functional genetic screening with transposons and CRISPR/Cas9 to illuminate cancer biology. *Curr. Opin. Genet. Dev.* **49**, 85–94 (2018).
 41. Carette, J. E. *et al.* Haploid genetic screens in human cells identify host factors used by pathogens. *Science* **326**, 1231–1235 (2009).
 42. Berns, K. *et al.* ARID1A mutation sensitizes most ovarian clear cell carcinomas to BET inhibitors. *Oncogene* **37**, 4611–4625 (2018).
 43. Mair, B., Kubicek, S. & Nijman, S. M. B. Exploiting epigenetic vulnerabilities for cancer therapeutics. *Trends Pharmacol. Sci.* **35**, 136–145 (2014).
 44. Chan, N. *et al.* Contextual synthetic lethality of cancer cell kill based on the tumor microenvironment. *Cancer Res.* **70**, 8045–8054 (2010).
 45. Steckel, M. *et al.* Determination of synthetic lethal interactions in KRAS oncogene-dependent cancer cells reveals novel therapeutic targeting strategies. *Cell Res.* **22**, 1227–1245 (2012).
 46. Vecchione, L. *et al.* A Vulnerability of a Subset of Colon Cancers with Potential Clinical Utility. *Cell* **165**, 317–330 (2016).
 47. Prahallad, A. *et al.* Unresponsiveness of colon cancer to BRAF(V600E) inhibition through feedback activation of EGFR. *Nature* **483**, 100–103 (2012).
 48. Ding, Y. *et al.* Synthetic lethality between HER2 and transaldolase in intrinsically resistant HER2-positive breast cancers. *Nat. Commun.* **9**, 4274 (2018).
 49. Huang, S. *et al.* MED12 controls the response to multiple cancer drugs through regulation of TGF- β receptor signaling. *Cell* **151**, 937–950 (2012).
 50. Jerby-Arnon, L. *et al.* Predicting cancer-specific vulnerability via data-driven detection of synthetic lethality. *Cell* **158**, 1199–1209 (2014).
 51. Sinha, S. *et al.* Systematic discovery of mutation-specific synthetic lethals by mining pan-cancer human primary tumor data. *Nat. Commun.* **8**, 15580 (2017).
 52. Dummer, R. *et al.* Cutaneous melanoma: ESMO Clinical Practice Guidelines for diagnosis, treatment and follow-up. *Ann. Oncol.* **26** Suppl 5, v126–32 (2015).
 53. Corcoran, R. B. *et al.* Combined BRAF and MEK Inhibition With Dabrafenib and Trametinib in BRAF V600-Mutant Colorectal Cancer. *J. Clin. Oncol.* **33**, 4023–4031 (2015).
 54. van Geel, R. M. J. M. *et al.* A Phase Ib Dose-Escalation Study of Encorafenib and Cetuximab with or without Alpelisib in Metastatic BRAF-Mutant Colorectal Cancer. *Cancer Discov.* **7**, 610–619 (2017).
 55. Corcoran, R. B. *et al.* Combined BRAF, EGFR, and MEK Inhibition in Patients with BRAFV600E-Mutant Colorectal Cancer. *Cancer Discov.* **8**, 428–443 (2018).
 56. Hong, D. S. *et al.* Phase IB Study of Vemurafenib in Combination with Irinotecan and Cetuximab in Patients with Metastatic Colorectal Cancer with BRAFV600E Mutation. *Cancer Discov.* **6**, 1352–1365 (2016).
 57. Kopetz, S. *et al.* Randomized trial of irinotecan and cetuximab with or without vemurafenib in BRAF-mutant metastatic colorectal cancer (SWOG S1406). *J. Clin. Orthod.* **35**, 3505–3505 (2017).
 58. BEACON (CRC). *Clinical trials* <https://clinicaltrials.gov/ct2/show/NCT02928224>.
 59. Kopetz, S. *et al.* Updated results of the BEACON CRC safety lead-in: Encorafenib (ENCO) + binimetinib (BINI) + cetuximab (CETUX) for BRAFV600E-mutant metastatic colorectal cancer (mCRC). *J. Clin. Orthod.* **37**, 688–688 (2019).
 60. FDA Grants Breakthrough Therapy Designation for Encorafenib Plus Binimetinib and Cetuximab in BRAF V600E-Mutant Metastatic Colorectal Cancer. <http://www.ascp.org/News/59160>.
 61. Guinney, J. *et al.* The consensus molecular subtypes of colorectal cancer. *Nat. Med.* **21**, 1350–1356 (2015).
 62. Oddo, D. *et al.* Molecular Landscape of Acquired Resistance to Targeted Therapy Combinations in BRAF-Mutant Colorectal Cancer. *Cancer Res.* **76**, 4504–4515 (2016).
 63. Popovici, V. *et al.* Identification of a Poor-Prognosis BRAF-Mutant-Like Population of

- Patients With Colon Cancer. *J. Clin. Orthod.* **30**, 1288–1295 (2012).
64. Tian, S. *et al.* A combined oncogenic pathway signature of BRAF, KRAS and PI3KCA mutation improves colorectal cancer classification and cetuximab treatment prediction. *Gut* **62**, 540–549 (2013).
 65. In 't Veld, S. G. J. G. *et al.* A Computational Workflow Translates a 58-Gene Signature to a Formalin-Fixed, Paraffin-Embedded Sample-Based Companion Diagnostic for Personalized Treatment of the BRAF-Mutation-Like Subtype of Colorectal Cancers. *High Throughput* **6**, (2017).
 66. Molecularly guided Trials with specific treatment strategies in patients with advanced newly molecular defined subtypes of Colorectal cancer. <http://www.motricolor.eu/>.
 67. Cremolini, C. *et al.* Vinorelbine in BRAF V600E mutant metastatic colorectal cancer: a prospective multicentre phase II clinical study. *ESMO Open* **2**, e000241 (2017).
 68. Masuishi, T. *et al.* Eribulin in BRAF V600E-mutant metastatic colorectal cancer: case series and potential rationale. *Ann. Oncol.* **29**, 1330–1331 (2018).
 69. T Masuishi H Taniguchi D Kotani H Bando Y Komatsu K Yamaguchi T E Nakajima T Satoh T Nishina T Esaki M Wakabayashi S Nomura S Sakamoto H Ono N Hirano N Fujishiro N Fuse A Sato A Ohtsu T Yoshino. BRAVERY study: A multicenter phase II study of eribulin in patients with BRAF V600E mutant metastatic colorectal cancer (EPOC1701). *Annals of Oncology* https://academic.oup.com/annonc/article/29/suppl_8/ndy281.153/5140513.
 70. Berns, K. *et al.* A functional genetic approach identifies the PI3K pathway as a major determinant of trastuzumab resistance in breast cancer. *Cancer Cell* **12**, 395–402 (2007).
 71. Nagata, Y. *et al.* PTEN activation contributes to tumor inhibition by trastuzumab, and loss of PTEN predicts trastuzumab resistance in patients. *Cancer Cell* **6**, 117–127 (2004).
 72. Eichhorn, P. J. A. *et al.* Phosphatidylinositol 3-kinase hyperactivation results in lapatinib resistance that is reversed by the mTOR/phosphatidylinositol 3-kinase inhibitor NVP-BE235. *Cancer Res.* **68**, 9221–9230 (2008).
 73. Loibl, S. *et al.* PIK3CA mutations are associated with lower rates of pathologic complete response to anti-human epidermal growth factor receptor 2 (her2) therapy in primary HER2-overexpressing breast cancer. *J. Clin. Oncol.* **32**, 3212–3220 (2014).
 74. Majewski, I. J. *et al.* PIK3CA mutations are associated with decreased benefit to neoadjuvant human epidermal growth factor receptor 2-targeted therapies in breast cancer. *J. Clin. Oncol.* **33**, 1334–1339 (2015).
 75. Baselga, J. *et al.* Relationship between Tumor Biomarkers and Efficacy in EMILIA, a Phase III Study of Trastuzumab Emtansine in HER2-Positive Metastatic Breast Cancer. *Clin. Cancer Res.* **22**, 3755–3763 (2016).
 76. Loibl, S. *et al.* PIK3CA mutations are associated with reduced pathological complete response rates in primary HER2-positive breast cancer: pooled analysis of 967 patients from five prospective trials investigating lapatinib and trastuzumab. *in early stage epithelial ovarian carcinoma. Gynecol Oncol* **93**, 301–306 (2004).
 77. Bianchini, G. *et al.* Biomarker analysis of the NeoSphere study: pertuzumab, trastuzumab, and docetaxel versus trastuzumab plus docetaxel, pertuzumab plus trastuzumab, or pertuzumab plus docetaxel for the neoadjuvant treatment of HER2-positive breast cancer. *Breast Cancer Res.* **19**, 16 (2017).
 78. Bajrami, I. *et al.* E-Cadherin/ROS1 Inhibitor Synthetic Lethality in Breast Cancer. *Cancer Discov.* **8**, 498–515 (2018).
 79. ROS1 Targeting With Crizotinib in Advanced E-cadherin Negative, ER Positive Lobular Breast Cancer or Diffuse Gastric Cancer Study (ROLO). *Clinical Trials* <https://clinicaltrials.gov/ct2/show/NCT03620643>.
 80. Corcoran, R. B. *et al.* Synthetic lethal interaction of combined BCL-XL and MEK inhibition promotes tumor regressions in KRAS mutant cancer models. *Cancer Cell* **23**, 121–128 (2013).
 81. Trametinib and Navitoclax in Treating Patients With Advanced or Metastatic Solid Tumors. *Clinical trials* <https://clinicaltrials.gov/ct2/show/NCT02079740>.
 82. Lugowska, I., Teterycz, P. & Rutkowski, P. Immunotherapy of melanoma. *Contemp. Oncol.* **22**, 61–67 (2018).
 83. Planchard, D. *et al.* Metastatic non-small cell lung cancer: ESMO Clinical Practice Guidelines for diagnosis, treatment and follow-up. *Ann. Oncol.* **29**, iv192–iv237 (2018).
 84. Overman, M. J. *et al.* Durable Clinical Benefit With Nivolumab Plus Ipilimumab in DNA Mismatch Repair-Deficient/Microsatellite Instability-High Metastatic Colorectal Cancer. *J. Clin. Oncol.* **36**, 773–779 (2018).
 85. Manguso, R. T. *et al.* In vivo CRISPR screening identifies Ptpn2 as a cancer immunotherapy target. *Nature* **547**, 413–418 (2017).
 86. Pan, D. *et al.* A major chromatin regulator determines resistance of tumor cells to T cell-mediated killing. *Science* **359**, 770–775 (2018).
 87. Patel, S. J. *et al.* Identification of essential genes for cancer immunotherapy. *Nature* **548**, 537–542 (2017).
 88. Mezzadra, R. *et al.* Identification of CMTM6 and CMTM4 as PD-L1 protein regulators. *Nature* **549**, 106–110 (2017).
 89. Bester, A. C. *et al.* An Integrated Genome-wide CRISPRa Approach to Functionalize lncRNAs in Drug Resistance. *Cell* **173**, 649–664.e20 (2018).
 90. Wang, L. *et al.* High-Throughput Functional Genetic and Compound Screens Identify

- Targets for Senescence Induction in Cancer. *Cell Rep.* **21**, 773–783 (2017).
91. Breslow, D. K. *et al.* A CRISPR-based screen for Hedgehog signaling provides insights into ciliary function and ciliopathies. *Nat. Genet.* **50**, 460–471 (2018).
 92. Horlbeck, M. A. *et al.* Mapping the Genetic Landscape of Human Cells. *Cell* **174**, 953–967. e22 (2018).
 93. Shen, J. P. *et al.* Combinatorial CRISPR-Cas9 screens for de novo mapping of genetic interactions. *Nat. Methods* **14**, 573–576 (2017).
 94. Kampmann, M., Bassik, M. C. & Weissman, J. S. Functional genomics platform for pooled screening and generation of mammalian genetic interaction maps. *Nat. Protoc.* **9**, 1825–1847 (2014).
 95. Boettcher, M. *et al.* Dual gene activation and knockout screen reveals directional dependencies in genetic networks. *Nat. Biotechnol.* **36**, 170–178 (2018).
 96. Dixit, A. *et al.* Perturb-Seq: Dissecting Molecular Circuits with Scalable Single-Cell RNA Profiling of Pooled Genetic Screens. *Cell* **167**, 1853–1866. e17 (2016).
 97. Adamson, B. *et al.* A Multiplexed Single-Cell CRISPR Screening Platform Enables Systematic Dissection of the Unfolded Protein Response. *Cell* **167**, 1867–1882. e21 (2016).
 98. Datlinger, P. *et al.* Pooled CRISPR screening with single-cell transcriptome read-out. *Nat. Methods* **14**, 297–301 (2017).
 99. Reinacher-Schick, A. *et al.* 519PMicrosatellite instability is associated with distinct clinical and molecular characteristics in early colon cancer: Analysis of a molecular registry of the AIO colorectal study group - Colopredict Plus. *Ann. Oncol.* **29**, (2018).



Chapter 2

Genetic and compound screens uncover factors modulating cancer cell response to indisulam

Ziva Pogacar^{1*}, Kelvin Groot^{1*}, Fleur Jochems¹, Matheus Dos Santos Dias¹, Antonio Mulero-Sánchez¹, Ben Morris², Mieke Roosen¹, Leyma Wardak¹, Giulia De Conti¹, Arno Velds³, Cor Liefink², Bram Thijssen¹, Roderick L. Beijersbergen^{1,2,3}, René Bernards^{1#}, Rodrigo Leite de Oliveira^{1,4#}

*These authors contributed equally

¹Division of Molecular Carcinogenesis, Oncode Institute. The Netherlands Cancer Institute, Plesmanlaan 121, 1066 CX Amsterdam, The Netherlands.

²The NKI Robotics and Screening Center, The Netherlands Cancer Institute, Plesmanlaan 121, 1066 CX Amsterdam, The Netherlands.

³Genomics core facility, The Netherlands Cancer Institute, Plesmanlaan 121, 1066 CX Amsterdam, The Netherlands.

⁴Present address: CRISPR Expertise Center, Cancer Center Amsterdam, Amsterdam University Medical Center, De Boelelaan 1117, 1081 HV Amsterdam, The Netherlands

#Shared corresponding authors

ABSTRACT

2

Discovering biomarkers of drug response and finding powerful drug combinations can support the reuse of previously abandoned cancer drugs in the clinic. Indisulam is an abandoned drug that acts as a molecular glue, inducing degradation of splicing factor RBM39 through interaction with CRL4^{DCAF15}. Here, we performed genetic and compound screens to uncover factors mediating indisulam sensitivity and resistance. First, a dropout CRISPR screen identified SRPK1 loss as a synthetic lethal interaction with indisulam that can be exploited therapeutically by the SRPK1 inhibitor SPHINX31. Moreover, a CRISPR resistance screen identified components of the degradation complex that mediate resistance to indisulam: DCAF15, DDA1, and CAND1. Lastly, we show that cancer cells readily acquire spontaneous resistance to indisulam. Upon acquiring indisulam resistance, pancreatic cancer (Panc10.05) cells still degrade RBM39 and are vulnerable to BCL-xL inhibition. The better understanding of the factors that influence the response to indisulam can assist rational reuse of this drug in the clinic.

INTRODUCTION

Personalised anti-cancer therapy is limited by high costs of drug development^{1,2}. One strategy to lower the costs is to reuse compounds already tested in the clinical setting but that were abandoned due to lack of single agent activity. As the majority of abandoned drugs are no longer patent protected, their reuse will be more affordable. The understanding of the molecular mechanism of action of those compounds allows identification of biomarkers of response and the discovery of combination treatments. This knowledge might lead to a rational strategy to reuse previously abandoned drugs.

One example of a previously abandoned drug is indisulam, which was first described as a sulfonamide with anti-cancer activity with an unknown mechanism of action^{3,4}. Indisulam was tested in multiple clinical trials, where it was proven to be safe and well tolerated, but had limited efficacy (clinical responses and stable disease in 17-35% of advanced stage cancer patients)⁵⁻¹³. Due to the modest response rates, the further clinical development of indisulam was halted. However, expired patent protection and the discovery of indisulam's molecular mechanism of action as a molecular glue, may facilitate the re-introduction into clinical development^{14,15}.

Molecular glues and proteolysis targeting chimeras (PROTACs) are a novel type of compounds that exploit the endogenous ubiquitin-proteasome system (UPS) to induce targeted protein degradation of neo-substrates¹⁶. As a molecular glue, indisulam facilitates the interaction between RNA Binding Motif Protein 39 (RBM39) and DDB1 And CUL4 Associated Factor 15 (DCAF15) in the cullin-RING E3 ubiquitin ligase 4 complex (CRL4^{DCAF15}) resulting in ubiquitination and proteasomal degradation of RBM39^{14,15}. The activity of cullin-RING ubiquitin ligases (CRLs) is regulated by post-translational modification with NEDD8¹⁷ which leads to the transfer of ubiquitin to a substrate. Furthermore, the exchange factor Cullin Associated And Neddylaton Dissociated 1 (CAND1) allows the exchange of the substrate receptor of de-neddylated CRL and increases the diversity of substrates that can be degraded¹⁸. Indisulam treatment leads to the interaction between CRL4^{DCAF15} and RBM39, as recently demonstrated by the resolved structure of the interacting complex¹⁹. RBM39 is a splicing factor involved in early spliceosome assembly²⁰ and its loss leads to the accumulation of splicing errors and cytotoxicity^{14,21,22}.

Understanding drug resistance mechanisms can further aid in biomarker discovery and help guide combination treatment. It has been described that point mutations in *RBM39* prevent the interaction with DCAF15 leading to resistance of HCT-116 colon cancer cells to indisulam^{14,22}. Similarly, knock-out of *DCAF15* prevents RBM39 degradation and confers resistance¹⁴. Recently, CAND1 loss has been described to induce resistance to multiple degraders, including indisulam²³. However, the clinical significance of these resistance mechanisms is still unclear.

Here we use functional genetic and compound screens to identify genes that modulate the response to indisulam.

RESULTS

SRPK1 loss is synthetic lethal with indisulam

In an effort to re-position indisulam for treatment of solid tumors, we first characterised the response to indisulam in a panel of solid tumor cell lines from different tissue types (pancreas, lung, breast, colon). We observed a range of responses of solid cancer cell lines to indisulam, with some cell lines being very sensitive to indisulam (colon cancer cell line HCT-116), others moderately sensitive (for example A549 lung cancer cell line) and some resistant up to 2 μ M of indisulam (for example SUM159 breast cancer cell line) (Figure 1A). Since splicing factor RBM39 is the molecular target of indisulam, we then characterized the dynamics of RBM39 degradation in these cell lines. The levels of residual RBM39 after 72 hours of indisulam treatment correlated with the sensitivity of the cell line. Sensitive cell lines showed no residual RBM39 after 72 hours whereas moderately sensitive cell lines and resistant cell lines still retained detectable RBM39 levels (Figure 1B).

The variable response to indisulam between solid cancer cell lines suggests that cell-intrinsic factors mediate sensitivity to indisulam. Additionally, since many cell lines do not respond to indisulam monotherapy there is a need to identify possible indisulam combination treatments. To address this, we performed a synthetic lethality CRISPR screen in the moderately sensitive line A549 using a sgRNA library targeting the human kinome²⁴. The cells were cultured for 10 days in the presence or absence of 0.35 μ M of indisulam. After this, sgRNAs were recovered by PCR and the abundance of gRNAs in the two conditions were determined by NGS as described previously²⁵. When we analyzed the relative abundance of sgRNAs in the indisulam treated condition compared to untreated, we observed a depletion of sgRNAs targeting *SRPK1* (Figure 1C). SRPK1 is a serine/arginine protein kinase which acts as a regulator of constitutive and alternative splicing²⁶. To validate the synthetic lethal interaction between indisulam and *SRPK1* loss, we generated single cell *SRPK1* knock-out clones in A549, SUM159 and DLD1 cells (Figure 1D, Supplemental figure 1A). *SRPK1* knock-out clones were more sensitive to indisulam than control cells in all cell lines, confirming the result of the CRISPR screen (Figure 1E, F, G, H, Supplemental figure 1B, C). Taken together, we show that loss of SRPK1 is synthetic lethal with indisulam treatment in multiple cancer cell lines.

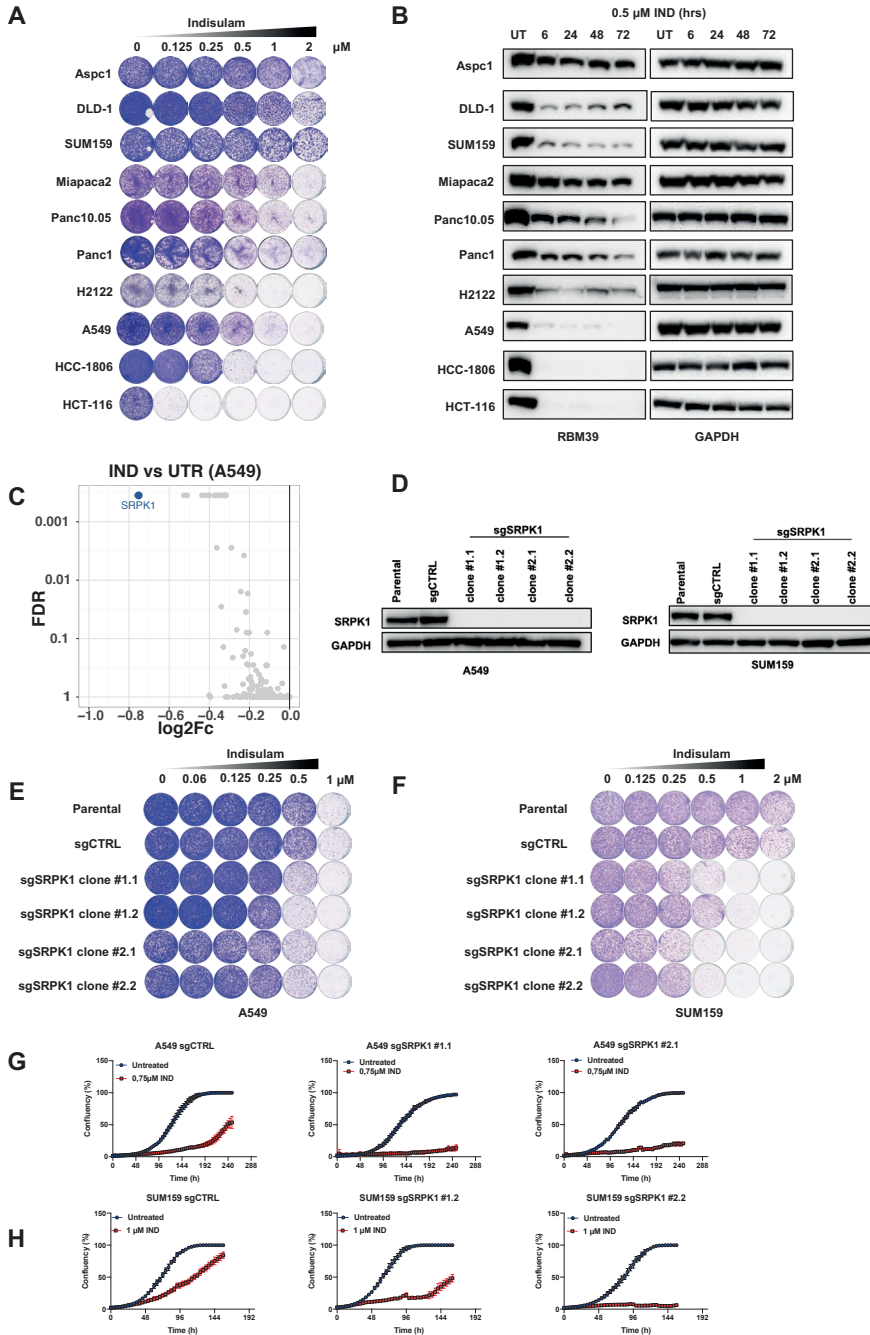


Figure 1: Dropout screen identifies SRPK1 as synthetic lethal with indisulam treatment

A Long-term colony formation assays of Aspc1, DLD-1, SUM159, Miapaca2, Panc10.05, Panc1, A549, H2122, HCC-1806 and HCT-116. Cells were treated with indicated doses of indisulam for 8-11 days.

B Western blot analysis of RBM39 levels in Aspc1, DLD-1, SUM159, Miapaca2, Panc10.05, Panc1, A549,

H2122, HCC-1806 and HCT-116 cells treated with 0.5 μM of indisulam for the indicated time periods. GAPDH was used as a loading control.

C Dropout CRISPR screen was performed in A549 treated with 0.35 μM indisulam. Volcano plot of indisulam treated samples compared to untreated. X axis shows \log_2 fold change of normalized read counts and Y axis shows false discovery rate (FDR). Each dot represents an individual gene and SRPK1 is highlighted.

D Western blot analysis of SRPK1 levels in A549 and SUM159 SRPK1 knock-out clones and control cells. Clones were generated from two independent sgRNAs. GAPDH was used as a loading control.

E Long-term colony formation assay of A549 cells. A549 *SRPK1* knock-out clones and control cells were treated with indicated doses of indisulam for 10 days.

F Long-term colony formation assay of SUM159 cells. SUM159 *SRPK1* knock-out clones and control cells were treated with indicated doses of indisulam for 7 days.

G Proliferation assay of A549 control and sgSRPK1 cells treated with 0,75 μM indisulam. One clone per sgRNA is shown. Mean of three technical replicates is shown and error bars indicate standard deviation.

H Proliferation assay of SUM159 control and sgSRPK1 cells treated with 1 μM indisulam. One clone per sgRNA is shown. Mean of three technical replicates is shown and error bars indicate standard deviation.

Combination of indisulam and SRPK1 inhibitor impairs cell proliferation

Next, we tested a specific SRPK1 inhibitor SPHINX31 and observed that combination of SPHINX31 and indisulam impaired proliferation of A549 (Figure 2A) as well as H2122 and SUM159 (Supplemental figure 2A). Furthermore, we observed an increase in apoptosis measured by caspase 3/7 activity in cells treated with the combination (Supplemental figure 2B, C). To investigate if the combination of indisulam and SPHINX31 is synergistic or additive we performed a viability experiment using a matrix of concentrations and calculated the Bliss synergy score. A Bliss score above 10 indicates synergy. We observed that the combination of indisulam and SPHINX31 is synergistic in A549 and SUM159, but less in H2122 (Figure 2B). We noticed that the cytotoxic effect of indisulam combined with SPHINX31 was more potent than the genetic knock-out of *SRPK1* combined with indisulam. To investigate potential off-target effects of SPHINX31 we performed a viability experiment using a matrix of concentrations of indisulam and SPHINX31 in *SRPK1* knock-out clones and control cells. We noticed that there was still synergy in clone #2.1 and less in clone #2.2. This indicates potential off-target activity of SPHINX31, which is not surprising, since it was reported to also target CLK1 and SRSF2²⁷ (Supplemental figure 2D). As CLK1 interacts with SRPK1 to facilitate spliceosome assembly, inhibiting both proteins might explain the observed synergy in *SRPK1* knock-out clones²⁸.

To study if the effect of indisulam combined with SPHINX31 is mediated by RBM39 loss, we used shRNAs to knock down *RBM39*. Since *RBM39* is an essential gene, only partial knockdown is achievable without compromising cell viability (Figure 2C, D). *RBM39* knock-down cells showed increased response to SPHINX31 (Figure 2E, F), consistent with the notion that indisulam-induced RBM39 degradation sensitized to SPHINX31.

Since both RBM39 and SRPK1 are involved in splicing, we asked whether the synergistic effect between indisulam and SPHINX31 can be explained by an increased amount of splicing errors. We treated A549 cells with indisulam, SPHINX31 and the combination for 24 hours and quantified splicing errors using transcriptome analysis. Treatment

with indisulam increased splicing errors, most notably skipped exons (Figure 2G). There were splicing errors detected in SPHINX31-treated cells, but at a much lower frequency. Interestingly, the combination of indisulam and SPHINX31 increased the number of skipped exons beyond what would be expected from the sum of the single treatments. This could indicate a threshold of splicing errors that is compatible with viability. To study the long term effects of the indisulam and SPHINX31 combination we performed a long term colony formation assay in A549, H2122 and SUM159 cells (Figure 2H, I, Supplemental figure 2E, F). Even though all cell lines acquired resistance to indisulam after 2-4 weeks of treatment, combination of indisulam and SPHINX31 prevented acquired resistance in all three cell lines.

Taken together, we show that synergy between indisulam and SPHINX31 is mediated by indisulam induced RBM39 degradation and that combination treatment prevents acquired resistance to indisulam.

Resistance to indisulam through CAND1 loss and reduced RBM39 degradation

To understand which factors mediate indisulam resistance, we performed a genome-wide resistance screen in A549 cells treated with indisulam. The cells were treated with 3 μ M of indisulam or control media for 3 weeks. After this, we identified the enriched sgRNAs between the two conditions by NGS of the recovered gRNAs. When comparing the treated versus untreated condition we observed enrichment of sgRNAs targeting *DCAF15*, *DDA1*, and *CAND1* (Figure 3A). Both *DCAF15* and *DDA1* are part of the CRL complex and their loss impairs the degradation of RBM39 as previously described^{14,23}. We therefore focused on validating *CAND1* as its function in indisulam resistance was less understood at the time. *CAND1* acts as a substrate receptor exchange factor regulating CRL complex activity^{29,30}. We knocked out *CAND1* in A549 cells and observed decreased sensitivity to indisulam in knock-out cells compared to control cells (Figure 3B, C, Supplemental figure 3A). We confirmed the resistance caused by *CAND1* knock-out in another moderately sensitive cell line, Panc10.05 (Figure 3E, Supplemental Figure 3B). We then investigated RBM39 degradation in *CAND1* knock-out cells and observed reduced degradation of RBM39 compared to control cells (Figure 3D, F). On the other hand, in the sensitive cell line HCT-116 we observed much less RBM39 stabilisation and there was no increase in resistance upon *CAND1* knock-out (Supplemental figure 3C, D, E). This suggests that the levels of RBM39 resulting from *CAND1* loss are not high enough to sustain HCT-116 cell viability upon indisulam treatment.

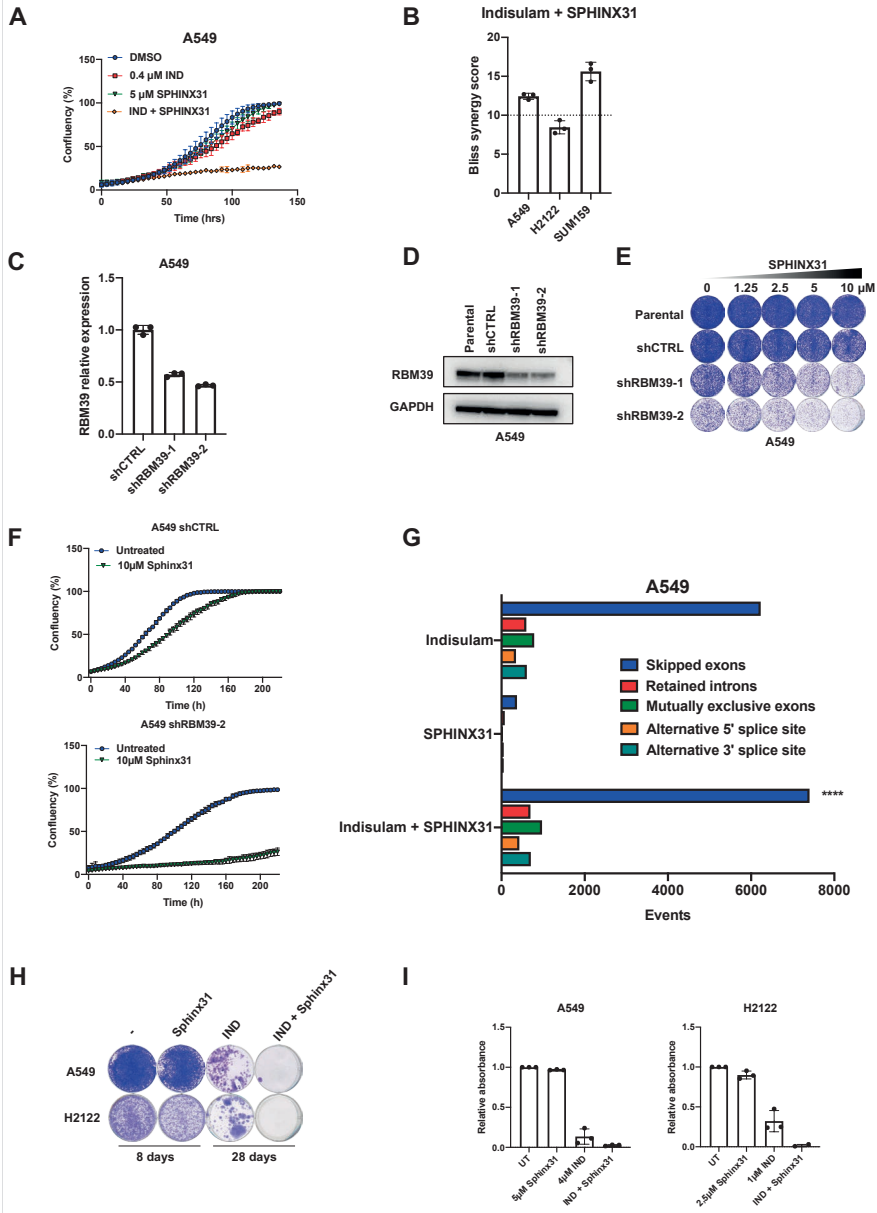


Figure 2: Combination of indisulam and SPRK1 inhibitor impairs cell proliferation and prevents acquired resistance to indisulam

A Proliferation assay of A549 cells treated with 0.4 μM indisulam, 5 μM SPHINX31 and the combination. Mean of three technical replicates is shown and error bars indicate standard deviation.

B Drug synergy analysis of a 6-day treatment with indisulam in combination with SPHINX31 in A549, H2122 and SUM159 cells. Bliss synergy score cut-off of 10 is shown, indicating likely synergy. Mean of three biological replicates is shown and error bars indicate standard deviation.

C qPCR analysis of RBM39 normalized to housekeeping gene RPL13 in A549. Mean of three technical replicates is shown and error bars indicate standard deviation.

D Western blot analysis of RBM39 levels in shRBM39 and control A549 cells. GAPDH was used as a loading control.

E Long-term colony formation assay of A549. shRBM39 and control cells were treated with indicated doses of indisulam for 10 days.

F Proliferation assay of shRBM39 and control A549 cells treated with 10 μ M SPHINX31. Mean of three technical replicates is shown and error bars indicate standard deviation.

G Quantification of splicing errors in RNA sequencing data from A549 cells treated for 24h with 0.5 μ M Indisulam, 5 μ M SPHINX31 and the combination. Data was analyzed based on two technical replicates and bars represent the number of events relative to untreated samples. Statistical difference was assessed by a Poisson test comparing the splicing errors in the combination to the sum of splicing errors of the individual treatments. Asterisks denote significance (**** $p < 0,0001$).

H Long-term colony formation assays of A549 and H2122. A549 were treated with 5 μ M SPHINX31, 4 μ M indisulam and the combination. H2122 cells were treated with 2,5 μ M SPHINX31, 1 μ M indisulam and the combination.

I Quantification of long-term colony formation assays of A549 and H2122 cells. Mean of three biological replicates is shown and error bars indicate standard deviation.

2

Next, we asked if a further increase in RBM39 stabilisation would lead to indisulam resistance in HCT-116 cells. We made use of MLN4924, a neddylation inhibitor which inhibits the NEDD8 activating E1 enzyme (NAE) and prevents the activation of CRLs (Figure 3G). Treatment with MLN4924 reduced CUL4A neddylation and prevented RBM39 degradation in both HCT-116, as well as in the moderately sensitive cell line A549 (Figure 3H). Additionally, we used the proteasome inhibitor MG-132 which prevents RBM39 degradation, but does not impair neddylation. Increasing the concentration of MLN4924 resulted in increased levels of RBM39 both in HCT-116 and A549 (Figure 3I). Notably, in the less sensitive cell line A549 a higher concentration of MLN429 still leads to less RBM39 stabilisation compared to HCT-116. Next, we treated HCT-116 and A549 cells with a combination of indisulam and MLN4924. We observed a rescue of indisulam toxicity when adding MLN4924 in HCT-116, but not in A549 cells (Figure 3J). Additionally, we performed a synergy analysis and observed antagonism of indisulam and MLN4924 in HCT-116 but not in A549 (Supplemental figure 3F, G). As A549 cells are less sensitive to indisulam, a higher concentration of MLN4924 is required to stabilize RBM39. Since MLN4924 becomes toxic at higher concentrations, there is no rescue of cell viability in A549. This is even more apparent in the synergy analysis, as it becomes clear that there is a much smaller window to detect antagonism in A549 (Supplemental figure 3G). These data indicate that increasing RBM39 levels either by *CAND1* knock-out or inhibition of neddylation results in indisulam resistance.

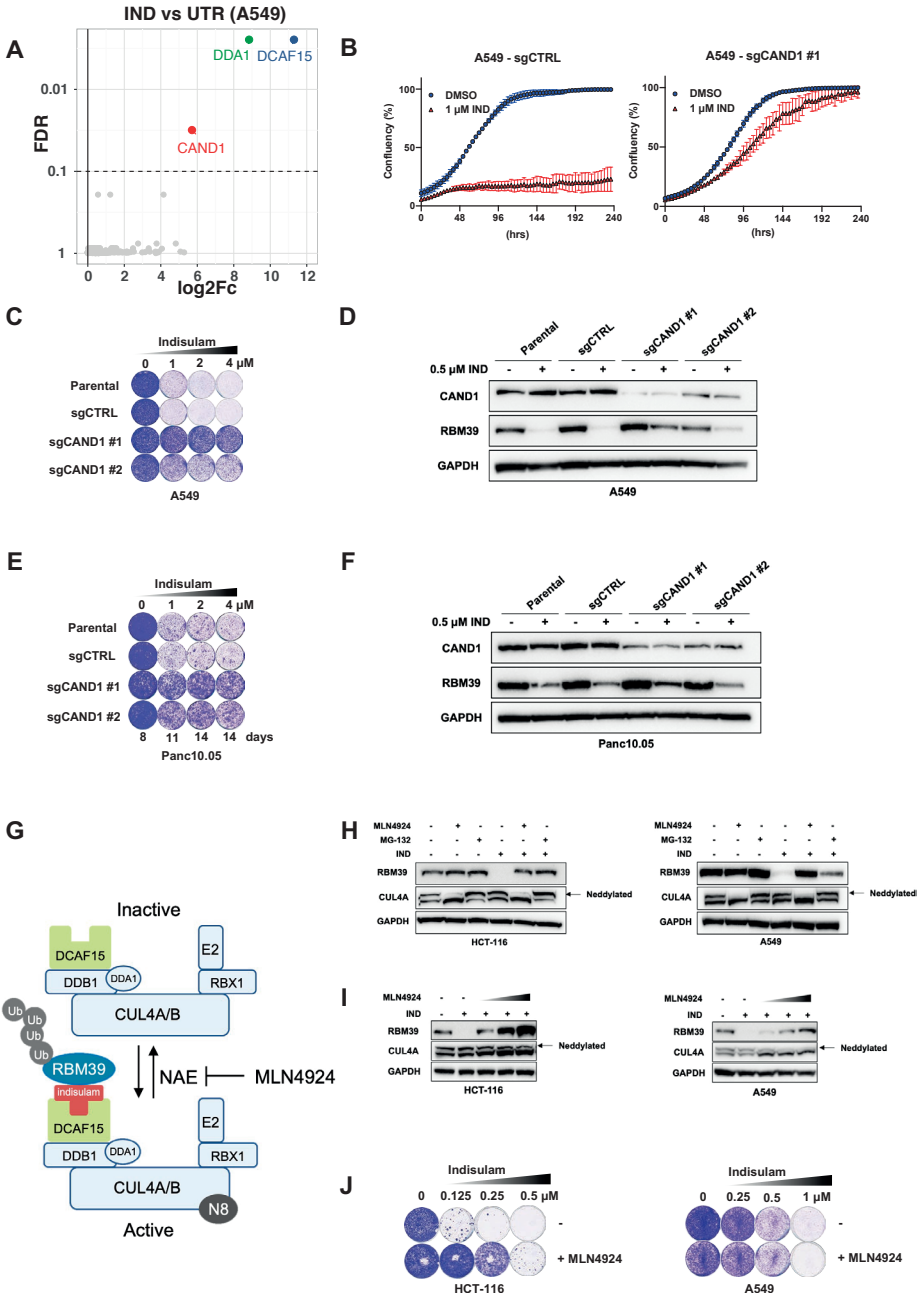


Figure 3: Resistance to indisulam is modulated through reduced RBM39 degradation and CAND1 loss

A Resistance screen was performed in A549 cells treated with 3 μM indisulam. Volcano plot of indisulam treated samples compared to untreated. X axis shows log₂ fold change of normalized read counts and Y axis shows false discovery rate (FDR). Each dot represents an individual gene and hits are highlighted.

- B** Proliferation assay of A549 control (sgCTRL) and sgCAND1 cells treated with 1 μ M indisulam. Mean of three technical replicates is shown and error bars indicate standard deviation.
- C** Long-term colony formation assay of A549. Wild-type, control and two individual sgCAND1 cells were treated with indicated doses of indisulam for 10 days.
- D** Western blot analysis of RBM39 and CAND1 in A549 cells. Wild-type, control and sgCAND1 cells were treated with 0.5 μ M of Indisulam for 8 days. GAPDH was used as loading control.
- E** Long-term colony formation assay of Panc10.05. Wild-type, control (sgCTRL) and two individual sgCAND1 cells were treated with indicated doses of indisulam for indicated number of days.
- F** Western blot analysis of RBM39 and CAND1 in Panc10.05 cells. Wild-type, control and sgCAND1 cells were treated with 0.5 μ M of Indisulam for 8 days. GAPDH was used as loading control.
- G** CUL4-DCAF15 E3 ubiquitin ligase (CRL) complexes get activated by neddylation (N8) which allows ubiquitination of the substrate (RBM39). Neddylation is reversed by NEDD8-Activating Enzyme (NAE), which can be inhibited by a small molecular inhibitor MLN4924 leading to inactive CRL complex and reduced substrate degradation.
- H** Western blot analysis of RBM39 and CUL4A in HCT-116 and A549 cells pretreated for 2 hrs with 1 μ M MLN4924 or 5 μ M MG-132 followed by a 6 hr treatment with 0.5 μ M Indisulam. GAPDH was used as loading control. The upper CUL4A band (arrow) represents neddylated CUL4A whereas the lower band represents the deneddylated CUL4A.
- I** Western blot analysis of RBM39 and CUL4A in HCT-116 (62.5, 125 and 250 nM MLN4924) and A549 (125, 250 and 500 nM MLN4924) cells treated with 0.5 μ M indisulam and increasing doses of MLN4924 for 24 hrs. The upper CUL4A band (arrow) represents neddylated CUL4A whereas the lower band represents the deneddylated CUL4A.
- J** Long-term colony formation assays of HCT-116 (62.5 nM MLN4924), HCC-1806 (62.5 nM MLN4924) and A549 (125 nM MLN4924) treated with indicated doses of indisulam and a fixed concentration of MLN4924 for 8-13 days depending on the cell line.

Cells with acquired resistance to indisulam are vulnerable to BCL-XL inhibition

In addition to loss of function mutations, gradual adaptation to drug treatment can also lead to drug resistance. To study spontaneous resistance to indisulam, we cultured various cell lines with increasing concentrations of indisulam. We observed that all tested cell lines acquired resistance to indisulam after three months of culture in the presence of the drug (Figure 4A, B). Next, we asked if resistant cells were still able to degrade RBM39. We observed a large difference in RBM39 degradation between cell lines (Figure 4C, D). Resistant HCT-116 cells showed an increase in RBM39 in the presence of indisulam, while HCC-1806 and A549 cells still showed some degradation of RBM39 in the presence of indisulam. Next, we tested if the differences in RBM39 levels could be explained by loss of CAND1 in resistant cells. We did not observe any changes of CAND1 levels between resistant and parental cells (Supplemental figure 4A) indicating that the differences in RBM39 are likely CAND1 independent. Interestingly, Panc10.05 cells show a strong reduction in RBM39 levels without impairing cell viability. Since this indicates an RBM39 independent resistance mechanism, we characterized this resistance further. As degradation of RBM39 results in the accumulation of splicing errors we first asked whether resistant Panc10.05 cells that degrade RBM39 still accumulate splicing errors. Transcriptome analysis of parental and resistant Panc10.05 cells treated with indisulam revealed that resistant cells had lower levels of splicing errors than control parental cells (Figure 4E). This could indicate that lowering the number of splicing errors allows the resistant cells to survive.

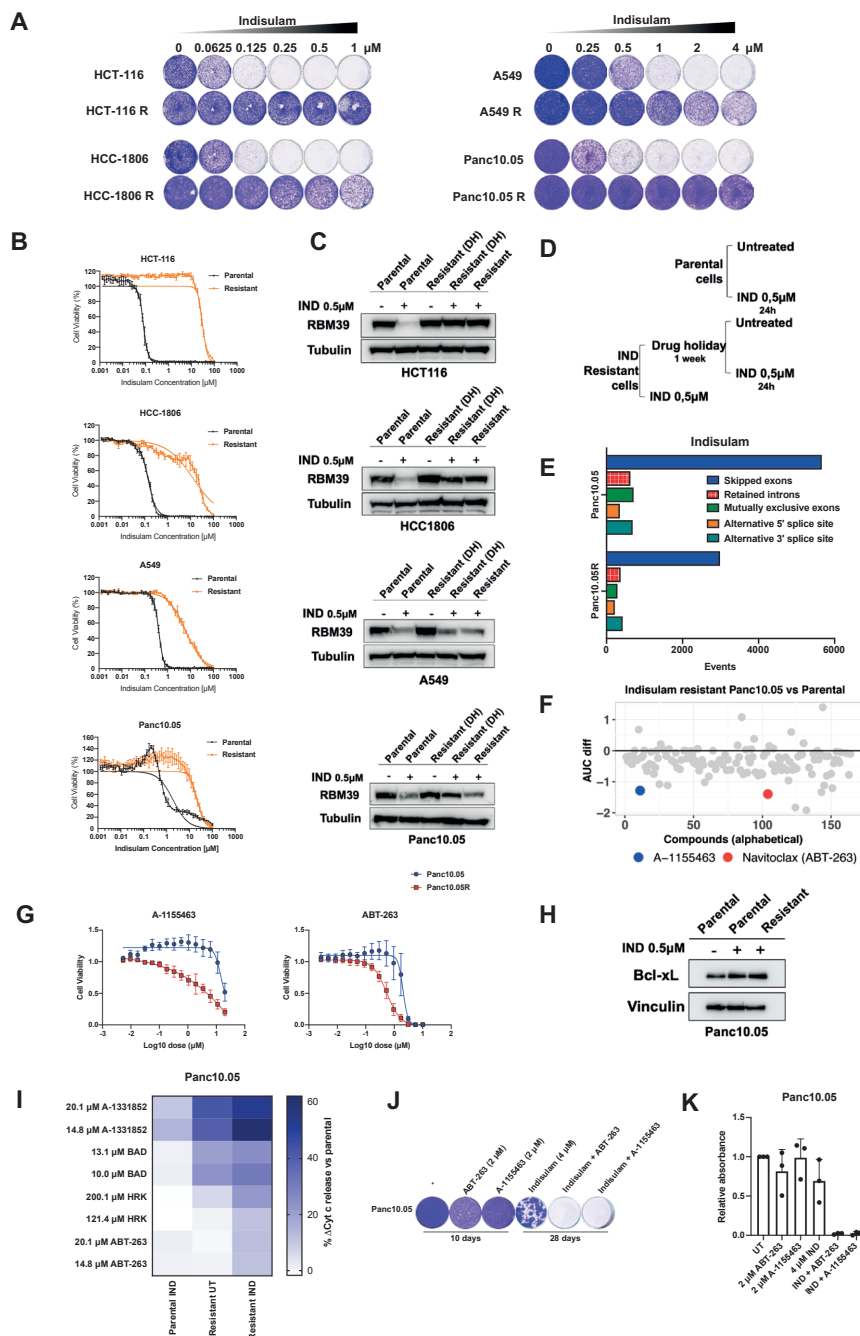


Figure 4: Cells with acquired resistance to indisulam are vulnerable to BCL-XL inhibition
A Long-term colony formation assays of HCT-116(R), HCC-1806(R), A549(R) and Panc10.05(R) treated with indicated doses of Indisulam for 8-10 days.
B Quantification of cell viability of HCT-116(R), HCC-1806(R), A549(R) and Panc10.05(R) treated with a dilution series of indisulam. Mean of three technical replicates is shown and error bars indicate

standard deviation.

C Western blot analysis of RBM39 in parental and resistant HCT-116, HCC-1806, A549 and Panc10.05. Tubulin was used as loading control. Experimental design is described in panel **D**.

D Parental cells were treated for 24 hrs with 0.5 μM of indisulam. Resistant cells were cultured without indisulam for 1 week (drug holiday- DH) and then treated for 24h with 0.5 μM of indisulam or cultured continuously in the presence of 0.5 μM Indisulam.

E Quantification of splicing errors in RNA sequencing data from Panc10.05 cells treated for 18 hrs with 2 μM indisulam and Panc10.05R cells cultured on 2 μM indisulam. Resistant cells cultured without indisulam for 1 week were considered untreated. Data was analyzed based on two technical replicates and bars represent the number of events compared to untreated samples.

F Compound screen in resistant and parental Panc10.05 cells. Dose response curves of various compounds were generated. Comparison of area under the curve of parental vs. resistant Panc10.05 is plotted for every compound. Compounds validated after a secondary screen are highlighted.

G Cell viability of Panc10.05(R) cells treated with ABT-263 and A-1155463. Indisulam-resistant cells were cultured in the presence of 0.5 μM Indisulam. Mean of three biological replicates is shown and error bars indicate standard deviation.

H Western blot analysis of BCL-xL in Panc 10.05 parental and resistant cells. Parental cells were treated with 0.5 μM of indisulam for 24h and resistant cells were cultured in the presence of 0.5 μM indisulam. Vinculin was used as a loading control.

I Heatmap of delta cytochrome c release compared to parental untreated cells (%) in Panc10.05(R) cells after BH3 profiling with A-1331852, BAD, HRK and ABT-263. Before profiling, parental Panc10.05 cells were treated with 0.5 μM of indisulam for 24 hrs. Resistant Panc10.05 cells were cultured in the absence of indisulam for 2 weeks and treated Panc10.05R cells were cultured in the presence of 0.5 μM indisulam. Mean of three technical replicates is shown.

J Long-term colony formation assay of Panc10.05 cells treated with 2 μM ABT-263, 2 μM A-1155463, 4 μM indisulam and the combinations for the indicated duration. Representative image of three independent biological replicates is shown.

K Quantification of long-term colony formation assays of Panc10.05. Mean of three biological replicates is shown and error bars indicate standard deviation.

Next, we studied if Panc10.05 cells resistant to indisulam also acquired a therapeutically exploitable vulnerability. We made use of a compound library consisting of 164 anti-cancer compounds (Supplemental Table 1). After screening the compounds on parental and resistant Panc10.05 cells, we identified a list of candidate compounds that had greater impact on viability of resistant than parental cells based on the difference in AUC (Figure 4F). Four of the highest scoring compounds were Rapamycin, Prexasertib, A-1155463 and ABT-263. After the secondary screen we focused on validation of A-1155463 and ABT-263 and excluded compounds with unclear dose response curves (Rapamycin) or those that showed very small difference between parental and resistant cells (Prexasertib). As we validated the effect of inhibitors targeting the anti-apoptotic protein BCL-xL on parental and resistant cells, we observed that indisulam resistant Panc10.05 cells were more sensitive to both ABT-263 (BCL-2, BCL-xL and BCL-W inhibitor) and A-1155463 (BCL-xL inhibitor) than parental control cells (Figure 4G). On the other hand, indisulam resistant A549 and HCC1806 did not show an increased sensitivity to ABT-263 and A-1155463 compared to parental cells, indicating that this might be cell line specific or specific to resistant cell lines with low RBM39 levels (Supplemental figure 4B).

2

ABT-263 and A-1155463 are BH3 mimetics as they mimic pro-apoptotic BH3-domain only proteins in targeting anti-apoptotic proteins. Since both ABT-263 and A-1155463 target BCL-xL, we checked the levels of BCL-xL in parental and resistant cells. There was a modest increase of BCL-xL protein both in parental cells treated with indisulam as well as resistant cells treated with indisulam (Figure 4H). Apoptosis is mostly regulated on the post-translational level and is highly dependent on the balance of anti- and pro-apoptotic signals³¹. To understand specific apoptotic dependencies of parental and indisulam resistant cells we made use of BH3 profiling, an assay that measures mitochondrial outer membrane permeabilization (MOMP) in response to BH3 peptides derived from BH3-domain only proteins³². We treated the parental and indisulam resistant Panc10.05 cells with various BH3 peptides and inhibitors and measured cytochrome c release using flow cytometry. Treatment with BAD, HRK as well as another BCL-xL inhibitor A-1331852 and ABT-263 triggered a stronger cytochrome C release in resistant cells compared to parental control cells (Figure 4I). This indicates a higher dependency of indisulam resistant Panc10.05 cells on BCL-xL, which could contribute to the resistance phenotype.

We then asked if we can exploit the dependency of resistant cells on BCL-xL to prevent the development of the resistance. To this end, we treated parental Panc10.05 cells with ABT-263, A-1155463, indisulam and the combinations. As expected, parental cells were not sensitive to monotherapy of either ABT-263 or A-1155463. Even though indisulam is initially effective, cells acquired resistance after 4 weeks of culture on indisulam. However, the combination of indisulam with ABT-263 and A-1155463 completely prevented the development of resistance in Panc10.05 cells (Figure 4J, K). We then asked whether other pancreatic cancer cell lines treated with indisulam also show a dependency on BCL-xL. We treated Panc1, Miapaca2 and Aspc1 cells with ABT-263, A-1155463, and indisulam (Supplemental figure 4C, D). All cell lines acquired resistance to indisulam after 4 weeks. The combination of ABT-263 and A-1155463 prevented resistance in Aspc1 cells and Panc1 cells. On the other hand, in Miapaca2 cell line we observed a reduction in resistance after treating the cells with the combination of indisulam and ABT-263, but not A-1155463. This might indicate that this cell line is more dependent on BCL-2 or BCL-w rather than on BCL-xL. Furthermore, we did not observe any major differences in BCL-2 and BCL-xL abundance upon indisulam treatment in Miapaca, Aspc1 and Panc1 (Supplemental figure 4E). Taken together, there seem to be different dependencies on anti-apoptotic proteins between cell lines treated with indisulam. However, in some cases combining indisulam with a BCL-xL inhibitor can prevent the development of spontaneous resistance.

DISCUSSION

Drug repurposing is an attractive strategy that can contribute to affordable healthcare³³. Here, we suggest that the previously abandoned anti-cancer compound indisulam has great potential to be reused due to expired patent protection, favourable safety profile in the clinic and a recently described molecular mechanism of action. Biomarkers of response and new combination treatments are instrumental for future clinical development of this drug. A great tool for both biomarker and combination treatment discovery are functional genetic screens³⁴. Here, we identify a synthetic lethal interaction with indisulam as well as resistance mechanisms to indisulam using CRISPR screens.

We show that the response to indisulam in solid cancer cell lines is variable, which is in line with the response rate in clinical trials⁵⁻¹³. Furthermore, the *in vitro* response seems to correlate with the residual RBM39 levels after indisulam treatment. Interestingly, RBM39 degradation was described as a biomarker of indisulam response in acute myeloid leukemia and DCAF15 levels were shown to correlate with indisulam response in hematopoietic and lymphoid cancers^{14,35}. As this correlation was not observed in solid cancers there might be other factors contributing to tissue specificity of sensitivity and resistance to indisulam.

To further explore the use of indisulam in solid tumors, we performed a dropout CRISPR screen and identified loss of *SRPK1* as a synthetic lethal interaction with indisulam. SRPK1 is a splicing factor that phosphorylates serine and arginine-rich (SR) proteins, such as SRSF1, which leads to their activation and enables splicing^{28,36-38}. A global proteomic analysis has shown that RBM39 is a direct target of SRPK1³⁸ which could explain the synthetic lethal interaction. Combination of SRPK1 inhibitor SPHINX31 and indisulam led to an increase of splicing errors. This could indicate that the cells can tolerate a certain amount of splicing errors, until a threshold is reached which leads to cytotoxicity. On the other hand, aberrant splicing of specific genes due to the combination might contribute to the synergy as well. Combining different splicing inhibitors may offer an advantage over single treatments³⁹. Furthermore, SRPK1 negative tumors might benefit from indisulam monotherapy treatment.

To anticipate resistance mechanisms to indisulam that can potentially arise in the clinic, we performed a whole genome resistance CRISPR screen. We identified two components of the CRL complex: DCAF15 and DDA1 as well as the substrate receptor exchange factor CAND1. This observation is in line with a previous screen that investigated resistance to multiple degraders²³. Loss of CAND1 was described to lock the CRL complex in a hyper neddylated state which leads to auto-degradation of substrate receptors²³. Curiously, both inhibition of neddylation and CAND1 loss lead to stabilisation of RBM39 levels and resistance. Similarly, spontaneously generated indisulam resistant cells showed

2

minor or no RBM39 degradation. The resistance in these cells may be mediated by point mutations in RBM39 that prevent its binding to CRL4^{DCAF15}, as described previously^{14,22}. On the other hand, indisulam resistant Panc10.05 cells still degraded RBM39. Since these cells also harbour less splicing errors, this could indicate a mechanism downstream of RBM39 that prevents splicing errors and allows survival. Interestingly, Panc10.05 cells depend on BCL-xL and spontaneous resistance can be prevented by co-treatment with BCL-xL inhibitors ABT-263 and A-1155463. This is in line with a previous report that showed synergy of splicing modulators and BCL-xL inhibitors⁴⁰. Combination treatment with BCL-xL inhibitors and indisulam could therefore prevent acquired resistance and lead to improved treatment success in the clinical setting.

Cancer types that harbour mutations in the spliceosome, such as haematopoietic and lymphoid malignancies, seem to be more sensitive to indisulam^{14,21,39}. Our data indicate that SRPK1 mutant solid tumors may be more sensitive to indisulam as well. However, this might be just one example of a synthetic lethal interaction and loss of other splicing factors could sensitize cells from different tissue types to indisulam as well. Furthermore, we propose that the combination of indisulam and SPHINX31 might present a better treatment strategy and that addition of either BCL-xL inhibitors or SPHINX31 might prevent acquired resistance. Recently, it has been shown that indisulam induced splicing errors can lead to neoantigen formation and that combining indisulam with immunotherapy improved treatment outcomes⁴¹. Further understanding of the factors involved in indisulam sensitivity and resistance might help in predicting which patients would benefit from this combination treatment.

METHODS

Cell lines

HCT-116, HCC-1806, Panc10.05, A549, Miapaca2 and H2122 cells were cultured in RPMI (Gibco) supplemented with 10% FBS (Serana) and 1% penicillin-streptomycin (Gibco). Aspc1, Panc1 and HEK293T cells were cultured in DMEM (Gibco) supplemented with 10% FBS and 1% penicillin-streptomycin (Gibco). SUM159 cells were cultured in DMEMF12 (Gibco) supplemented with 5% FBS (Serana), 1% penicillin-streptomycin (Gibco), 5 µg/mL insulin and 1 µg/mL hydrocortisone (Sigma-Aldrich). HCT-116, HCC-1806, Panc10.05, A549, Miapaca2, Aspc1, Panc1, H2122 and HEK293T were purchased from ATCC. SUM159 was a gift from Mettello Innocenti (NKI, Amsterdam). All cell lines were maintained in a humidified incubator at 37 °C and 5% CO₂ and were regularly tested for mycoplasma contamination using a PCR-based assay. To establish indisulam resistant cell lines, HCT-116, HCC-1806, Panc10.05 and A549 cells were treated with increasing doses of indisulam (from 0.125 to 1 µM) for at least 2 months. The dose of indisulam was doubled every two weeks. At the time of the experiments, indisulam

resistant cells were cultured at 0.5 μM indisulam.

Compounds and antibodies

Indisulam (E7070) (#201540), SPHINX31 (#555397), MLN4924 (#201924), Navitoclax (ABT-263) (#201970) and A-1155463 (#407213) were purchased from MedKoo Biosciences. MG-132 was purchased from Selleckchem. Phenylarsine oxide (PAO) was purchased from Sigma-Aldrich. All reagents were dissolved in DMSO at a stock solution of 10 mM. A-1331852 (#HY-19741) was obtained from MedChemExpress. Antibodies against CAND1 (#8759), CUL4A (#2699), GAPDH (#5174), Bcl-2 (#2872) and BCL-xL (#2764) were purchased from Cell Signalling Technology. Antibody against RBM39 (HPA001591) was purchased from Atlas Antibodies. Antibody against SRPK1 (611072) was purchased from BD Biosciences. Antibody against vinculin (V9131) was purchased from Sigma-Aldrich). Secondary anti-rabbit (#170-6515) and anti-mouse (#170-6516) antibodies were purchased from BIO-RAD.

CRISPR screens

For the dropout screen, A549 cells were screened using a custom sgRNA library targeting human kinases²⁴. Upon generating lentiviral vectors A549 cells were infected at multiplicity of infection (MOI) between 0.3 and 0.5, selected with puromycin and a reference sample (t=0) was collected. Cells were then cultured in presence or absence of 0.35 μM of indisulam for 10 population doublings while maintaining 1000x coverage of the library. gRNA sequences were then recovered, amplified and sequenced to determine the abundance. For sequence depth normalization, a relative total size factor was calculated for each sample by dividing the total counts of each sample by the geometric mean of all totals. All values within a sample were then divided by the respective relative total size factor and rounded off to integer values. A differential analysis between 'treated' versus 'untreated' condition was performed per sgRNA using DESeq2⁴². The results of this analysis was used as input for an analysis on the gene level for depletion, using MAGeCK's Robust Rank Algorithm (RRA)⁴³ which gives a test statistic, p-value and FDR value for enrichment of the sgRNAs of gene towards the top. In addition, we calculated a median log₂FoldChange per gene over the sgRNAs based on the DESeq2 output.

For the resistance screen, A549 cells were screened with genome-wide Brunello gRNA library⁴⁴. Cells were infected and selected as described above, and then cultured in the presence or absence of 3 μM of indisulam for 3 weeks. Data was normalized and analyzed as described above for the dropout screen, except for the RRA analysis which was performed for enrichment instead of depletion. Hits were selected based on FDR smaller or equal to 0.1 and median log₂FoldChange. All hits had log₂Fold Change greater or equal than 5.

Plasmids

Single gRNA oligonucleotides were cloned into LentiCRISPR 2.1 plasmid ²⁵ by BsmBI (New England Biolabs) digestion followed by Gibson Assembly (New England Biolabs). Control sgRNA: ACGGAGGCTAAGCGTCGCAA, sgRNA targeting CAND1 #1: AGTCTAGGGCTGGTCAACTG, sgRNA targeting CAND1 #2: AATGCAATGGATGCTGATGG, sgRNA targeting SRPK1 #1: GCAACAGAATGGCAGCGATC, sgRNA targeting SRPK1 #2: TGGTAGATCACTCTCAGAGT. The lentiviral shRNA vectors were selected from the arrayed TRC human genome-wide shRNA collection. Control shRNA: CCTAAGGTAAAGTCGCCCTCGCTCGAGCGAGGGCGACTTAACCTTAGG, shRNA targeting RBM39 #1: GCCGTGAAAGAAAGCGAAGTA, shRNA targeting RBM39 #2: GCTGGACCTATGAGGCTTTAT.

Lentiviral transduction

Second generation lentivirus packaging system (psPAX2 (Addgene #12260), pMD2.G (Addgene #12259) and pCMV-GFP as transfection control (Addgene #11153)) was used for lentiviral production. HEK293T cells were transfected using PEI and lentiviral supernatant was then filtered and used to infect target cells using 8mg/ml Polybrene. Infected cells were then selected with 2mg/ml puromycin until non-transduced control cells were dead.

Quantification of editing efficiency

Target sequences were amplified by PCR and SANGER sequenced (Macrogen), then purified by ISOLATE II PCR and Gel Kit (Bioline #BIO-52059) or the Exo-Cip Rapid PCR Cleanup Kit (New England Biolabs). Gene editing efficiency was analyzed using TIDE analysis software ⁴⁵. Each sample was corrected for background by subtracting the editing percentage in cells containing the control gRNA. PCR primers used are as follows: sgCAND1- #1 forward: GATCCCCGGAGTCAGTTTGG, sgCAND1 #1 reverse: CTGAAATCCAAAAGGCCGCT, sgCAND1 #2 forward: ATGCACTGGCATTTCACAA, sgCAND1 #2 reverse: CCTAGCCAAGAGAAAACAAGTGG.

Compound screen

The library consisted of 164 compounds with anti-cancer properties (Supplemental Table 1). The active range of every compound was selected based on literature, in order to set the highest screening concentration in the dilution range. Parental Panc10.05 (400 cells/well) and indisulam-resistant Panc10.05R cells on 0.5 μ M indisulam (500 cells/well) were seeded in 384 well plates using Multidrop Combi (Thermo Fisher). Cells were treated with the compound library in a 15-point 1:1.8 dilution series for 5 days using the MicroLab Starlet (Hamilton Robotics). Next, cell viability was measured using a resazurin assay on the EnVision plate reader (PerkinElmer). We used Phenylarsine oxide (PAO) as a positive control and DMSO as a negative control. For a random concentration per cell line a technical triplicate was taken along to determine the variance. Plate normalization

was performed using the normalized percent inhibition (NPI) method⁴⁶, setting values between 0 (for the median of the positive controls) and 1 (for the median of the negative controls). Response curves were fitted with parameters for high level set to 1 and low level set to 0, The Area under the curve (AUC) was calculated as a measure for overall viability. The AUC value of the parental cell line was subtracted from the AUC of the indisulam resistant cell line. The top 15 compounds in terms of this difference score were selected for validation. Secondary screen was performed in three biological replicates after which ABT-263 and A1155463 were the only compounds that validated with a substantial difference.

Dose response and Synergy assay

Antagonistic and synergistic interactions of MLN4924 and SPHINX31 with indisulam were determined in 6-day cell viability assays. Cells were seeded in 96-well plates and treated using a HP D300 Digital Dispenser. PAO and DMSO were used as a positive and negative control respectively. Drugs and medium were refreshed every 2-3 days. Cell viability was measured using resazurin assay on the EnVision plate reader (PerkinElmer). The data was corrected for PAO treated cells and normalised to DMSO treated cells. Drug antagonism and synergy was analyzed using SynergyFinder 2.0 using the Bliss model and viability as the readout⁴⁷. Data are displayed as means of 3 biological replicates.

RNA sequencing

For the indisulam and SPHINX31 experiment A549 cells were treated for 24h with 0.5 μ M indisulam, 5 μ M SPHINX31 and the combination. For the resistance experiment Panc10.05 cells were treated for 18h with 2 μ M indisulam. Resistant Panc10.05 were cultured in the absence of 2 μ M indisulam for one week, and treated Panc10.05R cells were continuously cultured in the presence of 2 μ M indisulam. Total RNA was extracted with RNeasy mini kit (Qiagen, cat# 74106) including a column DNase digestion (Qiagen, cat#79254), according to the manufacturer's instructions. Quality and quantity of total RNA was assessed by the 2100 Bioanalyzer using a Nano chip (Agilent, Santa Clara, CA). Total RNA samples having RIN>8 were subjected to library generation. Strand-specific libraries were generated using the TruSeq Stranded mRNA samples preparation kit (illumine Inc., San Diego, RS-122-2101/2) according to manufacturer's instructions (Illumina, part #15031047 Rev.E). Briefly, polyadenylated RNA from intact total RNA was purified using oligo-dT beads. Following purification, the RNA was fragmented, random primed and reverse transcribed using SuperScript II Reverse Transcriptase (Invitrogen, part # 18064-014) with the addition of Actinomycin D. Second strand synthesis was performed using Polymerase I and RNaseH with replacement of dTTP for dUTP. The generated cDNA fragments were 3' end adenylated and ligated to Illumina Paired-end sequencing adapters and subsequently amplified by 12 cycles of PCR. The libraries were analyzed on a 2100 Bioanalyzer using a 7500 chip (Agilent, Santa Clara, CA), diluted and pooled equimolar into a multiplex sequencing pool. The libraries were sequenced with

paired-end 150bp reads on a NovaSeq SP (Illumina inc., San Diego).

Splicing error quantification

The RNA was isolated and sequenced as described above. For the analysis, sequences were demultiplexed and adapter sequences were trimmed from using SeqPurge⁴⁸. Trimmed reads were aligned to GRCh38 using Hisat2⁴⁹ using the prebuilt genome_snp_tran reference. Splice event detection was performed using rMats version 4.0.2 by comparing the replicates of the treated groups to the replicates of the untreated group⁵⁰. rMats events in the different categories were considered significant when the following thresholds were met: having a minimum of 10 reads, an FDR less than 10% and an inclusion-level-difference greater than 10%, as described earlier²¹. For the statistical analysis of different treatments we assumed that splicing errors occur independently and with a constant rate; the splicing error rate of the combination treatment was then compared to the sum of the splicing error rates of the individual treatments using a Poisson test.

Long-term colony formation assays and proliferation assays

For long-term colony formation assay cells were seeded with densities between 10-20 000 cells per well, depending on the cell line. Cells were treated with the indicated doses of the drugs which were refreshed every 2-3 days. At the end of the assay, cells were fixed with 2% of formaldehyde (Millipore) in PBS, stained with 0.1% crystal violet (Sigma) in water and scanned. For proliferation assays cells were plated in 96 or 384-well plates with densities between 125-1000 cells per well. The cells were treated the following day using a HP D300 Digital Dispenser and drugs and medium were refreshed every 2-3 days. Plates were incubated at 37°C and images were taken every 4 hours using the IncuCyte® live cell imaging system. Confluency was calculated to generate growth curves. For apoptosis assay, caspase-3/7 green apoptosis assay reagent (Essen Bioscience #4440, 1:1000) was added to each well. Percentage of apoptotic cells was calculated by dividing the caspase-3/7 green signal by the confluence.

Western blot analysis

Cells were washed with PBS, lysed using RIPA buffer (25mM Tris-HCL pH 7.6, 150 mM NaCl, 1% NP-40, 1% sodium deoxycholate and 0.1% sodium dodecyl sulfate (SDS)) containing Halt Protease and Phosphatase Inhibitor Single-Use Cocktail (Thermo scientific). Loading buffer and reducing agent (both Thermo Fisher) were added to the samples, which were boiled for 5 min at 95°C and then separated on 4-12% polyacrylamide gradient gels (Invitrogen). After blotting, the PVDF membranes were incubated with primary antibodies diluted to 1:1000 in 5% BSA. Secondary antibodies were used at 1:10000 dilution. Immunodetection was conducted using ECL (BIO-RAD) and a BIO-RAD ChemiDoc Imaging System.

Quantitative RT-PCR

Total RNA extraction was performed using the ISOLATE II RNA mini kit (Bioline) according to the manufacturer's instructions. Next, RNA was reverse transcribed using the SensiFAST cDNA Synthesis Kit (Bioline) according to the manufacturer's protocol. Quantitative PCR analysis was carried out using SYBR green (SensiFast SYBR No-ROX kit) on an Applied Biosystems 7500 Fast Real-Time PCR System (Fisher Scientific) in technical triplicates. The results were analyzed using the $\Delta\Delta C_t$ method. The sequences of primers used are as follows: RBM39 forward GTCGATGTTAGCTCAGTGCCTC, RBM39 reverse ACGAAGCATATCTTCAGTTATG, RPL13 forward GGCCAGCAGTACCTGTTA, RPL13 reverse AGATGGCGGAGGTGCAG.

BH3 profiling by intracellular staining (iBH3)

BH3 peptides were purchased from New England Peptide: hBIM Acetyl-MRPEIWIQAQLRRIGDEFNA-Amide, mBAD Acetyl -LWAAQRYGRELRRMSDEFEGSFKGL-Amide, HRK-y Acetyl -SSAAQLTAARLKALGDELHQY- Amide. Corning Black 384 NBS plates were from Corning (#3575). To profile parental and indisulam-resistant Panc10.05 cells, parental Panc10.05 cells were treated for 24 hrs with 0.5 μM indisulam, whereas indisulam-resistant Panc10.05R cells were either cultured in the absence (one week) or presence of indisulam (0.5 μM indisulam). Subsequent iBH3 profiling was performed as in ³². In brief, 1×10^4 cells per 384-well were seeded in a plate containing titrated doses of BIM (100 – 0.1 μM), BAD (50 – 10 μM), HRK (200 – 10 μM), ABT-263 (20 – 1 μM), A-1331852, (20 – 1 μM) and alamethicin (Enzo, BML-A150-0005) (25 μM) in a total of 30 μL MEB buffer (150 mM Mannitol, 10 mM HEPES-KOH [pH 7.5], 150 mM KCl, 1 mM EGTA, 1 mM EDTA, 0.1% BSA, 5 mM Succinate) + 0.001% w/v digitonin. Cells were exposed to the peptides and BH3 mimetics for 50 min at 26 °C before cells were fixed using 10 μL of 4% formaldehyde for 10 min. Subsequently, 10 μL neutralization buffer (1.7 M Tris base, 1.25 M Glycine, pH 9.1) was added to neutralize the formaldehyde and terminate fixation. Afterwards, 10 μL of CytoC stain buffer (2% Tween20, 10% BSA (w/v) in PBS) + 1:400 Alexa Fluor 647 anti-cytochrome c antibody (Biolegend, cat#612310) + 1:100 DAPI (1 mg/mL, Thermofisher Scientific, #D3571) was added, vortexed and incubated overnight at 4 °C in the dark. Flow cytometric acquisition was performed on a BD Fortessa flow cytometer (BD Biosciences) and analyzed using FlowJo (V10.7.1). The gating strategy was set to live single cells positive for DAPI and positive for cytochrome c. Percentage of cytochrome (cyto) c release was calculated as follows:

$$\% \text{Cyto C release} = 100 - \frac{\% \text{Cyto c positive}_{\text{sample}} - \% \text{Cyto c positive}}{\% \text{Cyto c positive}_{\text{alamethicin}} - \% \text{Cyto c positive}_{\text{DMSO}}} \times 100$$

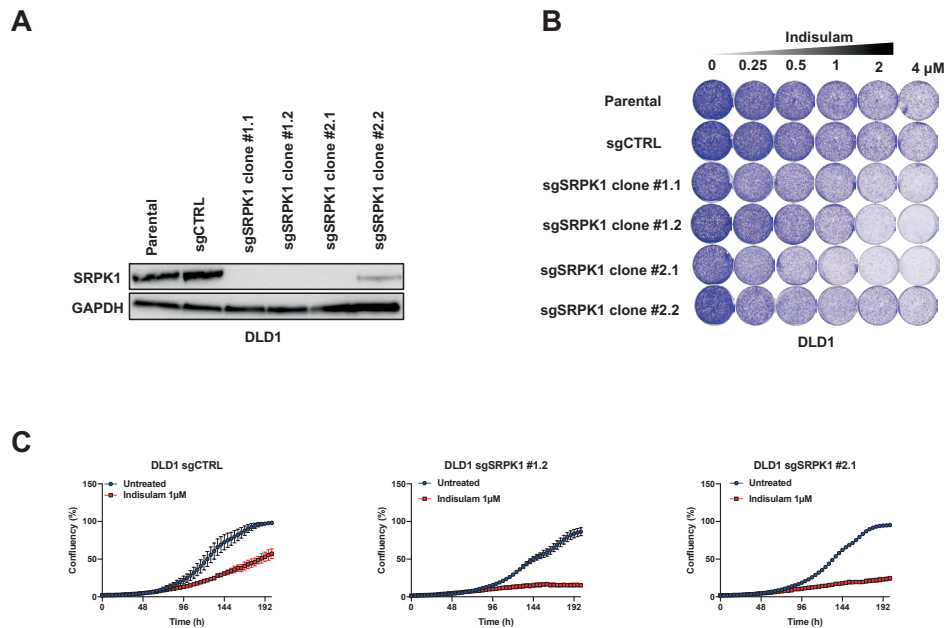
Data was represented as the mean of technical triplicates, and $\Delta\%$ Cyto c release is calculated as the %Cyto c release in resistant cells subtracted by their parental counterparts.

REFERENCES

1. Workman, P., Draetta, G. F., Schellens, J. H. M. & Bernards, R. How Much Longer Will We Put Up With \$100,000 Cancer Drugs? *Cell* **168**, 579–583 (2017).
2. Schlender, M., Hernandez-Villafuerte, K., Cheng, C.-Y., Mestre-Ferrandiz, J. & Baumann, M. How Much Does It Cost to Research and Develop a New Drug? A Systematic Review and Assessment. *Pharmacoeconomics* (2021) doi:10.1007/s40273-021-01065-y.
3. Owa, T. *et al.* Discovery of novel antitumor sulfonamides targeting G1 phase of the cell cycle. *J. Med. Chem.* **42**, 3789–3799 (1999).
4. Fukuoka, K. *et al.* Mechanisms of action of the novel sulfonamide anticancer agent E7070 on cell cycle progression in human non-small cell lung cancer cells. *Invest. New Drugs* **19**, 219–227 (2001).
5. Punt, C. J. A. *et al.* Phase I and pharmacokinetic study of E7070, a novel sulfonamide, given at a daily times five schedule in patients with solid tumors. A study by the EORTC-Early Clinical Studies Group (ECSG). *Ann. Oncol.* **12**, 1289–1293 (2001).
6. Raymond, E. *et al.* Phase I and pharmacokinetic study of E7070, a novel chloroindolyl sulfonamide cell-cycle inhibitor, administered as a one-hour infusion every three weeks in patients with advanced cancer. *J. Clin. Oncol.* **20**, 3508–3521 (2002).
7. Dittrich, C. *et al.* Phase I and pharmacokinetic study of E7070, a chloroindolyl-sulfonamide anticancer agent, administered on a weekly schedule to patients with solid tumors. *Clin. Cancer Res.* **9**, 5195–5204 (2003).
8. Terret, C. *et al.* Phase I clinical and pharmacokinetic study of E7070, a novel sulfonamide given as a 5-day continuous infusion repeated every 3 weeks in patients with solid tumours. A study by the EORTC Early Clinical Study Group (ECSG). *European Journal of Cancer* vol. 39 1097–1104 (2003).
9. Yamada, Y. *et al.* Phase I pharmacokinetic and pharmacogenomic study of E7070 administered once every 21 days. *Cancer Sci.* **96**, 721–728 (2005).
10. Haddad, R. I. *et al.* A phase II clinical and pharmacodynamic study of E7070 in patients with metastatic, recurrent, or refractory squamous cell carcinoma of the head and neck: modulation of retinoblastoma protein phosphorylation by a novel chloroindolyl sulfonamide cell cycle inhibitor. *Clin. Cancer Res.* **10**, 4680–4687 (2004).
11. Smyth, J. F. *et al.* Phase II study of E7070 in patients with metastatic melanoma. *Ann. Oncol.* **16**, 158–161 (2005).
12. Talbot, D. C. *et al.* A Randomized Phase II Pharmacokinetic and Pharmacodynamic Study of Indisulam as Second-Line Therapy in Patients with Advanced Non-Small Cell Lung Cancer. *Clin. Cancer Res.* **13**, 1816–1822 (2007).
13. Assi, R. *et al.* Final results of a phase 2, open-label study of indisulam, idarubicin, and cytarabine in patients with relapsed or refractory acute myeloid leukemia and high-risk myelodysplastic syndrome. *Cancer* vol. 124 2758–2765 (2018).
14. Han, T. *et al.* Anticancer sulfonamides target splicing by inducing RBM39 degradation via recruitment to DCAF15. *Science* **356**, (2017).
15. Uehara, T. *et al.* Selective degradation of splicing factor CAPERa by anticancer sulfonamides. *Nat. Chem. Biol.* **13**, 675–680 (2017).
16. Scholes, N. S., Mayor-Ruiz, C. & Winter, G. E. Identification and selectivity profiling of small-molecule degraders via multi-omics approaches. *Cell Chem Biol* **28**, 1048–1060 (2021).
17. Ohh, M. *et al.* An intact NEDD8 pathway is required for Cullin-dependent ubiquitylation in mammalian cells. *EMBO Rep.* **3**, 177–182 (2002).
18. Liu, J., Furukawa, M., Matsumoto, T. & Xiong, Y. NEDD8 modification of CUL1 dissociates p120(CAND1), an inhibitor of CUL1-SKP1 binding and SCF ligases. *Mol. Cell* **10**, 1511–1518 (2002).
19. Bussiere, D. E. *et al.* Structural basis of indisulam-mediated RBM39 recruitment to DCAF15 E3 ligase complex. *Nat. Chem. Biol.* **16**, 15–23 (2020).
20. Stepanyuk, G. A. *et al.* UHM-ULM interactions in the RBM39–U2AF65 splicing-factor complex. *Acta Crystallographica Section D: Structural Biology* **72**, 497–511 (2016).
21. Wang, E. *et al.* Targeting an RNA-Binding Protein Network in Acute Myeloid Leukemia. *Cancer Cell* **35**, 369–384.e7 (2019).
22. Ting, T. C. *et al.* Aryl Sulfonamides Degrade RBM39 and RBM23 by Recruitment to CRL4-DCAF15. *Cell Rep.* **29**, 1499–1510.e6 (2019).
23. Mayor-Ruiz, C. *et al.* Plasticity of the Cullin-RING Ligase Repertoire Shapes Sensitivity to Ligand-Induced Protein Degradation. *Mol. Cell* **75**, 849–858.e8 (2019).
24. Wang, C. *et al.* A CRISPR screen identifies CDK7 as a therapeutic target in hepatocellular carcinoma. *Cell Res.* **28**, 690–692 (2018).
25. Evers, B. *et al.* CRISPR knockout screening outperforms shRNA and CRISPRi in identifying essential genes. *Nat. Biotechnol.* **34**, 631–633 (2016).
26. Wang, H. Y. *et al.* Localization of serine kinases, SRPK1 (SFRSK1) and SRPK2 (SFRSK2), specific for the SR family of splicing factors in mouse and human chromosomes. *Genomics* **57**, 310–315 (1999).
27. Batson, J. *et al.* Development of Potent, Selective SRPK1 Inhibitors as Potential Topical Therapeutics for Neovascular Eye Disease. ACS

- Chemical Biology* vol. 12 825–832 (2017).
28. Aubol, B. E. *et al.* Release of SR Proteins from CLK1 by SRPK1: A Symbiotic Kinase System for Phosphorylation Control of Pre-mRNA Splicing. *Mol. Cell* **63**, 218–228 (2016).
 29. Reichermeier, K. M. *et al.* PIKES Analysis Reveals Response to Degraders and Key Regulatory Mechanisms of the CRL4 Network. *Mol. Cell* **77**, 1092–1106.e9 (2020).
 30. Liu, X. *et al.* Cand1-Mediated Adaptive Exchange Mechanism Enables Variation in F-Box Protein Expression. *Mol. Cell* **69**, 773–786.e6 (2018).
 31. Giam, M., Huang, D. C. S. & Bouillet, P. BH3-only proteins and their roles in programmed cell death. *Oncogene* **27 Suppl 1**, S128–36 (2008).
 32. Ryan, J. & Letai, A. BH3 profiling in whole cells by fluorimeter or FACS. *Methods* **61**, 156–164 (2013).
 33. Zhang, Z. *et al.* Overcoming cancer therapeutic bottleneck by drug repurposing. *Signal Transduct Target Ther* **5**, 113 (2020).
 34. Mulero-Sánchez, A., Pogacar, Z. & Vecchione, L. Importance of genetic screens in precision oncology. *ESMO Open* **4**, e000505 (2019).
 35. Hsiehchen, D., Goralski, M., Kim, J., Xie, Y. & Nijhawan, D. Biomarkers for RBM39 degradation in acute myeloid leukemia. *Leukemia* **34**, 1924–1928 (2020).
 36. Colwill, K. *et al.* The Clk/Sty protein kinase phosphorylates SR splicing factors and regulates their intranuclear distribution. *EMBO J.* **15**, 265–275 (1996).
 37. Gui, J. F., Lane, W. S. & Fu, X. D. A serine kinase regulates intracellular localization of splicing factors in the cell cycle. *Nature* **369**, 678–682 (1994).
 38. Varjosalo, M. *et al.* The protein interaction landscape of the human CMGC kinase group. *Cell Rep.* **3**, 1306–1320 (2013).
 39. Bonnal, S. C., López-Oreja, I. & Valcárcel, J. Roles and mechanisms of alternative splicing in cancer — implications for care. *Nature Reviews Clinical Oncology* vol. 17 457–474 (2020).
 40. Aird, D. *et al.* Sensitivity to splicing modulation of BCL2 family genes defines cancer therapeutic strategies for splicing modulators. *Nat. Commun.* **10**, 137 (2019).
 41. Lu, S. X. *et al.* Pharmacologic modulation of RNA splicing enhances anti-tumor immunity. *Cell* (2021) doi:10.1016/j.cell.2021.05.038.
 42. Love, M. I., Huber, W. & Anders, S. Moderated estimation of fold change and dispersion for RNA-seq data with DESeq2. *Genome Biol.* **15**, 550 (2014).
 43. Li, W. *et al.* MAGeCK enables robust identification of essential genes from genome-scale CRISPR/Cas9 knockout screens. *Genome Biol.* **15**, 554 (2014).
 44. Doench, J. G. *et al.* Optimized sgRNA design to maximize activity and minimize off-target effects of CRISPR-Cas9. *Nat. Biotechnol.* **34**, 184–191 (2016).
 45. Brinkman, E. K., Chen, T., Amendola, M. & van Steensel, B. Easy quantitative assessment of genome editing by sequence trace decomposition. *Nucleic Acids Res.* **42**, e168 (2014).
 46. Boutros, M., Brás, L. P. & Huber, W. Analysis of cell-based RNAi screens. *Genome Biol.* **7**, R66 (2006).
 47. Ianevski, A., Giri, A. K. & Aittokallio, T. SynergyFinder 2.0: visual analytics of multi-drug combination synergies. *Nucleic Acids Res.* **48**, W488–W493 (2020).
 48. Sturm, M., Schroeder, C. & Bauer, P. SeqPurge: highly-sensitive adapter trimming for paired-end NGS data. *BMC Bioinformatics* **17**, 208 (2016).
 49. Kim, D., Paggi, J. M., Park, C., Bennett, C. & Salzberg, S. L. Graph-based genome alignment and genotyping with HISAT2 and HISAT-genotype. *Nat. Biotechnol.* **37**, 907–915 (2019).
 50. Shen, S. *et al.* rMATS: robust and flexible detection of differential alternative splicing from replicate RNA-Seq data. *Proc. Natl. Acad. Sci. U. S. A.* **111**, E5593–601 (2014).

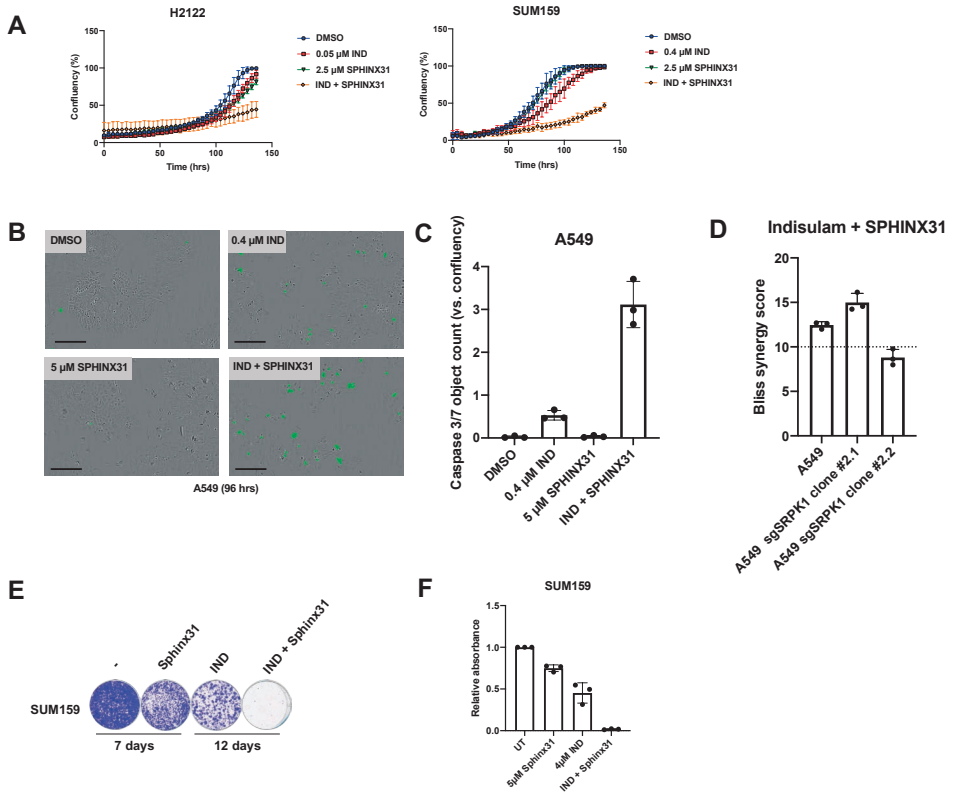
SUPPLEMENTARY FILES

**Supplemental Figure 1: SRPK1 is synthetic lethal with indisulam in DLD-1 cells**

A Western blot analysis of SRPK1 levels in DLD1 SRPK1 knock-out clones and control cells. Clones were generated from two independent sgRNAs. GAPDH was used as a loading control.

B Long-term colony formation assay of DLD1 cells. DLD1 *SRPK1* knock-out clones and control cells were treated with indicated doses of indisulam for 8 days.

C Proliferation assay of DLD1 control and sgSRPK1 cells treated with 1 μ M indisulam. One clone per sgRNA is shown. Mean of three technical replicates is shown and error bars indicate standard deviation.



Supplemental Figure 2: Combination of indisulam and SRPK1 inhibitor leads to apoptosis and prevents resistance to indisulam

A Proliferation assay of H2122 and SUM159 cells treated with 0.05 μ M indisulam (H2122) and 0.4 μ M indisulam (SUM159), 2.5 μ M SPHINX31 and the combination. Mean of three technical replicates is shown and error bars indicate standard deviation.

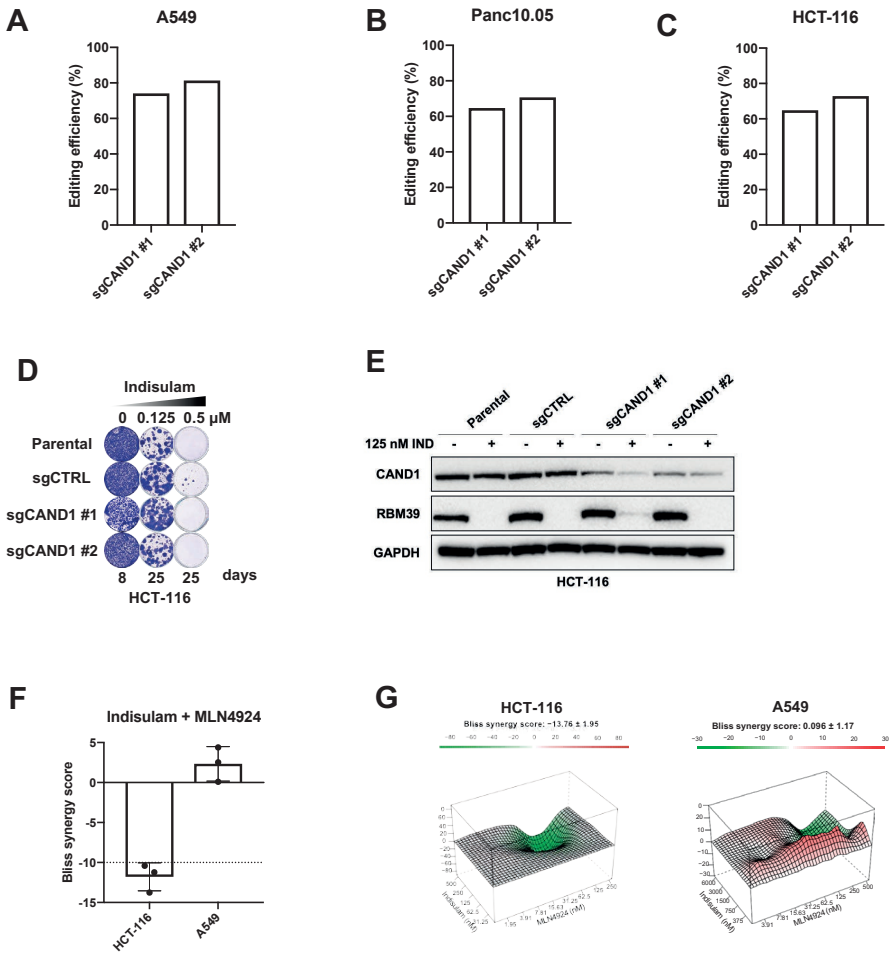
B Caspase 3/7 assay of A549 cells treated with 0.4 μ M indisulam, 5 μ M SPHINX31 and the combination for 4 days. Scale bar indicates 300 μ m.

C Quantification of caspase 3/7 object count normalized to confluency of A549 cells. Cells were treated with 0.4 μ M indisulam, 5 μ M SPHINX31 and the combination for 4 days. Mean of three technical replicates is shown and error bars indicate standard deviation.

D Drug synergy analysis of a 6-day treatment with indisulam in combination with SPHINX31 in A549 SRPK1 knock-out and control cells. Mean of three biological replicates is shown and error bars indicate standard deviation.

E Long-term colony formation assays of SUM159 cells. SUM159 were treated with 5 μ M SPHINX31, 4 μ M indisulam and the combination.

F Quantification of long-term colony formation assays of SUM159 cells. Mean of three biological replicates is shown and error bars indicate standard deviation.



Supplemental Figure 3: Loss of CAND1 does not rescue RBM39 degradation in HCT-116 cells

A CAND1 gene editing efficiency in A549 sgCAND1-1 and sgCAND1-5 cells determined by TIDE analysis.

B CAND1 gene editing efficiency in PANC10.05 sgCAND1-1 and sgCAND1-5 cells determined by TIDE analysis.

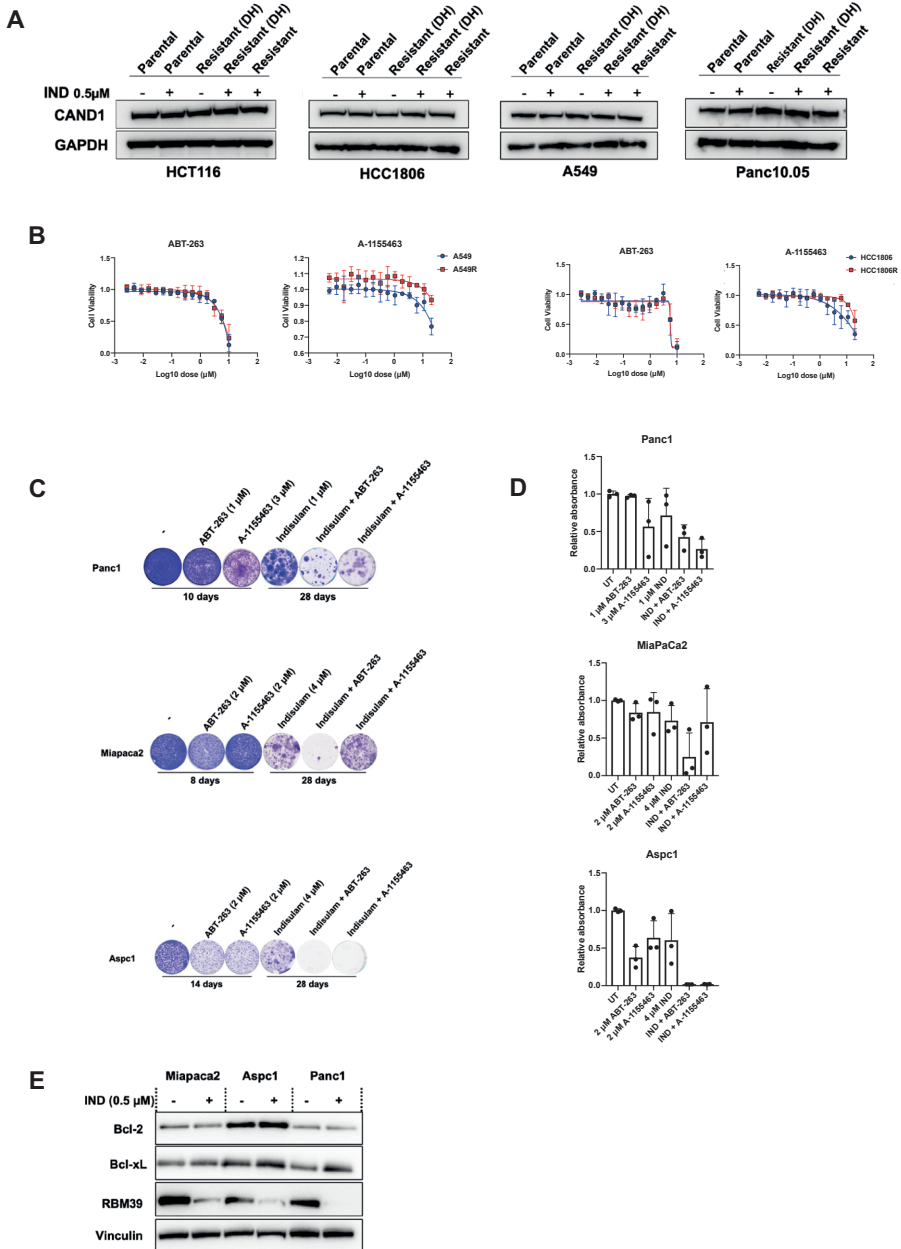
C CAND1 gene editing efficiency in HCT-116 sgCAND1-1 and sgCAND1-5 cells determined by TIDE analysis.

D Long-term colony formation assay of HCT-116. Wild-type, control and two individual sgCAND1 cells were treated with indicated doses of indisulam for indicated number of days.

E Western blot analysis of RBM39 and CAND1 in HCT-116 cells. Wild-type, control and sgCAND1 cells were treated with 0.125 μ M of indisulam for 8 days. GAPDH was used as loading control.

F Drug synergy analysis of indisulam and MLN4924 combination in HCT-116 and A549 cells. Mean of three biological replicates is shown and error bars indicate standard deviation.

G 3D representation of the synergy matrix of indisulam and MLN4924 in HCT-116 and A549 cells. Red areas represent high Bliss score and green areas represent low Bliss score. Mean of three biological replicates is shown.



Supplemental Figure 4: Acquired resistance to indisulam is CAND1 independent and can be prevented by inhibiting Bcl-xL

A Western blot analysis of CAND1 in parental and resistant HCT-116, HCC-1806, A549 and Panc10.05. GAPDH was used as loading control. Experimental design is described in figure 4D.

B Cell viability of A549(R) and HCC-1806(R) cells treated with ABT-263 and A-1155463. Indisulam-resistant cells were cultured in the presence of 0.5 μM indisulam. Mean of three biological replicates is shown and error bars indicate standard deviation.

C Long-term colony formation assays of Panc1, Miapaca2 and Aspc1. Both Miapaca2 and Aspc1

were treated with 2 μ M ABT-263, 2 μ M A-1155463, 4 μ M indisulam and the combination for the indicated duration. Panc1 was treated with 1 μ M ABT-263, 3 μ M A-1155463, 1 μ M indisulam and the combination.

D Quantification of long-term colony formation assays of Panc1, Miapaca2 and Aspc1 cells. Mean of three biological replicates is shown and error bars indicate standard deviation.

E Western blot analysis of BCL-2, Bcl-xL and RBM39 in Panc10.05, Miapaca2, Aspc1 and Panc1 parental and resistant cells. Parental cells were treated with 0.5 μ M of indisulam for 24h and resistant cells were cultured in the presence of 0.5 μ M Indisulam. Vinculin was used as a loading control.

Supplemental Table 1

Compound no.	Cat. No.	Product Name	Target	CAS No.	Solvent	M.Wt	Stock Conc. (mM)	Desired Highest Conc. (µM)
1	HY-50876	(E)-Daporinad	Autophagy; Namp1	658084-64-1	DMSO	391.51	10	5
2	HY-16106	Talazoparib	PARP	1207456-01-6	DMSO	380.35	10	10
3	HY-18174	Prexasertib	Checkpoint Kinase (Chk)	1234015-52-1	DMSO	365.39	10	10
4	HY-13925	PD0166285	Apoptosis; Wee1	185039-89-8	DMSO	512.43	10	10
5	HY-103617	PKM2-IN-1	Pyruvate Kinase	94164-88-2	DMSO	345.48	10	10
6	HY-112037	IACS-10759	Apoptosis	1570496-34-2	DMSO	562.56	10	10
7	HY-112897	IITZ-01	Apoptosis; Autophagy; PI3K	1807988-47-1	DMSO	482.51	10	10
8	HY-18072	GSK2606414	Apoptosis; Autophagy; PERK	1337531-36-8	DMSO	451.44	10	10
9	HY-107455	A-485	Epigenetic Reader Domain; Histone Acetyltransferase	1889279-16-6	DMSO	536.48	10	10
10	HY-15142	Doxorubicin (hydrochloride)	ADC Cytotoxin; AMPK; Apoptosis; Autophagy; HBV; HCV; HIV; Mitophagy; Topoisomerase	25316-40-9	DMSO	579.98	10	10
11	HY-12859	BAY1217389	Mps1	1554458-53-5	DMSO	561.50	10	5
12	HY-12814	TH588	DNA/RNA Synthesis	1609960-31-7	DMSO	295.17	10	10
13	HY-12113	Oprozomb	Autophagy; Proteasome	935888-69-0	DMSO	532.61	10	2
14	HY-90006	5-Fluorouracil	HIV; Nucleoside Antimetabolite/Analog	51-21-8	DMSO	130.08	10	10
15	HY-13629	Etoposide	Apoptosis; Autophagy; Mitophagy; Topoisomerase	33419-42-0	DMSO	588.56	10	10
16	HY-10586	5-Azacytidine	Autophagy; DNA Methyltransferase; Nucleoside Antimetabolite/Analog	320-67-2	DMSO	244.20	10	10
17	HY-13946	BML-277	Apoptosis; Checkpoint Kinase (Chk)	516480-79-8	DMSO	363.80	10	10
18	HY-15520	CGK733	ATM/ATR	905973-89-9	DMSO	555.84	10	10
19	HY-13002	Torin 2	Apoptosis; Autophagy; DNA-PK; mTOR	1223001-51-1	DMSO	432.40	10	10
20	HY-18690	Enasidenib	Isocitrate Dehydrogenase (IDH)	1446502-11-9	DMSO	473.38	10	10
21	HY-14715B	CCT241533 (hydrochloride)	Checkpoint Kinase (Chk)	1431697-96-9	DMSO	478.94	10	10
22	HY-10453	Ixazomb	Autophagy; Proteasome	1072833-77-2	DMSO	361.03	10	1
23	HY-100016	AZD0156	ATM/ATR	1821428-35-6	DMSO	461.56	10	10
24	HY-101566A	BAY-1895344 (hydrochloride)	ATM/ATR	1876467-74-1	DMSO	411.89	10	10

Supplemental Table 1 continued.

Compound no.	Cat. No.	Product Name	Target	CAS No.	Solvent	M.Wt	Stock Conc. (mM)	Desired Highest Conc. (µM)
25	HY-10993	Adavoseritib	Wee1	955365-80-7	DMSO	500.60	10	10
26	HY-10422	AZD-8055	Apoptosis; Autophagy; mTOR	1009298-09-2	DMSO	465.54	10	10
27	HY-10126	Barasertib-HQPA	Aurora Kinase	722544-51-6	DMSO	507.56	10	10
28	HY-12137	Volasertib	Apoptosis; Polo-like Kinase (PLK)	755038-65-4	DMSO	618.81	10	10
29	HY-17026	Gemcitabine	Autophagy; DNA/RNA Synthesis; Nucleoside Antimetabolite/Analog	95058-81-4	DMSO	263.20	10	10
30	HY-50759	Ispinesib	Apoptosis; Kinesin	336113-53-2	DMSO	517.06	10	2
31	HY-19707	4J8C	IRE1	14003-96-4	DMSO	204.18	10	10
32	HY-100017	BAY-876	Others	1799753-84-6	DMSO	496.42	10	10
33	HY-B1123	Auranofin	Bacterial	34031-32-8	DMSO	680.50	10	10
34	HY-50877	GSK461364	Polo-like Kinase (PLK)	929095-18-1	DMSO	543.60	10	10
35	HY-13734	PX-12	Others	141400-58-0	DMSO	188.31	10	10
36	HY-13780	Vinblastine (sulfate)	Autophagy; Microtubule/Tubulin	143-67-9	DMSO	909.05	10	2
37	HY-10194	YM-155	Autophagy; Survivin	781661-94-7	DMSO	443.29	10	5
38	HY-10212	BIIB021	Autophagy; HSP	848695-25-0	DMSO	318.76	10	10
39	HY-100006A	MRT68921 (dihydrochloride)	ULK	2080306-21-2	DMSO	471.04	10	10
40	HY-10221	Vorinostat	Autophagy; HDAC; HIV; Mitophagy	149647-78-9	DMSO	264.32	10	10
41	HY-10211	Tanespimycin	Apoptosis; Autophagy; HSP; Mitophagy	75747-14-7	DMSO	585.69	10	10
42	HY-12248	Telaglenastat	Autophagy; Glutaminase	1439399-58-2	DMSO	571.57	10	10
43	HY-12024	Alvespimycin (hydrochloride)	Apoptosis; HSP	467214-21-7	DMSO	653.21	10	10
44	HY-12325	GSK2194069	Others	1332331-08-4	DMSO	428.48	10	10
45	HY-10299	GSK-923295	Apoptosis; Kinesin	1088965-37-0	DMSO	592.13	10	10
46	HY-111621	DC661	Apoptosis; Autophagy	1872387-43-3	DMSO	552.58	10	10
47	HY-15187	Filanesib	Kinesin	885060-09-3	DMSO	420.48	10	5
48	HY-19725	A-1155463	Bcl-2 Family	1235034-55-5	DMSO	669.79	10	10
49	HY-15531	Venetoclax	Autophagy; Bcl-2 Family	1257044-40-8	DMSO	868.44	10	10
50	HY-10455	Carfilzomib	Apoptosis; Autophagy; Proteasome	868540-17-4	DMSO	719.91	10	1
51	HY-13322	Pracinostat	Apoptosis; HDAC	929016-96-6	DMSO	358.48	10	10

Supplemental Table 1 continued.

Compound no.	Cat. No.	Product Name	Target	CAS No.	Solvent	M.Wt	Stock Conc. (mM)	Desired Highest Conc. (µM)
52	HY-50514	AT9283	Apoptosis; Aurora Kinase; Autophagy; Bcr-Abi; FLT3; JAK	896466-04-9	DMSO	381.43	10	10
53	HY-12858	Empesertib	Mps1	1443763-60-7	DMSO	559.61	10	10
54	HY-17537	APY29	IRE1	1216665-49-4	DMSO	332.36	10	10
55	HY-10082	3-AP	DNA/RNA Synthesis	143621-35-6	DMSO	195.24	10	10
56	HY-13820	GSK2656157	Apoptosis; Autophagy; PERK	1337532-29-2	DMSO	416.45	10	10
57	HY-A0004	Decitabine	Apoptosis; DNA Methyltransferase	2353-33-5	DMSO	228.21	10	10
58	HY-10971	Alisertib	Apoptosis; Aurora Kinase; Autophagy	1028486-01-2	DMSO	518.92	10	10
59	HY-10992	AZD-7762	Checkpoint Kinase (Chk)	860352-01-8	DMSO	362.42	10	10
60	HY-100549	(S)-Crizotinib	Apoptosis; DNA/RNA Synthesis	1374356-45-2	DMSO	450.34	10	10
61	HY-16966	SBI-0206965	Apoptosis; Autophagy; ULK	1884220-36-3	DMSO	489.32	10	10
62	HY-13253	AMG 900	Aurora Kinase	945595-80-2	DMSO	503.58	10	10
63	HY-12683	BPTES	Glutaminase	314045-39-1	DMSO	524.68	10	10
64	HY-12750	AZD3965	Monocarboxylate Transporter	1448671-31-5	DMSO	515.51	10	10
65	HY-13062	Daunorubicin (Hydrochloride)	ADC Cytotoxin; Apoptosis; Autophagy; DNA/RNA Synthesis; Topoisomerase	23541-50-6	DMSO	563.98	10	10
66	HY-10450	Dapagliflozin	SGLT	461432-26-8	DMSO	408.87	10	10
67	HY-15433	Quisinosat	HDAC	875320-29-9	DMSO	394.47	10	5
68	HY-15287	Nelfinavir	HIV; HIV Protease	159989-64-7	DMSO	567.78	10	10
69	HY-101533	AZD-5991	Bcl-2 Family	2143061-81-6	DMSO	672.26	10	10
70	HY-114490	ULK-101	ULK		DMSO	460.45	10	10
71	HY-10547	OSU-03012	Autophagy; PDK-1	742112-33-0	DMSO	460.45	10	10
72	HY-15532	SCH900776	Checkpoint Kinase (Chk)	891494-63-6	DMSO	376.25	10	50
73	HY-100888	Simurosertib	CDK	1330782-76-7	DMSO	341.43	10	10
74	HY-19710	MKC3946	IRE1	1093119-54-0	DMSO	380.46	10	10
75	HY-14846	Litromesib	Kinesin	910634-41-2	DMSO	511.70	10	5
76	HY-15230	Geldanamycin	Bacterial; HSP	30562-34-6	DMSO	560.64	10	10
77	HY-112167A	GDC-0575 dihydrochloride	Checkpoint Kinase (Chk)	1657014-42-0	DMSO	451.19	10	10

Supplemental Table 1 continued.

Compound no.	Cat. No.	Product Name	Target	CAS No.	Solvent	M.Wt	Stock Conc. (mM)	Desired Highest Conc. (µM)
78	HY-109566	AZD1390	ATM/ATR	2089288-03-7	DMSO	477.57	10	10
79	HY-10496	SC75741	Influenza Virus; NF-κB	913822-46-5	DMSO	565.67	10	10
80	HY-100538A	DTP3 (TFA)	DNA/RNA Synthesis; JNK	1809784-29-9	DMSO	639.62	10	10
81	HY-101462	RAD51 Inhibitor B02	Apoptosis; RAD51	1290541-46-6	DMSO	339.39	10	50
82	HY-14720	Rabusertib	Autophagy; Checkpoint Kinase (Chk)	911222-45-2	DMSO	436.30	10	10
83	HY-W013009	5-Methyl-1H-pyrazol-3(2H)-one		4344-87-0	DMSO	98.10	10	10
84	HY-106376A	L-Buthionine-(S)-sulfoximine	Ferroptosis	83730-53-4	mQ	222.31	100	100
85	HY-B1370	Hydroxychloroquine sulfate	Autophagy; Parasite; Toll-like Receptor (TLR)	747-36-4	mQ	433.95	100	100
86	HY-10224	Panobinostat	Apoptosis; Autophagy; HDAC; HIV	404950-80-7	DMSO	349.43	10	5
87	HY-12495	ISRIB (trans-isomer)	Apoptosis; Autophagy; PERK	1597403-47-8	DMSO	451.34	10	10
88	HY-70044	GSK-1070916	Apoptosis; Aurora Kinase	942918-07-2	DMSO	507.63	10	10
89	HY-13468	KW-2478	HSP	819812-04-9	DMSO	574.66	10	10
90	HY-10162	Olaparib	Autophagy; Mitophagy; PARP	763113-22-0	DMSO	434.46	10	10
91	HY-101966	NCT-503	Others	1916571-90-8	DMSO	408.48	10	10
92	HY-10087	Navitoclax	Bcl-2 Family	923564-51-6	DMSO	974.61	10	10
93	HY-101570	Nedisertib	DNA-PK	1637542-33-6	DMSO	481.91	10	10
94	HY-B0015	Paclitaxel	ADC Cytotoxin; Autophagy; Microtubule/Tubulin	33069-62-4	DMSO	853.91	10	5
95	HY-14842B	Givinostat (hydrochloride monohydrate)	HDAC	732302-99-7	DMSO	475.97	10	10
96	HY-B0542	Ouabain (Octahydrate)	Autophagy; Na ⁺ /K ⁺ ATPase	11018-89-6	DMSO	728.77	10	10
97	HY-10161	Tozasertib	Aurora Kinase; Autophagy	639089-54-6	DMSO	464.59	10	10
98	HY-10219	Rapamycin	Autophagy; FKBP; mTOR	53123-88-9	DMSO	914.17	10	5
99	HY-10179	Danusertib	Aurora Kinase; Autophagy	827318-97-8	DMSO	474.55	10	10
100	HY-14981	GSK2334470	PDK-1	1227911-45-6	DMSO	462.59	10	10
101	HY-100437	HA15	Apoptosis; Autophagy; HSP	1609402-14-3	DMSO	466.58	10	10

Supplemental Table 1 continued.

Compound no.	Cat. No.	Product Name	Target	CAS No.	Solvent	M.Wt	Stock Conc. (mM)	Desired Highest Conc. (µM)
102	HY-100430	CCF642	Others	346640-08-2	DMSO	378.45	10	10
103	HY-13812	QNZ	NF-κB; TNF Receptor	545380-34-5	DMSO	356.42	10	10
104	HY-13902	Berzosertib	ATM/ATR	1232416-25-9	DMSO	463.55	10	10
105	HY-18958	CCT245737	Checkpoint Kinase (Chk)	1489389-18-5	DMSO	379.34	10	10
106	HY-19323	Ceralasertib	ATM/ATR	1352226-88-0	DMSO	412.51	10	10
107	HY-B0782	Acetazolamide	Autophagy; Carbonic Anhydrase	59-66-5	DMSO	222.25	10	10
108	HY-13252	MK-5108	Aurora Kinase; Autophagy	1010085-13-8	DMSO	461.94	10	10
109	HY-12069	SB-743921	Kinesin	940929-33-9	DMSO	553.52	10	10
110	HY-15317	RI-1	RAD51	415713-60-9	DMSO	361.61	10	50
111	HY-17029	Epothilone B	Apoptosis; Microtubule/Tubulin	152044-54-7	DMSO	507.68	10	1
112	HY-50907	ABT-737	Apoptosis; Bcl-2 Family; Mitophagy	852808-04-9	DMSO	813.43	10	10
113	HY-50698	BI 2536	Apoptosis; Epigenetic Reader Domain; Polo-like Kinase (PLK)	755038-02-9	DMSO	521.65	10	5
114	HY-100023	LY3177833	CDK	1627696-51-8	DMSO	309.30	10	10
115	HY-N0488	Vincristine (sulfate)	Apoptosis; Microtubule/Tubulin	2068-78-2	DMSO	923.04	10	10
116	HY-10619	Niraparib		1038915-60-4	DMSO	320.34	100	100
117	HY-17393	Carboplatin		41575-94-4	mQ	371.25	10	100
118	HY-16107	BMS-303141		943962-47-8	DMSO	424.3	50	100
119	HY-17589	Chloroquine (diphosphate)		50-63-5	mQ	515.86	100	100
120	HY-N0018	Daidzin		552-66-9	DMSO	416.38	100	100
121	HY-10617	Rucaparib	PARP	283173-50-2	DMSO	421.36	100	100
122	HY-13653	(-)Epigallocatechin Gallate		989-51-5	DMSO	458.37	100	100
123	HY-110287	Apcin		300815-04-7	DMSO	438.65	100	100
124	HY-107569	Garcinol		78824-30-3	DMSO	602.8	40	100
125	HY-101071	(S)-Monastrol		254753-54-3	DMSO	292.35	100	100
126	HY-111510	PI-3063	PI3K delta	1425043-73-7	DMSO	455.51	10	10
127	HY-19708	kir66	IRE1	1589527-65-0	DMSO	518.53	5	10

Supplemental Table 1 continued.

Compound no.	Cat. No.	Product Name	Target	CAS No.	Solvent	M.Wt	Stock Conc. (mM)	Desired Highest Conc. (µM)
128	HY-18961	PD 407824	CHK1 and WEE1	622864-54-4	DMSO	328,32	10	10
129	HY-17394	Cisplatin	Alkylating	15663-27-1	DMF	300,05	33,3	100
130	HY-103709S	VX 984 (M9831)	DNA-PK	1562396-65-9	DMSO	415,49	10	10
131		ND 646	ACC1/ACC2	1434639-57-2	DMSO	568,64	10	10
132	SML0021-5MG	16F16	PDI	922507-80-0	DMSO	320,77	10	10
133	SML0781-5MG	NSC 109555	CHK2	15427-93-7	mQ	600,67	10	10
134	5054770001	pevonedistat (MLN4924)	NAE		DMSO	452,53	10	10
135		Oxaliplatin		61325-94-3	DMF	397,29	10	100
136	S1362	Rigosertib	PLK1	1225497-78-8	DMSO	473,47	10	10
137	S1570	KU-60019	ATM		DMSO	547,67	10	10
138	S8061	Sabutoclax	Bcl-2 Bcl-xl Mcl-1	1228108-65-3	DMSO	700,78	10	10
139	S6718	MKT 077	HSP 70	147366-41-4	DMSO	432	10	10
140	S7771	STF-083010	IRE1	307543-71-1	DMSO	317,38	10	100
141	S1069	Luminespib	HSP 90	747412-64-2	DMSO	465,54	10	10
142	HY-107427	PF 3644022	MK2	1276121-88-0	DMSO	574,46	10	10
143	HY-10985	Marizomib	Proteasome	437742-34-2	DMSO	313,78	10	1
144	HY-108643	CMPD1	MK2	41179-33-3	DMSO	349,4	10	10
145	HY-100558	Bafilomycin A1	Endosome acidification	88899-55-2	DMSO	622,83	10	5
146	S7547	XL 413	CDC7		mQ	326,18	10	5
147	HY-15149	Romidepsin	HDAC	128517-07-7	DMSO	540,7	10	10
148		Bortezomib	Proteasome	179324-69-7	DMSO	384,24	10	1
149	HY-124955	ProTAME	APC	1362911-19-0	DMSO		10	10
150	HY-A0098	Tunicamycin	Glycosylation	11089-65-9	DMSO	844,94	10	10
151	Cat. No. 5921	D9	TrxR		DMSO	596,43	10	2
152		RSL3			DMSO		10	10
153		Indisulam			DMSO		10	10
154		Thapsigargin			DMSO		10	10
155	HY-100110	KNK437	HSP	218924-25-5	DMSO	245,23	100	100

Supplemental Table 1 continued.

Compound no.	Cat. No.	Product Name	Target	CAS No.	Solvent	M.Wt	Stock Conc. (mM)	Desired Highest Conc. (µM)
156	HY-18085	Quercetin	Autophagy; Mitophagy; PI3K	117-39-5	DMSO	302.24	100	100
157	HY-N0182	Fisetin	PPAR; Sirtuin; TNF Receptor	528-48-3	DMSO	286.24	100	100
158	HY-13513	U-104	Carbonic Anhydrase	178606-66-1	DMSO	309.32	100	100
159	HY-112683	V-9302	Others	1855871-76-9	DMSO	538.68	100	100
160	HY-14650	DHEA	Androgen Receptor; Endogenous Metabolite	53-43-0	DMSO	288.42	100	100
161	HY-19959	Mirin	Others	1198097-97-0	DMSO	220.25	100	100
162	HY-12364A	trans-C75	Fatty Acid Synthase (FAS)	191282-48-1	DMSO	254.32	100	100
163	HY-15453	Devimistat	Apoptosis	95809-78-2	DMSO	388.59	100	100
164	HY-19693	Cariporide	Sodium Channel	159138-80-4	DMSO	283.35	100	100



Chapter 3

Indisulam synergizes with palbociclib to induce senescence through inhibition of CDK2 kinase activity

Ziva Pogacar¹, Jackie L. Johnson¹, Lenno Krenning², Giulia De Conti¹, Fleur Jochems¹, Cor Liefink³, Arno Velds⁴, Leyma Wardak¹, Kelvin Groot¹, Arnout Schepers¹, Liqin Wang¹, Ji-Ying Song⁵, Marieke van de Ven⁶, Olaf van Tellingen⁷, Rene H. Medema², Roderick L. Beijersbergen^{1,3}, Rene Bernards^{1*} and Rodrigo Leite de Oliveira^{1,8*}

¹Division of Molecular Carcinogenesis, Oncode Institute. The Netherlands Cancer Institute, Plesmanlaan 121, 1066 CX Amsterdam, The Netherlands.

³The NKI Robotics and Screening Center, The Netherlands Cancer Institute, Plesmanlaan 121, 1066 CX Amsterdam, The Netherlands.

²Division of Cell Biology, Oncode Institute, The Netherlands Cancer Institute, Plesmanlaan 121, 1066 CX Amsterdam, The Netherlands.

⁴Genomics core facility, The Netherlands Cancer Institute, Plesmanlaan 121, 1066 CX Amsterdam, The Netherlands.

⁵Division of Animal Pathology, The Netherlands Cancer Institute, Amsterdam, The Netherlands

⁶Mouse Clinic for Cancer and Aging, Netherlands Cancer Institute, Amsterdam, The Netherlands

⁷Division of Pharmacology. The Netherlands Cancer Institute, Plesmanlaan 121, 1066 CX Amsterdam, The Netherlands

⁸Present address: CRISPR Expertise Center, Cancer Center Amsterdam, Amsterdam University Medical Center, De Boelelaan 1117, 1081 HV Amsterdam, The Netherlands

* Shared corresponding authors

ABSTRACT

Inducing senescence in cancer cells is emerging as a new therapeutic strategy. In order to find ways to enhance senescence induction by palbociclib, a CDK4/6 inhibitor approved for treatment of metastatic breast cancer, we performed functional genetic screens in palbociclib-resistant cells. Using this approach, we found that loss of *CDK2* results in strong senescence induction in palbociclib-treated cells. Treatment with the CDK2 inhibitor indisulam, which phenocopies genetic CDK2 inactivation, led to sustained senescence induction when combined with palbociclib in various cell lines and lung cancer xenografts. Treating cells with indisulam led to downregulation of cyclin H, which prevented CDK2 activation. Combined treatment with palbociclib and indisulam induced a senescence program and sensitized cells to senolytic therapy. Our data indicate that inhibition of CDK2 through indisulam treatment can enhance senescence induction by CDK4/6 inhibition.

INTRODUCTION

Cellular senescence is a stable cell cycle arrest and can be induced by a variety of stressors, including cancer therapies (referred to as therapy induced senescence [TIS])¹. Senescence is characterized by changes in cellular physiology, such as changes of cell morphology, changes in gene expression and metabolism, and secretion of a variety of proteins (collectively referred to as the senescence associated secretory phenotype [SASP])². Induction of senescence as an anti-cancer treatment can be advantageous in the short term because cell proliferation is halted and immune cells are recruited through the SASP. However, in the long term, persistence of senescent cancer cells can lead to chronic inflammation, tumor progression and migration³. We postulated that a “one-two punch” approach to cancer therapy, in which a first drug induces senescence and the second drug either targets the senescent cancer cells for death (senolysis) or enhances the efficacy of the immune infiltrate may be an effective anti-cancer strategy^{4,5}.

Several cancer treatments have been shown to induce senescence, including chemotherapeutics and targeted agents (reviewed in⁶). For instance, targeting CDK4 and 6 with inhibitors (such as palbociclib, ribociclib and abemaciclib) induced senescence in various cancer models⁷⁻¹¹. CDK4/6 are important kinases in the cell cycle, regulating the transition from G1 to S phase by phosphorylating and partially inactivating the retinoblastoma protein RB. Upon subsequent further phosphorylation of RB by CDK2, RB is functionally fully inactivated, leading to complete de-repression of E2F transcriptional activity and entry into S phase¹². Since the majority of cancer cells have an intact *RB1* gene and thus depend on CDK4/6 kinase activity for sustained proliferation, CDK4/6 emerged as a potential target for cancer therapy. CDK4/6 inhibitors have been approved for treatment of hormone receptor positive (HR+) and human epidermal growth factor receptor 2 (HER2) negative (HER2-) breast cancer in combination with anti-hormonal therapy¹³⁻¹⁵.

Due to the efficacy, safety and tolerability of the CDK4/6 inhibitors in HR+ breast cancer, and multiple nodes of oncogenic signals converging on CDK4/6 in multiple cancer types¹⁶, there has been significant interest in extending their use to other cancer types. Several clinical trials using CDK4/6 inhibitors in various cancer types, such as non-small cell lung cancer, ovarian cancer and triple negative breast cancer were recently completed¹⁷⁻²⁰. However, translating the use of CDK4/6 inhibitors to other tumor types has proven to be challenging, due to limited senescence induction and intrinsic resistance²¹⁻²³. Better understanding of the limitations of senescence induction by CDK4/6 inhibitors may help in broadening the clinical utility of this class of cancer therapeutics.

A potential solution is using CDK4/6 inhibitors in a rational combination. For example, combining CDK4/6 inhibitors with PI3K inhibition was effective in multiple preclinical models^{24,25}. Furthermore, combining CDK4/6 inhibition with the MEK inhibitor trametinib

was shown to increase senescence induction in lung cancer and colorectal cancer cells^{26,27}.

Indisulam was originally identified as a sulfonamide with anticancer effects that acts as an indirect CDK2 inhibitor²⁸. However, after various phase 1 and 2 clinical trials showed a response and stable disease in only 17-36% of patients, development was halted²⁹⁻³⁵. On a molecular level, indisulam was recently identified as being a molecular glue, targeting the splicing factor RBM39 to DCAF15, a component of a ubiquitin ligase complex, leading to degradation of RBM39³⁶. Here, we identify an unexpected synergy between indisulam and palbociclib in induction of senescence in multiple cancer types. Moreover, we find that cancer cells made senescent with palbociclib and indisulam are sensitive to the senolytic agent ABT-263.

RESULTS

CDK2 loss is synergistic with palbociclib in inducing senescence in triple negative breast cancer

Palbociclib has only modest cytostatic activity in triple negative breast cancer (TNBC) cell lines. To capture the heterogeneity of TNBC, we chose three independent cell lines as models for kinome-based shRNA synthetic lethality screens to identify genes whose suppression enhances the response to palbociclib (Supplemental Figure 1A). We performed synthetic lethality screens in CAL-51, CAL-120 and HCC1806, all of which are resistant to palbociclib (Figure 1A, Supplemental Figure 1C). Depleted shRNAs were identified by deep sequencing as described previously³⁷. When comparing the relative abundance of shRNAs in palbociclib-treated to untreated cells, shRNAs targeting *CDK2* were depleted in all three cell lines (Figure 1A). Furthermore, *CDK2* was the only common hit between all three screening cell lines (Figure 1B). To validate this observation, we used individual shRNAs to knock down *CDK2* in the cell lines used for the screens (Supplemental Figure 1B). Even though *CDK2* knockdown had no effect on proliferation, we observed a decrease in proliferation in *CDK2* knockdown cells treated with palbociclib (Supplemental Figure 1C,D). Similarly, CAL-51-*CDK2* knockout cells had no changes in proliferation, but were more sensitive to palbociclib treatment (Figure 1C, D, E).

CDK2 knockout cells treated with palbociclib showed a change in morphology indicative of senescence. To better characterize these cells, we stained them for senescence-associated β -galactosidase (SA- β -gal), an established marker of senescence³⁸. We observed an increase in the number of cells positive for SA- β -gal in all three TNBC cell lines when cells lacking *CDK2* were treated with palbociclib (Figure 1F,G, S1E, F).

Given that senescent cancer cells can promote inflammation and support metastasis, senolytic therapies are being developed to obliterate the senescent cells⁶. We tested

the senolytic compound navitoclax (ABT-263, an inhibitor of BCL-2, BCL-xL and BCL-W) in *CDK2* knockout TNBC cells rendered senescent with palbociclib. After pre-treating sgCDK2 and control cells with palbociclib, only cells lacking CDK2 were killed upon treatment with ABT-263 (Figure 1H).

CDK2 inhibition is synergistic with palbociclib in multiple cancer types

Due to the heterogeneity of TNBC cell lines we hypothesized that the interaction between CDK2 and palbociclib may be a general dependency and could therefore be applied broadly to other cancer types. To address this, we tested an additional TNBC cell line (SUM159) as well as lung cancer cell lines A549 and H2122 and colorectal cancer cell lines DLD-1 and RKO. We knocked out *CDK2* (Figure 2A, F, S2A) and observed an increased sensitivity to palbociclib in cells harboring sgCDK2 compared to control cells (Figure 2B, C, G, H, S2B). Furthermore, cells harboring sgCDK2 treated with palbociclib showed an increased number of SA- β -gal positive cells in SUM159 and A549 (Figure 2D, E, I, J) and the enlarged size and flat morphological features of cellular senescence. SUM159 CDK2 knock-out cells also showed sensitivity to the senolytic agent ABT-263 (Supplemental Figure 2C). Unequivocal identification of senescence in cancer cells can be difficult due to the lack of gold-standard markers of the senescent state. Previous studies have identified gene signatures associated with senescence^{2,39} or list of genes differentially expressed in senescence^{40,41}. We therefore used transcriptome analyses to further characterize these cells. We observed that A549 cells showed enrichment in four out of five tested senescence signatures in RNA-seq experiments when comparing treated and untreated sgCDK2 cells (Figure 2K). This shows that senescence induction upon *CDK2* loss and CDK4/6 inhibition has little context-dependency.

Indisulam phenocopies CDK2 loss and induces senescence in combination with palbociclib

Even though the interaction between *CDK2* loss and palbociclib induces senescence in a broad panel of cell lines, the lack of a selective CDK2 inhibitor complicates further development of this concept. While a variety of compounds targeting CDK2 are available, they tend to be non-specific and also target other CDKs, such as CDK1/5/7/9 (reviewed in ⁴²) which diminishes their utility. Furthermore, the off-target effects of these compounds often lead to toxicity and prevent their use in combination therapies. In search of a CDK2 inhibitor we came across indisulam, a sulfonamide that was described as an indirect CDK2 inhibitor²⁸. When we treated the cells with the combination of palbociclib and indisulam we observed a decrease in proliferation in all tested cell lines (Figure 3A, B, S3A, B). Furthermore, treatment with indisulam and palbociclib showed an increase in the number of cells positive for SA- β -gal (Figure 3C, D, S3C, D). Both SUM159 and A549, as well as CAL-51, DLD-1 and RKO senescent cells induced by palbociclib and indisulam were sensitive to ABT-263 (Figure 3E, S3E).

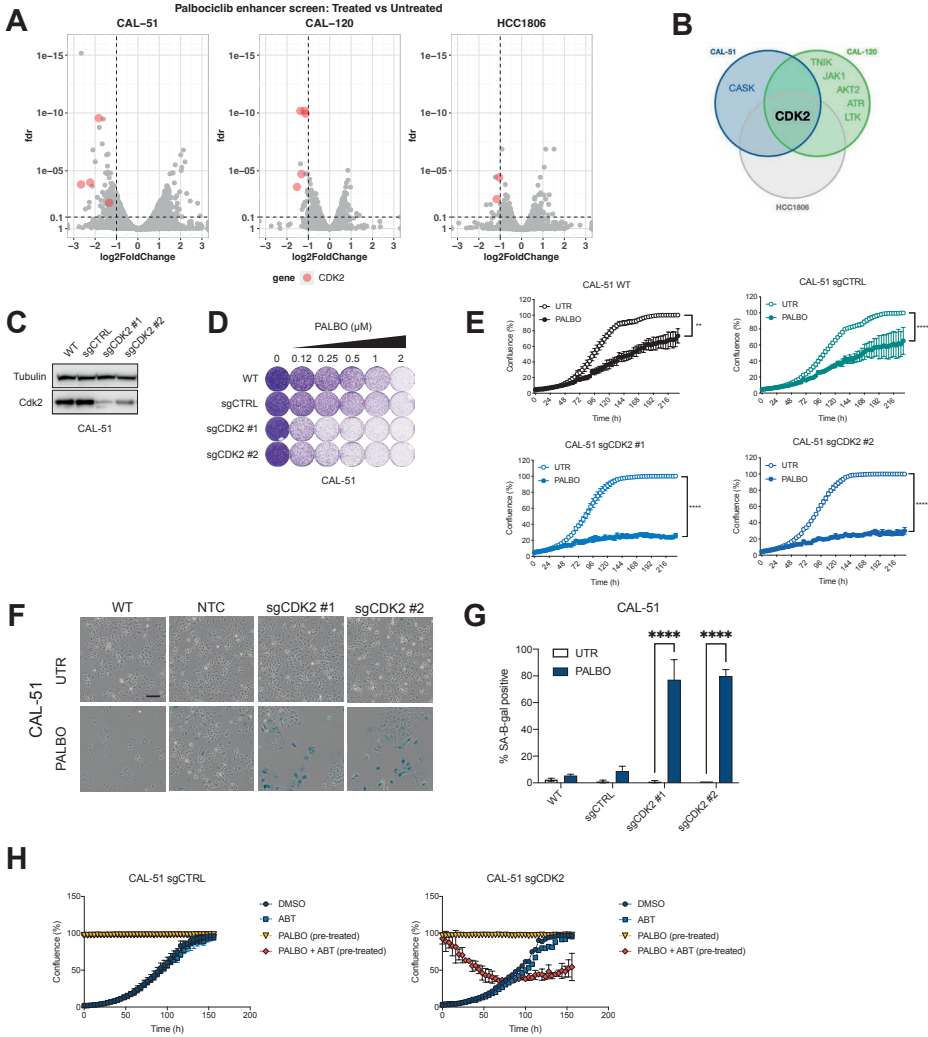


Figure 1: CKD2 loss is synergistic with palbociclib in induction of senescence in triple negative breast cancer

A Volcano plot of hit selection. shRNA counts of CAL-51, CAL-120 and HCC1806 were compared between palbociclib treated and untreated conditions. Each dot represents an individual shRNA. Y axis shows the false discovery rate (FDR) and X axis shows fold change between conditions. The cutoffs of 0.1 FDR and -1 log₂ fold change are represented by the dashed lines. Red dots indicate shRNAs targeting CDK2. Hits were selected as genes that were represented with at least 2 independent shRNAs.

B Venn diagram shows overlap of hits between CAL-51, CAL-120 and HCC-1806. Hits were selected as genes that were represented with at least 2 independent shRNAs.

C-G Screen validation: CDK2 was knocked out with two independent sgRNAs in CAL-51 cells. Polyclonal population of sgCDK2 cells was used for experiments.

C Western blot analysis of CDK2 levels in CAL-51 sgCDK2 and control cells. Tubulin was used as loading control. Representative images of two independent experiments are shown (n=2).

D Long term colony formation assay of CAL-51. Wild-type, control and sgCDK2 cells were treated with indicated doses of palbociclib for 10 days. Representative of three independent experiments is shown (n=3).

E Proliferation assay of CAL-51. Cells were treated with 0.5 μM of palbociclib or DMSO. Mean of three technical replicates representative of two independent experiments (n=2) is shown and error bars

indicate standard deviation. The end point confluency of all conditions were analysed using two-way ANOVA with Šidák's post-hoc test (** $p < 0.01$ **** $p < 0.0001$).

F SA- β -gal staining in CAL-51 cells treated for 10 days with 0.5 μM of palbociclib. Scale bar indicates 100 μm . Representative images of two independent experiments are shown (n=2).

G Quantification of SA- β -gal positive cells shown in **F**. CAL-51 cells were treated for 10 days with 0.5 μM of palbociclib. Bars represent mean \pm SD of triplicates. Data was analysed using two-way ANOVA with Šidák's post-hoc test (**** $p < 0.0001$).

H Proliferation assay of CTRL or CAL-51 sgCDK2 cells treated with senolytic drug ABT-263. Cells were pre-treated with 2 μM of palbociclib for 10 days to induce senescence, then seeded in high density (100% confluence) and treated with palbociclib or a combination of palbociclib and 5 μM ABT-263. Proliferating cells, which were not pre-treated, were seeded at low density and treated with DMSO or ABT-263. Mean of three technical replicates representative of two independent experiments (n=2) is shown and error bars indicate standard deviation.

We then set out to further characterize the senescence phenotype by testing four different senescence markers by Western blot. We observed a decrease in phosphorylated RB and increase in p21 in both cell lines. There was also an increase in γH2AX , although less apparent in A549. Furthermore, there was an increase in p16INK4A in SUM159. Since A549 cells are p16 null, we examined an additional marker Lamin B1, which was reduced upon the combination treatment. We observed a reduction in CDK2 protein levels in palbociclib treated samples. However CDK2 was not further reduced upon the combination treatment samples since indisulam is an indirect CDK2 inhibitor that does not influence the protein abundance (Figure 3F, S3H).

Next, we treated A549 and SUM159 cells with indisulam, palbociclib and the combination, and performed RNA-sequencing. We observed enrichment in senescence signatures when comparing the combination-treated cells to single drugs or untreated conditions (Figure 3G). Additionally, we tested the recently developed PF-0687360 compound, which is described to inhibit CDK2/4/6^{43,44}. Treatment with PF-0687360 led to an increase of SA- β -gal positive cells in SUM159 and A549 (Figure S3F,G) as well as enrichment in senescence signatures (Figure S3I), further validating inhibition of CDK2 with CDK4/6 as a senescence inducing combination.

Combination of indisulam and palbociclib impairs tumor growth *in vivo*

To extend the findings to an *in vivo* model, we tested if *CDK2* loss leads to growth arrest when combined with palbociclib treatment in mice xenografts. We generated *CDK2* KO clones in A549 and CAL-51 cells and then engrafted A549 subcutaneously and CAL-51 orthotopically in NMRI nude mice. However, *CDK2* seems to be essential for growth *in vivo* as the growth of *CDK2* knock-out tumors was severely impaired, making genetic validation technically not feasible (Figure S4A, B). We then proceeded to test the combination of palbociclib and indisulam *in vivo*. Firstly, we performed a PK/PD experiment and determined that both drugs were stable in plasma (Figure S4C, D). Next, we engrafted A549 cells subcutaneously and treated the mice with vehicle, palbociclib, indisulam or the combination. We observed a reduction in tumor growth in

animals treated with the drug combination compared to the single treatments (Figure 4A). Furthermore, immunohistochemical analysis showed decrease of the proliferation marker Ki67 and increase of the CDK inhibitor p21 in tumors treated with the drug combination, compared to single treatments or control groups (Figure 4B, C). We conclude that the combination of indisulam and palbociclib is well tolerated *in vivo* and leads to impaired tumor growth and reduced proliferation.

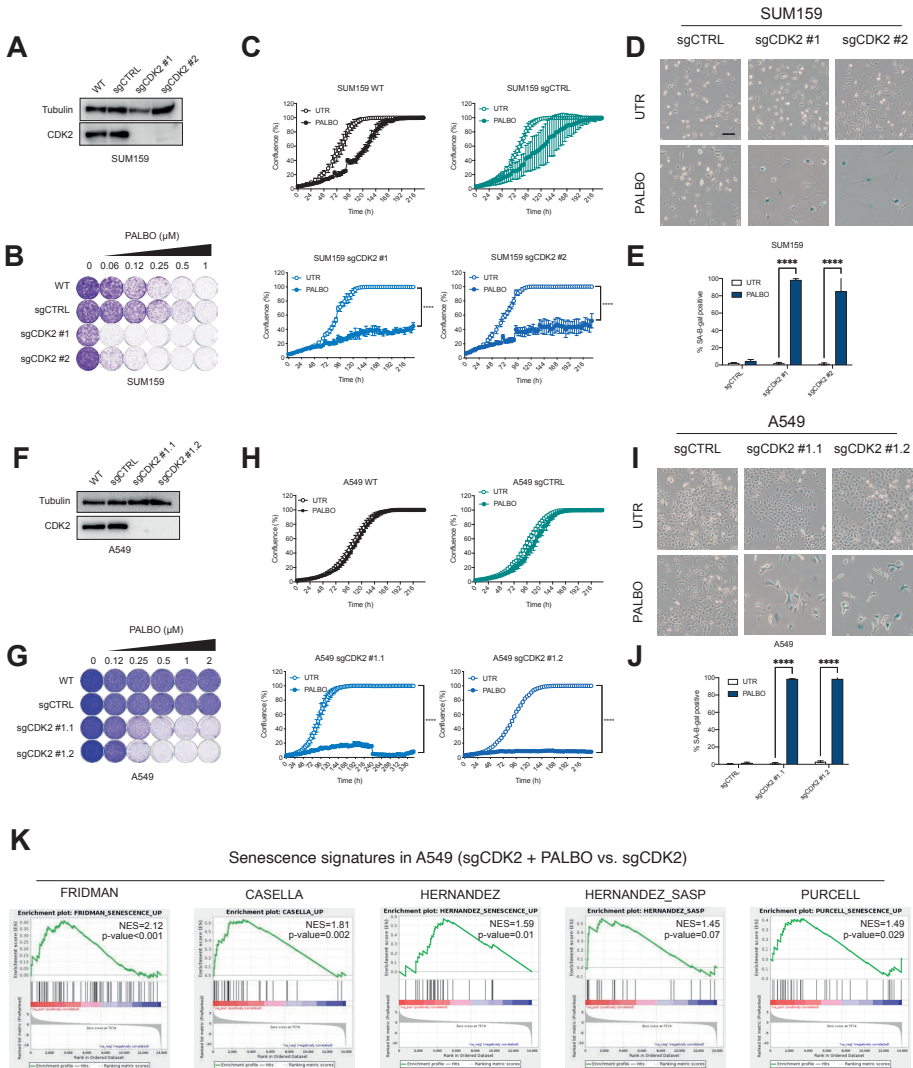


Figure 2: CDK2 inhibition is synergistic with palbociclib in multiple cancer types

A-E CDK2 was knocked out in SUM159 cells using two independent sgRNAs.

A Western blot analysis of SUM159 sgCDK2 cells and control cells. Tubulin was used as a loading control. Representative images of two independent experiments are shown (n=2).

B Long term colony formation assay of SUM159 sgCDK2 and control cells with palbociclib was performed for 8 days. Representative of two independent experiments are shown (n=2).

C Proliferation assay of SUM159 sgCDK2 and control cells treated with 0.25 μM of palbociclib. Mean of three technical replicates representative of two independent experiments (n=2) is shown and error bars indicate standard deviation. The end point confluency of all conditions were analysed using two-way ANOVA with Šidák's post-hoc test (**** $p < 0.0001$).

D SA- β -gal staining in SUM159 sgCDK2 and control cells treated with 0.25 μM of palbociclib for 8 days. Scale bar indicates 100 μm . Representative images of two independent experiments are shown (n=2).

E Quantification of SA- β -gal positive cells shown in **D**. SUM159 cells were treated for 8 days with 0.25 μM of palbociclib. Bars represent mean \pm SD of triplicates. Data was analysed using two-way ANOVA with Šidák's post-hoc test (**** $p < 0.0001$).

F-J CDK2 was knocked out in A549 and two single cell clones were selected.

F Western blot analysis of A549 sgCDK2 cells and control cells. Tubulin was used as a loading control. Representative images of two independent experiments are shown (n=2).

G Long term colony formation assay of A549 sgCDK2 and control cells with palbociclib was performed for 10 days. Representative of two independent experiments are shown (n=2).

H Proliferation assay of A549 sgCDK2 and control cells treated with 0.5 μM of palbociclib. Mean of three technical replicates representative of two independent experiments (n=2) is shown and error bars indicate standard deviation. The end point confluency of all conditions were analysed using two-way ANOVA with Šidák's post-hoc test (**** $p < 0.0001$).

I SA- β -gal staining in A549 sgCDK2 and control cells treated with 0.5 μM of palbociclib for 10 days. Scale bar indicates 100 μm . Representative images of two independent experiments are shown (n=2).

J Quantification of SA- β -gal positive cells shown in **I**. A549 cells were treated for 10 days with 0.5 μM of palbociclib. Bars represent mean \pm SD of triplicates. Data was analysed using two-way ANOVA with Šidák's post-hoc test (**** $p < 0.0001$).

K GSEA of previously published senescence gene sets comparing A549 sgCDK2 cells treated with 2 μM palbociclib for 10 days with untreated cells. Normalized enrichment score (NES) and p-values of enrichment score are shown. The experiment was performed in duplicates.

Indisulam prevents activation of CDK2 leading to cell cycle arrest when combined with palbociclib

To better understand the effects of indisulam on CDK2 we first performed an *in vitro* kinase activity assay. In short, we added indisulam to different cyclin/CDK complexes *in vitro* and measured the kinase activity as previously described⁴⁵. We did not observe a direct and specific inhibition of CDK2 by indisulam, which was in line with previous reports on indisulam being an indirect CDK2 inhibitor (Figure S5A). Recently, indisulam has been characterized as a molecular degrader, bringing together a splicing factor RBM39 with DCAF15 substrate receptor of CUL4a/b ubiquitin ligase complex³⁶. This leads to ubiquitination and proteasomal degradation of RBM39, leading to accumulation of splicing errors. We therefore asked whether RBM39 degradation plays a role in the senescence induction by palbociclib and indisulam. Indeed, we observed a degradation of RBM39 in cells treated with indisulam or the combination with palbociclib (Figure 5A). To understand if the combination effect of palbociclib and indisulam is dependent on RBM39 we used shRNAs to knock down RBM39 (Figure 5B). We observed that cells with reduced RBM39 expression and treated with palbociclib showed a reduction in growth (Figure 5C) and became positive for SA- β -gal staining (Figure 5D, E). This suggests that the senescence induction upon indisulam and palbociclib treatment is mediated through RBM39 degradation.

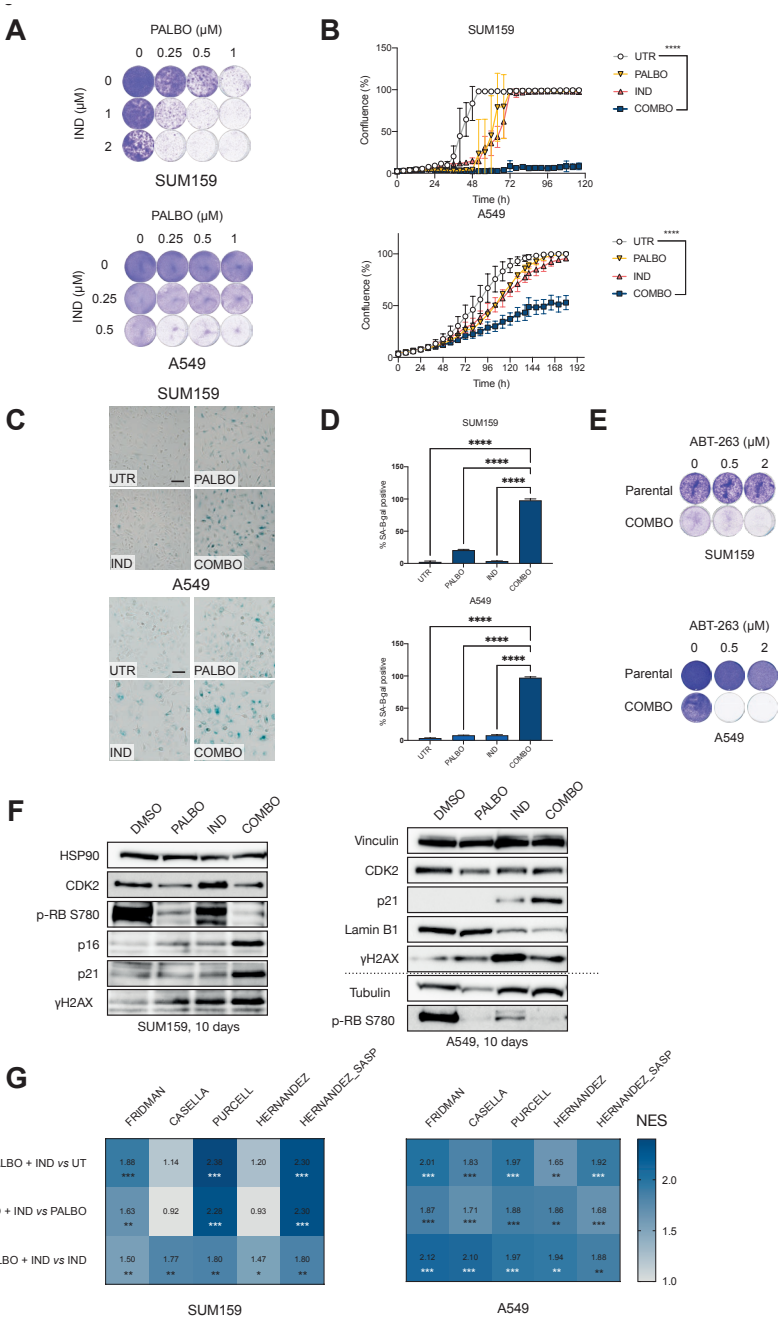


Figure 3: Indisolam phenocopies CDK2 loss and induces senescence in combination with palbociclib
A Long term colony formation assay of SUM159 and A549 cells treated with palbociclib, indisolam and the combination for 10 days. Representative of three independent experiments are shown (n=3).
B Proliferation assay of SUM159 and A549 cells treated with palbociclib, indisolam and the combination. SUM159 cells were treated with 0.5 μM of palbociclib and 2 μM indisolam and A549 with 2 μM palbociclib and 0.5 μM indisolam. Mean of three technical replicates representative of two independent experiments (n=2) is shown and error bars indicate standard deviation. The end point confluency of all conditions were

analysed using one-way ANOVA with Dunnett's post-hoc test (**** $p < 0.0001$).

C SA- β -gal staining in SUM159 and A549 cells treated with palbociclib, indisulam and combination. SUM159 were treated with 0.5 μM of palbociclib and 2 μM indisulam and A549 with 2 μM palbociclib and 0.5 μM indisulam for 10 days. Scale bar indicates 100 μm . Representative images of three independent experiments are shown (n=3).

D Quantification of SA- β -gal positive cells shown in **C**. SUM159 were treated with 0.5 μM of palbociclib and 2 μM indisulam and A549 with 2 μM palbociclib and 0.5 μM indisulam for 10 days. Bars represent mean \pm SD of triplicates. Data was analysed using one-way ANOVA with Dunnett's post-hoc test (**** $p < 0.0001$).

E Long term colony formation assay of SUM159 and A549 cells pre-treated with 0.5 μM of palbociclib plus 2 μM of indisulam for SUM159 and 2 μM of palbociclib plus 0.5 μM of indisulam for A549 for 2 weeks. Senescent and parental cells were then treated with 0.5 μM and 2 μM of ABT-263 for 1 week. Representative of two independent experiments are shown (n=2).

F Western blot analysis of SUM159 and A549 cells treated with palbociclib, indisulam and combination. SUM159 were treated with 0.5 μM of palbociclib and 2 μM indisulam and A549 with 2 μM palbociclib and 0.5 μM indisulam for 10 days. HSP90, vinculin and tubulin were used as a loading control. Dotted line indicates a separate experiment. Representative images of two independent experiments are shown (n=2).

G GSEA of previously published senescence gene sets comparing A549 and SUM159 cells treated with palbociclib, indisulam or the combination. SUM159 were treated with 0.5 μM of palbociclib and 2 μM indisulam and A549 with 2 μM palbociclib and 0.5 μM indisulam for 10 days. Comparisons of normalized enrichment scores of combination with untreated, and combination with single drugs is shown. Numbers indicate p-value (* $p < 0.05$; ** $p < 0.01$; *** $p < 0.001$).

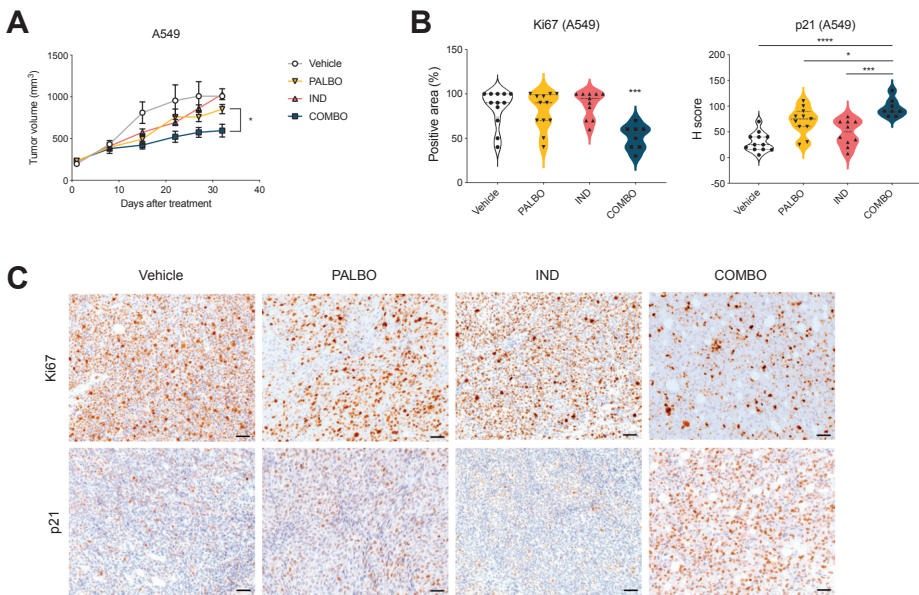


Figure 4: Combination of indisulam and palbociclib impairs tumor growth *in vivo*

A Tumor growth of A549 xenografts in NMRI nude mice. Upon tumors reaching 200 mm³ the mice were randomly assigned to treatment with vehicle, indisulam, palbociclib or combination. Palbociclib was administered by oral gavage daily at 100 mg/kg and indisulam by intraperitoneal injection three times per week at 5 mg/kg. Every group consisted of 8-12 mice. Error bars indicate SEM. Tumor volumes of palbociclib and combination treated mice at end point were analysed using unpaired t-test (* $p < 0.05$).

B Quantification of IHC staining for Ki67 and p21 of A549 tumor xenografts (n= 8-12). Positive area of the tumor was quantified in tumors treated with vehicle, palbociclib, indisulam or combination. One-way ANOVA was performed with Dunnett's post-hoc test (* $p < 0.05$; *** $p < 0.001$; **** $p < 0.0001$). For the Ki67 staining, combination is compared to vehicle or single treatments.

C Representative images from (B) of IHC staining for Ki67 and p21 of A549 tumor xenografts treated with vehicle, palbociclib, indisulam or combination. Images were taken at 20x magnification and the scale bar indicates 50 μm .

To characterize splicing errors downstream of RBM39 degradation we treated A549 and SUM159 cells with indisulam, palbociclib or the combination and collected an RNA-seq data. Upon quantifying the splicing errors (see methods) we detected an increase of splicing errors in indisulam-treated and combination-treated cells with skipped exons being the most common splicing error class detected (Figure 5F).

To elucidate how indisulam-induced splicing errors affect CDK2 activity, we made use of a CDK2 reporter construct that changes its subcellular localization depending on CDK2 activity⁴⁶. Cells with low CDK2 activity show fluorescence in the nucleus and cells with active CDK2 show fluorescence in the cytoplasm. Upon 24 hours treatment with a matrix of increasing concentrations of indisulam, palbociclib and the combination we imaged fixed cells and determined the nuclear and cytoplasmic fluorescence signal, indicative of CDK2 activity. We observed a decrease of CDK2 activity in cells treated with the combination of indisulam and palbociclib (Figure 5G). To exclude a potential confounding effect of cell cycle arrest leading to reduced CDK2 activity in the combination treatment, we performed a FACS-based experiment using the concentrations of indisulam and palbociclib that showed reduced CDK2 activity in the imaging experiment. We did not observe cell cycle differences between the single treatments and the combination after 24h (Figure 5H), which indicates that CDK2 inactivation happens upstream of cell cycle arrest.

To investigate the dynamic of CDK2 inactivation upon treatment we performed a live imaging experiment using CDK2 reporter cells. We included a positive control, a CDK1/2 inhibitor SNS-032. After beginning the imaging, the drugs were added and cells were followed through their next cell cycle. We first followed the cells that showed the fluorescence signal in the cytoplasm, indicative of active CDK2. We observed inactivation of CDK2 when we added SNS-032, but not the other drugs. Next, we followed the cells that showed fluorescence in the nucleus, and therefore had low activity of CDK2. We observed that treatments with SNS-032 and palbociclib prevented CDK2 activation, as expected. Remarkably, treatment with indisulam prevented CDK2 activation as well (Figure 5I).

When examining the effects of the combination treatment on the cell cycle proteins we observed a stronger reduction in phosphorylated RB in the combination treated cells (Figure 5J, S5B). While levels of total CDK2 were only slightly reduced, the difference is likely in the levels of active CDK2. Additionally, Cyclin E levels were increased upon palbociclib treatment, which can be explained by reduced CDK2 activity regulating cyclin E levels^{47,48}. We also observed a decrease in Cyclin H, a member of the CDK activating complex (CAK). CAK phosphorylates and activates CDK2 and we hypothesized that indisulam-induced downregulation of Cyclin H could prevent CDK2 activation. To this end, we tested the expression levels of *CCNH* upon treatment with indisulam using qPCR

and observed a downregulation in both A549 and SUM159 cells (Figure 5K). Additionally, cells with knockdown of RBM39 also showed a reduction in *CCNH* (Figure 5L). This might indicate that indisulam-induced *CCNH* downregulation prevents CDK2 activation through the CAK complex inactivation. We then analyzed the RNA-seq data generated in Figure 5F by performing a kinase enrichment analysis⁴⁹. Genes associated with CDK1 and CDK2 were over-represented in the list of differentially expressed genes in A549 and SUM159 cells treated with indisulam (Figure S5C). This further indicates that treatment with indisulam reduces the activity of CDK2. To confirm the effect of indisulam on CDK2, we overexpressed CDK2 in A549 cells using both transient transfection (Figure 5M) and stable integration of lentiviral vectors (Supplemental figure 5D). We observed an increase in proliferation rescuing the senescence induction in cells that overexpressed CDK2 compared to control cells (Figure 5N, S5E). Senescence induction was not fully rescued by CDK2 overexpression, which is in line with the observation that the activity and not only abundance of CDK2 determine senescence induction. Furthermore, CDK2 independent effects of indisulam might play a role in senescence induction as well. Taken together, indisulam downregulates *CCNH*, which prevents CDK2 activation and leads to senescence induction when combined with palbociclib (Figure 5O).

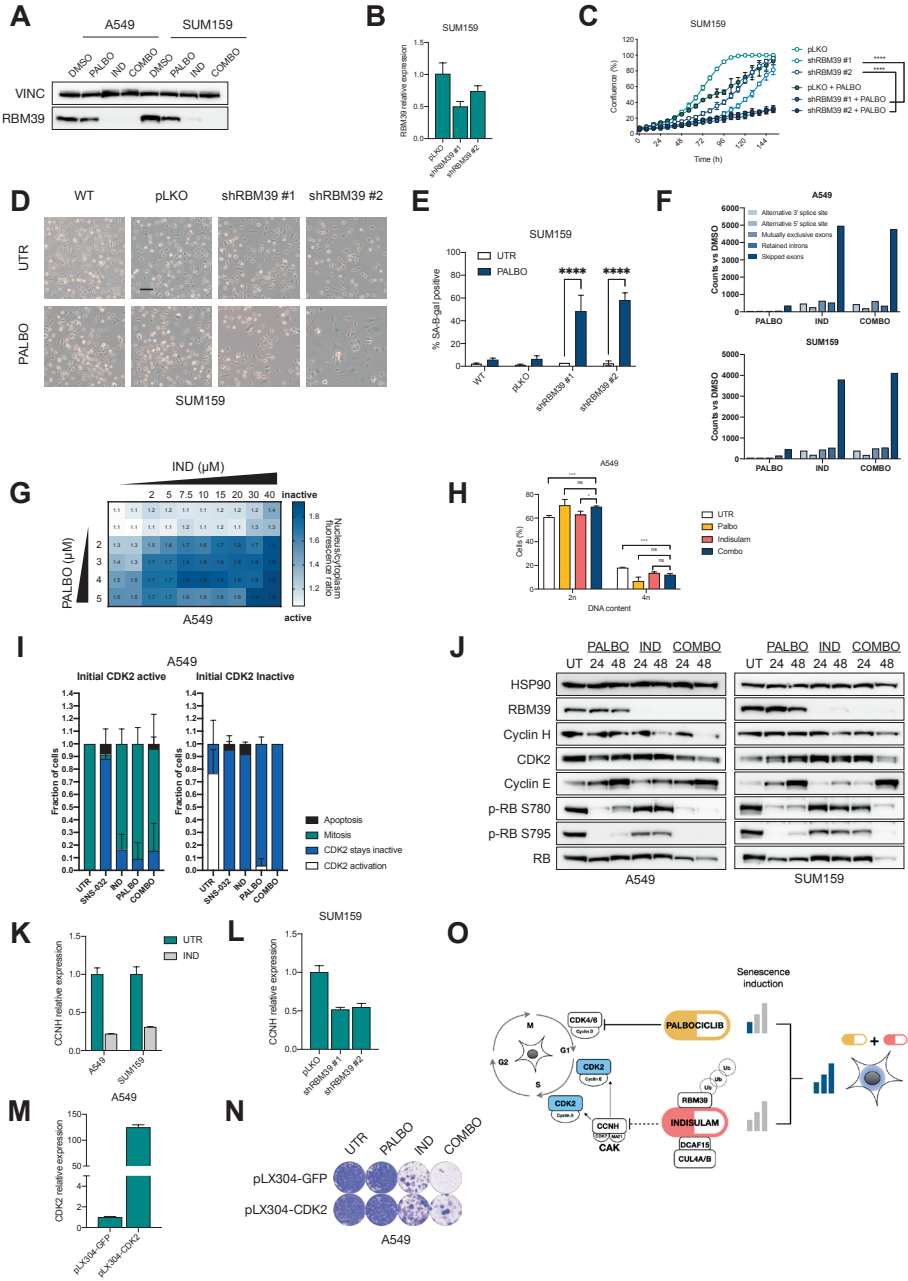


Figure 5: Indisulam prevents activation of CDK2 leading to cell cycle arrest when combined with palbociclib

A Western blot analysis of RBM39 in SUM159 and A549 cells treated with palbociclib, indisulam or combination. SUM159 were treated with 0.5 μM of palbociclib and 2 μM indisulam and A549 with 2 μM palbociclib and 0.5 μM indisulam for 12 days. Vinculin was used as a loading control. Representative images of three independent experiments are shown (n=3).

B-E RBM39 was knocked-down in SUM159 cells with two independent shRNAs.

- B** qPCR analysis of RBM39 normalized to housekeeping gene RPL13 in SUM159. Mean of three technical replicates is shown and error bars indicate standard deviation.
- C** Proliferation assay was performed in RBM39 knock-down and control SUM159 using 0.25 μM of palbociclib. Mean of three technical replicates representative of two independent experiments ($n=2$) is shown and error bars indicate standard deviation. The end point confluency of all conditions were analysed using two-way ANOVA with Šidák's post-hoc test (**** $p < 0.0001$).
- D** SA- β -gal staining in RBM39 knock-down and control SUM159 cells treated with 0.125 μM of palbociclib for 10 days. Scale bar indicates 100 μm . Representative images of two independent experiments are shown ($n=2$).
- E** Quantification of SA- β -gal positive cells shown in **D**. SUM159 cells were treated for 10 days with 0.125 μM of palbociclib. Bars represent mean \pm SD of triplicates. Data was analysed using two-way ANOVA with Šidák's post-hoc test (**** $p < 0.0001$).
- F** Quantification of splicing errors in RNA-sequencing data in A549 and SUM159 cells treated for 16h with 2 μM palbociclib, 3 μM indisulam and the combination, in technical duplicates. Bars represent counts compared to untreated samples.
- G** A549 cells expressing a CDK2 reporter DHB-iRFP and H2B-GFP were treated with a matrix of different concentrations of palbociclib (2-5 μM) and indisulam (2-40 μM). After 24h, CDK2 reporter localization and nuclei were imaged by spinning disk microscopy, and the nucleo/cytoplasmic distribution of the CDK2 reporter was analyzed using ImageJ. Matrix shows the average CDK2 reporter ratio of two independent experiments ($n=2$).
- H** Flow cytometry analysis of A549 cells treated with 5 μM of palbociclib, 40 μM of indisulam or combination for 24h. Mean of three technical replicates representative of two independent experiments ($n=2$) is shown and error bars represent standard deviation. Unpaired t-test was performed (* $p < 0.05$; ** $p < 0.01$).
- I** A549 cells expressing CDK2 reporter DHB-iRFP and H2B-GFP were treated with 10 μM of SNS-032, 40 μM of indisulam or 5 μM palbociclib and immediately imaged for 24h. CDK2 activity was quantified in cells with initial high CDK2 activity (left plot) and cells with initial low CDK2 activity (right plot). At least 10 cells per condition were quantified and results show the mean of two independent experiments ($n=2$). Error bars indicate standard deviation.
- J** Western blot analysis of A549 and SUM159 cells treated with 2 μM palbociclib, 5 μM indisulam and the combination for either 24 or 48 hours. HSP90 was used as a loading control. Representative images of three independent experiments are shown ($n=3$).
- K** qPCR analysis of A549 and SUM159 cells treated with 3 μM of indisulam for 24h. CCNH expression was normalized to the housekeeping gene RPL13. Mean of three technical replicates is shown and error bars indicate standard deviation.
- L** qPCR analysis of SUM159 cells harbouring shRBM39 or control cells for CCNH (as in B). Expression was normalised to the housekeeping gene RPL13. Mean of three technical replicates is shown and error bars indicate standard deviation.
- M** qPCR analysis of CDK2 overexpressing A549 cells compared to GFP control cells. Expression was normalized to the housekeeping gene RPL13. Mean of three technical replicates is shown and error bars indicate standard deviation.
- N** Long term colony formation assay of CDK2 and GFP overexpressing A549 cells treated with 0.5 μM palbociclib, 0.5 μM indisulam and the combination for 10 days.
- O** Schematic overview of palbociclib and indisulam senescence induction. Palbociclib inhibits CDK4/6 leading to weak senescence induction and increased dependence on CDK2 for cell cycle progression. Indisulam induces RBM39 degradation through DCAF15 and CUL4A/B leading to splicing errors and downregulation of CCNH. As CCNH is part of CDK2 activating CAK complex, indisulam treatment prevents the activation of CDK2 through CAK. Combination of palbociclib and indisulam therefore induces strong senescent phenotype in cancer cells.

DISCUSSION

Since proliferation of cancer cells depends heavily on the core components of the cell cycle machinery, inhibitors of CDKs could have significant anticancer activity in many tumor types. However, translating the success of CDK4/6 inhibitors from HR+ breast cancer to other cancer types has been hampered by intrinsic resistance^{23,50}. Here we identify a treatment strategy that exploits the synergy between CDK2 loss (i.e., indisulam treatment) and palbociclib treatment in induction of senescence in a diverse panel of cell lines.

Genetic screens are a powerful tool to identify genetic dependencies in an unbiased manner⁵¹. Here, we identified *CDK2* loss as an enhancer of the palbociclib effect using genetic screens in three TNBC cell lines. We further validated this interaction in a diverse panel of cell lines, demonstrating that this synergy shows little context dependency. The interaction between *CDK2* loss and CDK4/6 inhibition is not surprising, as CDK2 acts downstream of CDK4/6 in the cell cycle progression. Furthermore, the majority of clinically relevant resistance mechanisms to CDK4/6 inhibition, such as loss of RB and overexpression of *CCNE*²⁰, could be circumvented by CDK2 inhibition. As such, *CDK2* depletion was previously shown to re-sensitize both CDK4/6 inhibitor sensitive and resistant cells^{22,24,43,52,53}.

Unfortunately, the lack of a specific CDK2 inhibitor has until now prevented exploiting the synergy between CDK2 inhibition and CDK4/6 inhibition. In spite of this, multiple targeting strategies were previously described to increase sensitivity to CDK4/6 inhibition, such as using a multi CDK inhibitor roscovitine²⁴, knock-in of analog-sensitive CDK2²² and use of triple CDK2/4/6 inhibitor PF-06873600^{43,44}. Unfortunately, the use of roscovitine in the clinic is hindered by off-target effects and toxicity, and analog-sensitive CDK2 lacks translational potential. Even though PF-06873600 is in clinical development (phase 1 clinical trial ongoing: NCT03519178), the compound also inhibits CDK1, which might lead to toxicity as seen with other multi-CDK inhibitors⁴³. Interestingly, comparing palbociclib to two other CDK4/6 inhibitors abemaciclib and ribociclib shows that abemaciclib is more effective compared to palbociclib and ribociclib, possibly due to the notion that it also targets CDK2⁴⁵. However, both intrinsic and acquired resistance are still an issue, indicating a need for a different therapeutic strategy. We propose using the indirect CDK2 inhibitor indisulam, which has previously shown a favorable toxicity profile in the clinic. We demonstrate that combination of palbociclib and indisulam induces senescence in a diverse cell line panel, which points to a broad applicability across tumor types. Additionally, our preliminary data indicate that the combination can be effective in vivo.

Even though indisulam was described as an indirect CDK2 inhibitor, later studies revealed that it targeted a splicing factor—RBM39—for degradation. Interestingly, we observed an effect of indisulam on CDK2 activity only in cells where CDK2 is initially inactive, indicating that indisulam prevents CDK2 activation. Regulation of CDK2 activity is based on its interaction with cyclins, removal of inhibitory phosphorylation by CDC25 and activating phosphorylation by the CDK Activating Kinase (CAK) complex. We observed that cyclin H, which is a part of the CAK complex, is downregulated upon indisulam treatment in an RBM39 dependent manner. As we observed no splicing errors in *CCNH* transcripts or other CDK2 regulators, it is still unclear how reduction of RBM39 leads to *CCNH* downregulation. As *CCNH* is an essential gene, loss of function genetic experiments are technically challenging to perform. Additionally, other CDKs might be involved in senescence induction through indisulam since CAK regulates CDK1, 4 and 6 in addition to CDK2. Furthermore, as activity and not amount of CDK2 seems to play a role in indisulam sensitivity, overexpression of CDK2 is at best expected to partially rescue the senescence induction, which is indeed what we observed here. Lastly, we observed accumulation of thousands of splicing errors in cells treated with indisulam, which might sensitize the cells to palbociclib in CDK2 independent manner and further explain the partial rescue of CDK2 overexpression.

Combining palbociclib with indisulam might be a potential treatment strategy for cell types that are intrinsically resistant to palbociclib. In addition, acquired resistance to palbociclib has been shown to be reversed by depleting CDK2. For example, loss of RB leads to resistance to palbociclib and the combination of palbociclib with a MEK inhibition²⁶. However, RB deficient cells are still sensitive to knockdown of CDK2⁵³. It is therefore likely that the combination of palbociclib and indisulam would still be effective in palbociclib resistant cells, although the mechanism of senescence induction in RB deficient cells is not yet well understood. Furthermore, recent reports on Cyclin D regulation described *AMBRA1* loss as a resistance mechanism to CDK4/6 inhibition⁵⁴, but as those cells still depend on CDK2 activity, combination with indisulam could still be effective. Senescence induction is increasingly in focus as a potential cancer therapeutic strategy, supported by the findings that senolytic compounds can be effective in eradicating senescent cancer cells⁶. Here, we have shown that senescence induction by palbociclib and indisulam sensitizes the cells to the established senolytic drug navitoclax. Finally, senescent cells attract immune cells, and together with the notion that indisulam induced splicing errors could lead to generation of neoantigens, the combination of senescence induction and immunotherapy might be a potential future treatment strategy^{26,55}.

METHODS

Cell lines

TNBC cell line CAL-51 was grown in DMEM (Gibco) supplemented with 20% fetal bovine serum (FBS, Serana), 1% penicillin-streptomycin (P/S, Gibco) and 2mM L-glutamine (Gibco). TNBC cell line CAL-120 was grown in DMEM supplemented with 10% FBS, 1% P/S and 2 mM L-glutamine. TNBC cell line HCC1806, lung cancer cell lines A549 and H2122, colon cancer cell lines DLD-1 and RKO were grown in RPMI (Gibco) supplemented with 10% FBS, 1% P/S and 2 mM L-glutamine. TNBC cell line SUM159 was grown in DMEM/F12 (Gibco) supplemented with 10% FBS, 1% P/S, 5 µg/ml insulin (Sigma-Aldrich) and 1µg/ml hydrocortisone (Sigma-Aldrich).

HCC1806, A549, RKO, H2122 and DLD-1 were purchased from ATCC. SUM159 was a gift from Metello Innocenti (NKI, Amsterdam). CAL-51 and CAL-120 were obtained from DSMZ. All cell lines were regularly tested for mycoplasma contamination using a PCR assay and STR profiled (Eurofins).

Compounds and antibodies

Palbociclib, indisulam and ABT-263 were purchased from MedKoo (Cat:#123215, #201540 and #201970). PF-06873600 was purchased from Selleck chem. Antibodies against CDK2 and tubulin were purchased from Abcam. Antibodies against vinculin and p-H2AX S139 were purchased from Sigma Aldrich. Antibodies against p-RB S780, p-RB S795, RB (9309-4H1), Lamin B1, Cyclin H and Cyclin E were purchased from Cell Signalling Technology. Antibodies against HSP90 and p21 were purchased from Santa Cruz Biotechnology. Antibody against RBM39 was purchased from Atlas Antibodies. Antibody against p16 was purchased from Proteintech.

Kinome dropout shRNA screens

TNBC cell lines CAL-51, CAL-120 and HCC1806 were screened using a kinome shRNA library targeting 518 human kinases and 17 kinase-related genes. The kinome library was assembled from the RNAi Consortium (TRCHs 1.5 and 2.0) shRNA collection and included 243 hairpins targeting essential and 272 targeting non-essential genes. Upon generating lentiviral shRNA vectors, CAL-51, CAL-120 and HCC1806 cells were infected using a low infection efficiency of <30%, reference sample t=0 was collected and cells were then cultured in the presence or absence of palbociclib (0.4 µM for CAL-51, 1 µM for CAL-120 and 0.2 µM for HCC1806), while maintaining 1000x coverage of the library. shRNA sequences were then recovered by PCR from genomic DNA, and the abundance was quantified by deep sequencing. The analysis was performed using DESeq⁵⁶. Hit selection was done in two steps: initially the hits were selected based on the comparison of treated to untreated arm with the criteria of at least two shRNAs per gene with log₂ fold change <-1, FDR <0.1 and baseMeanA > 100 and no hit shRNAs in the opposite direction. To exclude the shRNAs that are increased in the untreated condition, instead

of decreased in treated compared to reference t=0 sample, we performed an additional selection step in which sgRNA should have log₂ fold change < -1 in treated condition compared to reference t=0 condition. Hits that overlapped between the three cell lines were prioritized for validation.

Plasmids

The lentiviral shRNA vectors were selected from the arrayed TRC human genome-wide shRNA collection in pLKO backbone. shRNA targeting CDK2 #1: CTATGCCTGATTACAAGCCAA, shRNA targeting CDK2 #2: GCCCTCTGAACTTGCCTTAAA, shRNA targeting RBM39 #1: GCCGTGAAAGAAAGCGAAGTA, shRNA targeting RBM39 #2: GCTGGACCTATGAGGCTTTAT. Single gRNAs were cloned into LentiCRISPR 2.1 plasmid⁵⁷ by BsmBI (New England BioLabs) digestion and Gibson Assembly (New England BioLabs); control sgRNA: ACGGAGGCTAAGCGTCGCAA, sgRNA targeting CDK2 #1: GTTCGTA CTACACCCATGG, sgRNA targeting CDK2 #2: CATGGGTGTAAGTACGAACG. For overexpression experiments pLX304-Blast-V5 were used, with either GFP or CDK2 (ID ccsbBroad304_00276). Additionally, pCMV-GFP (Addgene #11153) and pCMV-CDK2⁵⁸ were used to transiently transfect the target cells.

Lentiviral transduction

Second generation lentivirus packaging system consisting of psPAX2 (Addgene #12260), pMD2.G (Addgene #12259) and pCMV-GFP as transfection control (Addgene #11153) was used to produce lentivirus particles. After transient transfection in HEK293T cells using polyetylenamine (PEI), lentiviral supernatant was filtered and used to infect target cells using 8 mg/ml polybrene. After infection, the cells were selected with 2 mg/ml puromycin or 10 mg/ml blasticidin. After 48-72h or until non-transduced control cells were dead, the selection was complete.

RNA sequencing and GSEA

Total RNA was extracted with RNeasy mini kit (Qiagen, cat# 74106) including a column DNase digestion (Qiagen, cat#79254), according to the manufacturer's instructions. Quality and quantity of total RNA was assessed by the 2100 Bioanalyzer using a Nano chip (Agilent, Santa Clara, CA). Total RNA samples having RIN>8 were subjected to library generation. Strand-specific libraries were generated using the TruSeq Stranded mRNA samples preparation kit (illumine Inc., San Diego, RS-122-2101/2) according to manufacturer's instructions (Illumina, part #15031047 Rev.E). Briefly, polyadenylated RNA from intact total RNA was purified using oligo-dT beads. Following purification, the RNA was fragmented, random primed and reverse transcribed using SuperScript II Reverse Transcriptase (Invitrogen, part # 18064-014) with the addition of Actinomycin D. Second strand synthesis was performed using Polymerase I and RNaseH with replacement of dTTP for dUTP. The generated cDNA fragments were 3' end adenylated and ligated to Illumina Paired-end sequencing adapters and subsequently amplified by

12 cycles of PCR. The libraries were analyzed on a 2100 Bioanalyzer using a 7500 chip (Agilent, Santa Clara, CA), diluted and pooled equimolar into a multiplex sequencing pool. The libraries were sequenced with single-end 65bp reads on a HiSeq 2500 using V4 chemistry (Illumina inc., San Diego).

For the analysis, reads were first aligned to a reference genome (hg38) and the datasets were normalized for sequence depth using a relative total size factor. We then performed gene set enrichment analysis (GSEA) using GSEA software⁵⁹ with log2FoldChange ranked list as an input. The GSEA preranked tool was used to run the analysis. We used two senescence gene signatures^{2,39} as well as gene sets of genes upregulated in senescence from^{40,41} to assess enrichment of senescence-associated genes (Table S1).

In genetic experiments we compared sgCDK2 cells treated with palbociclib with untreated cells and for pharmacological experiments cells treated with palbociclib and indisulam to untreated cells or single treatments. When using PF-0687360 we compared cells treated with the compound to untreated cells. All experiments were performed in duplicates. The *P*-value estimates the statistical significance of the enrichment score and is shown in the figure, unless $P < 0.001$.

Splicing error quantification

The RNA was isolated and libraries were prepared as described above. The libraries were sequenced with 75bp paired-end reads on a NextSeq550 using the High Output Kit v2.5, 150 Cycles (Illumina Inc., San Diego). For the analysis, sequences were demultiplexed and adapter sequences were trimmed from using SeqPurge⁶⁰. Trimmed reads were aligned to GRCh38 using Hisat2⁶¹ using the prebuilt genome_snp_tran reference. Splice event detection was performed using rMats version 4.0.2 by comparing the replicates of the treated groups to the replicates of the untreated group⁶². rMats events in the different categories were considered significant when the following thresholds were met: having a minimum of 10 reads, an FDR less than 10% and an inclusion-level-difference greater than 10%, as described earlier⁶³.

Kinase enrichment analysis

RNA-seq data generated from the splicing experiment was filtered for adjusted *p*-value <0.05 and analysed using the Enrichr software⁶⁴ using kinase enrichment analysis⁴⁹.

CDK2 activity experiments

CDK2 reporter DHB-iRFP was modified from DHB-Venus (Addgene #136461)⁴⁶. Venus was replaced for iRFP713 through Gibson Assembly. In brief, iRFP713 was amplified adding sequence homology and assembled into the BamHI and HpaI sites of the original CDK2 reporter plasmid. The following primers were used to amplify iRFP713; F:AC-CGATAATCAAGAACTGGATCCGGGGCCAGGGCAGCGGCATGGCGGAAGGCTCCGTC

R: GTTGATTATCGATAAGCTTGATCCCTCGATGCGGCCGCTTACTCTTCCATCACGCCGATC.

A549 cells were stably transduced with a lentiviral vector containing H2B-GFP (Addgene #25999) and a lentiviral vector containing DHB-iRFP, and subsequently GFP/iRFP double positive cells were isolated by FACS. In order to determine CDK2 activity following 24h drug treatment, cells were seeded in 96 well plate, treated with indisulam and palbociclib for 24h and then imaged on a spinning disc microscope using Andor 505 Dragonfly system equipped with 20x 0.75 NA objective and Zyla 4.2+, sCMOS camera. CDK2 activity was determined by calculating the nucleo/cytoplasmic ratio of the CDK2 reporter, using a custom macro for ImageJ, as described before⁶⁵. For real-time analysis of CDK2 activity immediately following drug treatment, cells were seeded in chambered covered slides (LabtekII), and subsequently imaged for 25h. Inhibitors were added following the first round of image acquisition. Imaging was performed using a Deltavision Elite (Applied Precision) that was maintained at 5% CO₂ and 37°C, equipped with a 20x 0.75 NA lens (Olympus) and cooled Hamamatsu ORCA R2 Black and White CCD-camera.

Flow cytometry

A549 cells were treated for 24h with indicated doses of palbociclib and indisulam. Cells were then harvested, fixed in ice cold 70% ethanol and stained with DAPI 8 µg/ml in PBS. Samples were acquired with LSRFortessa (BD Biosciences) and analysis was performed with FlowJo10 software. Single cells were gated via DAPI-A and DAPI-H signals and DNA content was gated based on DAPI-A histogram profile.

Western blot

Cells were lysed using RIPA buffer and protein was extracted and quantified using BCA assay (Pierce). Loading buffer and reducing agent (both Thermo Fisher) were added to the samples, which were then boiled for 5 min at 95°C. The samples were resolved on a 5-15% Bis-Tris gel (Thermo Fisher) followed by blotting. Membranes were incubated with primary antibodies diluted to 1:1000 in 5% BSA. Secondary antibodies were used at 1:10000 dilution and were purchased from Biorad. Signal was visualized by the ECL solution (Biorad) using the ChemiDoc Imaging system (Biorad). To quantify, the intensity of each band was measured using ImageJ and normalized to the loading control and untreated condition. All uncropped Western blot images are provided as supplemental material (Supplemental Images 1).

Kinase inhibition assay

Inhibition of CDK/cyclin complexes by indisulam was measured by Z'LYTE - SelectScreen Kinase Profiling Services (ThermoFisher). Briefly, CDK/cyclin complexes were incubated with indisulam, substrates and ATP. The kinase activity of the CDK/cyclin complex was measured as ATP consumption, as described in detail previously⁴⁵.

Quantitative reverse transcription PCR

RNA was extracted using Isolate II Mini kit (Bioline), following manufacturer's instructions. cDNA was generated using SensiFast cDNA synthesis kit (Bioline) following manufacturer's instructions. For qPCR reaction 1 µg of cDNA was used with SensiFast Sybr Lo-Rox mix (Bioline) and respective primer pair. All reactions were performed in triplicates and the results were analyzed using the deltadelta Ct method. The sequences of primers used are as follows:

RPL13 forward GCCCCAGCAGTACCTGTTTA, *RPL13* reverse AGATGGCGGAGGTGCAG, *RBM39* forward GTCGATGTTAGCTCAGTGCCTC, *RBM39* reverse ACGAAGCATATCTTCAGT-TATG, *CCNH* forward TGTTCCGGTGTTTAAGCCAGCA, *CCNH* reverse TCCTGGGGTGATATTC-CATTACT.

Senescence associated B-galactosidase staining

Cells were stained using the Senescence Cells Histochemical Staining kit (CS0030) from Sigma Aldrich according to the manufacturer's instructions. Stained cells were imaged at 100x magnification and at least 3 pictures per condition were taken. The staining was quantified by counting at least 100 cells from 3 independent images. To evaluate the increase in SA-β-gal positive cells in combination treatment compared to individual drug treatments we performed one-way ANOVA comparing each treatment group to the combination.

Colony formation assay and proliferation assay

Cells were plated in 6-well plates with densities between 10-40000 cells per well, depending on the cell line. Medium and drugs were refreshed every 3-4 days. After 10 days the cells were fixed with 4% formaldehyde (Millipore) in PBS, stained with 2% Crystal Violet (Sigma) in water and scanned. For proliferation assays, cells were plated in 96-well plates with densities between 500-2000 cells per well, depending on cell line. Plates were incubated at 37°C and images were taken every 4 hours using the IncuCyte® live cell imaging system. Medium and drugs were refreshed every 3-4 days. Confluency was calculated to generate growth curves.

In vivo experiments

All animal experiments were approved by the Animal Ethics Committee of the Netherlands Cancer Institute and were performed in accordance with institutional, national and European guidelines for Animal Care and Use. CDK2 KO clones used in vivo were generated through transient transfection of a plasmid containing Cas9 and gRNA sequences, followed by the brief puromycin selection and characterisation of the clones. For the genetic experiments one million of CAL-51 CDK2 KO single cell clone or control cells in PBS were mixed 1:1 with matrigel and injected orthotopically in the mammary fat pad of 8 weeks female NMRI nude mice (JAX labs), 5-6 mice per group. Furthermore,

one million of A549 CDK2 KO single cell clones or control cells in PBS were mixed 1:1 with matrigel and injected subcutaneously in the right flank of NMRI nude mice, 5-6 mice per group. Tumor volume was monitored twice a week and tumor volume was calculated based on the calliper measurements following modified ellipsoidal formula (tumor volume = $\frac{1}{2}$ [length x width²]). For the intervention experiment, one million of A549 cells in PBS were mixed 1:1 with matrigel and injected subcutaneously in the right flank of NMRI nude mice. Upon reaching 200 mm³, mice were randomized to four treatment groups of 8-12 mice per group: vehicle, indisulam, palbociclib or combination. Palbociclib (dissolved in 50 mM sodium lactate) was administered by oral gavage daily at 100 mg/kg and indisulam (dissolved in 3.5% DMSO, 6.5% Tween 80, 90% saline) by intraperitoneal injection three times per week at 5 mg/kg. Four mice were excluded from the study due to complications of daily intraperitoneal injections (peritonitis). Anesthesia was administered in a form of isoflurane (3% induction, 2% maintenance) and analgesia in form of carprofen. The mice were sacrificed using CO₂. The following humane end points were applied according to the Code of Practice Animal Experiments in cancer research to alleviate suffering:

- Waiting for spontaneous death is NOT allowed;
- Animal loses more than 15% of body weight within 2 days;
- Animal has lost more than 20% of body weight since start of experiment;
- Animal has circulation or breathing problems;
- Animal shows aberrant behaviour/movement;
- The tumour causes clinical symptoms (as a result of location, invasive growth or ulceration);
- The tumour has reached the size of more than 10% of the normal bodyweight or has a diameter of 15 mm (is approx. 2 cm³).

Immunohistochemistry

Tumors were collected and fixed in EAF fixative (ethanol/acetic acid/formaldehyde/saline at 40:5:10:45 v/v) and embedded in paraffin. For immunohistochemistry, 4 μ m-thick sections were made on which antibodies against Ki67 and p21 were applied. The sections were reviewed with a Zeiss Axioskop2 Plus microscope (Carl Zeiss Microscopy) and images were captured with a Zeiss AxioCam HRc digital camera and processed with AxioVision 4 software (both from Carl Zeiss Vision). Histological samples were analyzed by an experienced pathologist. Scoring was performed by quantifying positive area for Ki67 and H-score for p21.

PK/PD experiment for PD and IN

Blood was collected either from the tail vein or by cardiac puncture at different time points indicated in Supplementary Figure 4C and D. Samples were collected on ice using tubes with potassium EDTA as anticoagulant. After cooling, tubes were centrifuged for

10 min 5000xg 4°C to separate the plasma fraction, which was then transferred into clean vials and stored at -20°C until analysis. Sample pre-treatment was accomplished by mixing 5 µL (plasma) with 60 µL of formic acid in acetonitrile (1 + 99) containing the internal standard. After centrifugation, the clear supernatant was diluted 1 + 8 with water and 5 µL was injected into the LC-MS/MS system. The samples were assayed twice by liquid chromatography triple quadrupole mass spectrometry (LC-MS/MS) using an API4000 detector (Sciex). Indisulam is detected in negative ionization mode (MRM: 384.2/171.9) and palbociclib in positive ionization mode (MRM: 448.5/320.0). In both cases, LC separation was achieved using a Zorbax Extend C18 column (100 x 2.0 mm: ID). Mobile phase A and B comprised 0.1% formic acid in water and methanol, respectively. The flow rate was 0.4 ml/min and a linear gradient from 20%B to 95%B in 2.5 min, followed by 95%B for 2 min, followed by re-equilibration at 20%B for 10 min was used for elution.

STATISTICAL ANALYSIS

Unpaired t-test and ANOVA were performed with Graphpad Prism (v8.4.3).

Materials availability

Plasmid generated in this study is available from the corresponding authors upon request.

Data and Code availability

Raw RNA-sequencing data is available in GEO, accession numbers:

GSE197600 - Transcriptomic expression of A549 CDK2 KO cells treated or untreated with palbociclib

GSE197601 - Transcriptomic expression of SUM159 cells treated with palbociclib and indisulam

GSE197602 - Transcriptomic expression of A549 and SUM159 cells treated with palbociclib and indisulam

GSE197603 - Transcriptomic expression of A549 cells treated with palbociclib and indisulam or PF-06873600 and SUM159 cells treated with PF-06873600

GSE197604 - Senescence associated gene signatures.

ACKNOWLEDGEMENTS

We would like to thank Artur Burylo, Natalie Proost, Jordi van Iersel and Marcio Sousa for help with experiments and Katrien Berns for critical discussion on screening techniques. We also thank the NKI Bioimaging facility, Genomics core facility and pre-Clinical Intervention Unit for their technical support.

AUTHOR CONTRIBUTIONS

Conceptualization, Z.P, J.L.J, R.B and R.L.O.; Methodology, L.K.; Software C.L., A.V. and

K.G.; Validation, Z.P. and R.L.O.; Formal analysis, Z.P., G.D.C., C.L., A.V., K.G., Le. W., F.J., J.Y.S. and R.L.O.; Investigation, Z.P., J.L.J., L.K., G.D.C., Le.W., F.J., K.G., A.S., Li.W., J.Y.S. and R.L.O.; Data curation, C.L. and A.V.; Writing - Original Draft, Z.P., R.B. and R.L.O.; Writing - Review and Editing, J.L.J., F.J., A.S., Li.W., O.vT. and R.L.B.; Visualization, Z.P., L.K., G.D.C., C.L., A.V., Le.W., F.J., K.G. and R.L.O.; Supervision, M.vdV., O.vT., R.H.M., R.L.B. and R.B.; Funding Acquisition, R.H.M and R.B.

COMPETING INTERESTS

R.B is the founder of the company Oncosence (<https://www.oncosence.com>), which aims to develop senescence-inducing and senolytic compounds to treat cancer. This does not alter our adherence to PLOS ONE policies on sharing data and materials.

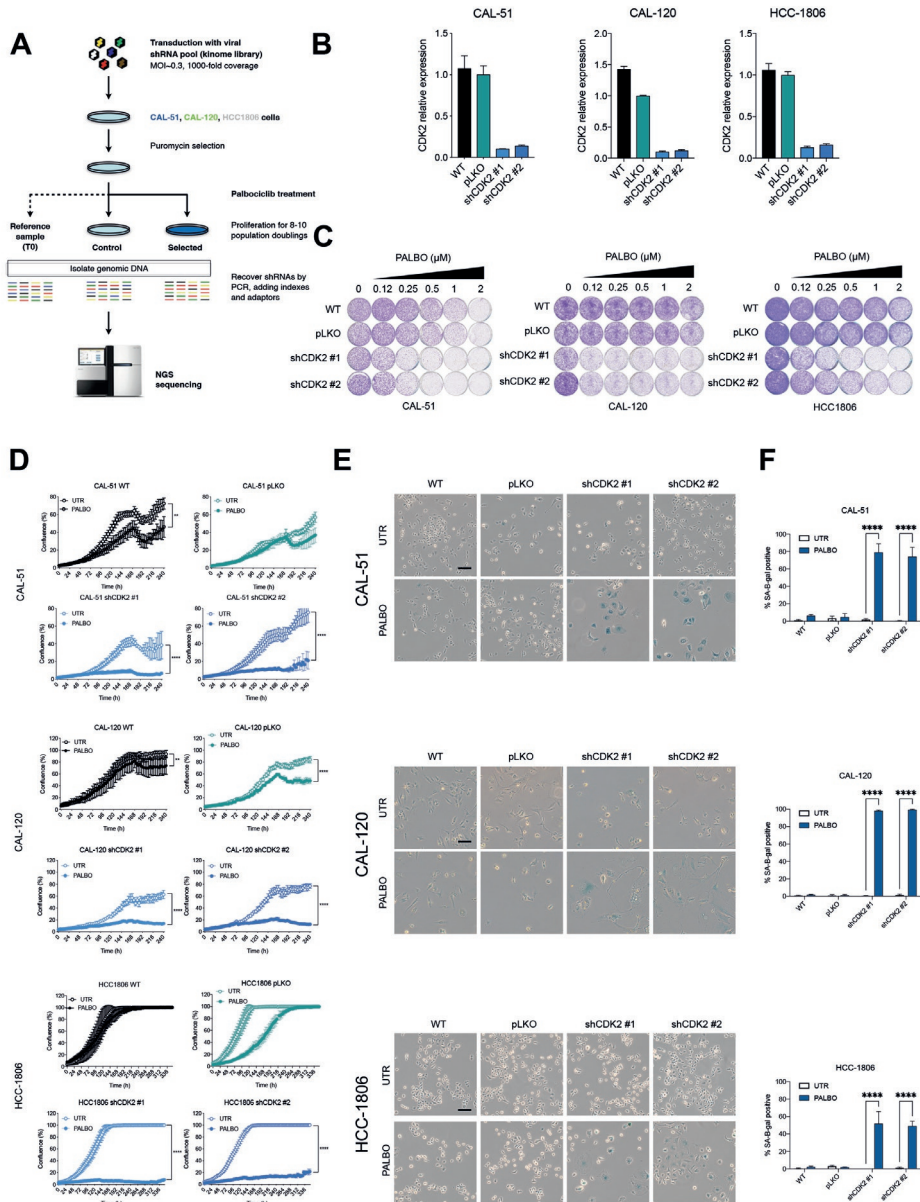
REFERENCES

1. Ewald, J. A., Desotelle, J. A., Wilding, G. & Jarrard, D. F. Therapy-induced senescence in cancer. *J. Natl. Cancer Inst.* **102**, 1536–1546 (2010).
2. Fridman, A. L. & Tainsky, M. A. Critical pathways in cellular senescence and immortalization revealed by gene expression profiling. *Oncogene* **27**, 5975–5987 (2008).
3. Milanovic, M. *et al.* Senescence-associated reprogramming promotes cancer stemness. *Nature* vol. 553 96–100 (2018).
4. Wang, C. *et al.* Inducing and exploiting vulnerabilities for the treatment of liver cancer. *Nature* **574**, 268–272 (2019).
5. Guerrero, A. *et al.* Cardiac glycosides are broad-spectrum senolytics. *Nat Metab* **1**, 1074–1088 (2019).
6. Saleh, T. *et al.* Therapy-Induced Senescence: An ‘Old’ Friend Becomes the Enemy. *Cancers* **12**, 822 (2020).
7. Guan, X. *et al.* Stromal Senescence By Prolonged CDK4/6 Inhibition Potentiates Tumor Growth. *Mol. Cancer Res.* **15**, 237–249 (2017).
8. Muñoz-Espín, D. *et al.* A versatile drug delivery system targeting senescent cells. *EMBO Mol. Med.* **10**, (2018).
9. Miettinen, T. P. *et al.* Thermal proteome profiling of breast cancer cells reveals proteasomal activation by CDK4/6 inhibitor palbociclib. *EMBO J.* **37**, (2018).
10. Torres-Guzmán, R. *et al.* Preclinical characterization of abemaciclib in hormone receptor positive breast cancer. *Oncotarget* **8**, 69493–69507 (2017).
11. Iyengar, M. *et al.* CDK4/6 inhibition as maintenance and combination therapy for high grade serous ovarian cancer. *Oncotarget* **9**, 15658–15672 (2018).
12. Malumbres, M. & Barbacid, M. To cycle or not to cycle: a critical decision in cancer. *Nat. Rev. Cancer* **1**, 222–231 (2001).
13. Sledge, G. W. *et al.* MONARCH 2: Abemaciclib in Combination With Fulvestrant in Women With HR+/HER2– Advanced Breast Cancer Who Had Progressed While Receiving Endocrine Therapy. *J. Clin. Orthod.* **35**, 2875–2884 (2017).
14. Rugo, H. S. *et al.* Impact of palbociclib plus letrozole on patient-reported health-related quality of life: results from the PALOMA-2 trial. *Ann. Oncol.* **29**, 888–894 (2018).
15. Hortobagyi, G. N. *et al.* First-line ribociclib (RIB) + letrozole (LET) in hormone receptor-positive (HR+), HER2-negative (HER2–) advanced breast cancer (ABC): MONALEESA-2 biomarker analyses. *J. Clin. Orthod.* **36**, 1022–1022 (2018).
16. Sherr, C. J., Beach, D. & Shapiro, G. I. Targeting CDK4 and CDK6: From Discovery to Therapy. *Cancer Discov.* **6**, 353–367 (2016).
17. Schettini, F. *et al.* CDK 4/6 Inhibitors as Single Agent in Advanced Solid Tumors. *Front. Oncol.* **8**, 608 (2018).
18. Gopalan, P. K. *et al.* A phase II clinical trial of the CDK 4/6 inhibitor palbociclib (PD 0332991) in previously treated, advanced non-small cell lung cancer (NSCLC) patients with inactivated CDKN2A. *Journal of Clinical Oncology* vol. 32 8077–8077 (2014).
19. Konecny, G. E. *et al.* A multicenter open-label phase II study of the efficacy and safety of palbociclib a cyclin-dependent kinases 4 and 6 inhibitor in patients with recurrent ovarian cancer. *J. Clin. Orthod.* **34**, 5557–5557 (2016).
20. Turner, N. C. *et al.* Cyclin E1 Expression and Palbociclib Efficacy in Previously Treated Hormone Receptor-Positive Metastatic Breast Cancer. *J. Clin. Oncol.* **37**, 1169–1178 (2019).
21. Morris-Hanon, O. *et al.* Palbociclib Effectively Halts Proliferation but Fails to Induce Senescence in Patient-Derived Glioma Stem Cells. *Mol. Neurobiol.* **56**, 7810–7821 (2019).
22. Fassl, A. *et al.* Increased lysosomal biomass is responsible for the resistance of triple-negative breast cancers to CDK4/6 inhibition. *Sci Adv* **6**, eabb2210 (2020).
23. Haines, E. *et al.* Palbociclib resistance confers dependence on an FGFR-MAP kinase-mTOR-driven pathway in KRAS-mutant non-small cell lung cancer. *Oncotarget* **9**, 31572–31589 (2018).
24. Herrera-Abreu, M. T., Palafox, M., Asghar, U. & Rivas, M. A. Early adaptation and acquired resistance to CDK4/6 inhibition in estrogen receptor-positive breast cancer. *Cancer Res.* (2016).
25. Vora, S. R. *et al.* CDK 4/6 inhibitors sensitize PIK3CA mutant breast cancer to PI3K inhibitors. *Cancer Cell* **26**, 136–149 (2014).
26. Ruscetti, M., Leibold, J., Bott, M. J. & Fennell, M. NK cell-mediated cytotoxicity contributes to tumor control by a cytostatic drug combination. (2018).
27. Lee, M. S. *et al.* Efficacy of the combination of MEK and CDK4/6 inhibitors in vitro and in vivo in KRAS mutant colorectal cancer models. *Oncotarget* **7**, 39595–39608 (2016).
28. Haddad, R. I. *et al.* A phase II clinical and pharmacodynamic study of E7070 in patients with metastatic, recurrent, or refractory squamous cell carcinoma of the head and neck: modulation of retinoblastoma protein phosphorylation by a novel chloroindolyl sulfonamide cell cycle inhibitor. *Clin. Cancer Res.* **10**, 4680–4687 (2004).
29. Smyth, J. F. *et al.* Phase II study of E7070 in patients with metastatic melanoma. *Ann. Oncol.* **16**, 158–161 (2005).
30. Talbot, D. C. *et al.* A Randomized Phase II Pharmacokinetic and Pharmacodynamic Study of Indisulam as Second-Line Therapy in Patients with Advanced Non-Small Cell Lung Cancer.

- Clin. Cancer Res.* **13**, 1816–1822 (2007).
31. Punt, C. J. A. *et al.* Phase I and pharmacokinetic study of E7070, a novel sulfonamide, given at a daily times five schedule in patients with solid tumors. A study by the EORTC-Early Clinical Studies Group (ECSG). *Annals of Oncology* vol. 12 1289–1293 (2001).
 32. Raymond, E. *et al.* Phase I and pharmacokinetic study of E7070, a novel chloroindolyl sulfonamide cell-cycle inhibitor, administered as a one-hour infusion every three weeks in patients with advanced cancer. *J. Clin. Oncol.* **20**, 3508–3521 (2002).
 33. Dittrich, C. *et al.* Phase I and pharmacokinetic study of E7070, a chloroindolyl-sulfonamide anticancer agent, administered on a weekly schedule to patients with solid tumors. *Clin. Cancer Res.* **9**, 5195–5204 (2003).
 34. Yamada, Y. *et al.* Phase I pharmacokinetic and pharmacogenomic study of E7070 administered once every 21 days. *Cancer Sci.* **96**, 721–728 (2005).
 35. Han, T. *et al.* Anticancer sulfonamides target splicing by inducing RBM39 degradation via recruitment to DCAF15. *Science* **356**, (2017).
 36. Prahallad, A. *et al.* Unresponsiveness of colon cancer to BRAF(V600E) inhibition through feedback activation of EGFR. *Nature* **483**, 100–103 (2012).
 37. Gorgoulis, V. *et al.* Cellular Senescence: Defining a Path Forward. *Cell* **179**, 813–827 (2019).
 38. Casella, G. *et al.* Transcriptome signature of cellular senescence. *Nucleic Acids Res.* **47**, 11476 (2019).
 39. Purcell, M., Kruger, A. & Tainsky, M. A. Gene expression profiling of replicative and induced senescence. *Cell Cycle* **13**, 3927–3937 (2014).
 40. Hernandez-Segura, A. *et al.* Unmasking Transcriptional Heterogeneity in Senescent Cells. *Curr. Biol.* **27**, 2652–2660.e4 (2017).
 41. Tadesse, S. *et al.* Targeting CDK2 in cancer: challenges and opportunities for therapy. *Drug Discov. Today* **25**, 406–413 (2020).
 42. Fukuoka, K. *et al.* Mechanisms of action of the novel sulfonamide anticancer agent E7070 on cell cycle progression in human non-small cell lung cancer cells. *Invest. New Drugs* **19**, 219–227 (2001).
 43. Kumarasamy, V., Vail, P., Nambiar, R., Witkiewicz, A. K. & Knudsen, E. S. Functional Determinants of Cell Cycle Plasticity and Sensitivity to CDK4/6 Inhibition. *Cancer Res.* **81**, 1347–1360 (2021).
 44. Freeman-Cook, K. *et al.* Expanding control of the tumor cell cycle with a CDK2/4/6 inhibitor. *Cancer Cell* **39**, 1404–1421.e11 (2021).
 45. Hafner, M. *et al.* Multiomics Profiling Establishes the Polypharmacology of FDA-Approved CDK4/6 Inhibitors and the Potential for Differential Clinical Activity. *Cell Chem Biol* **26**, 1067–1080.e8 (2019).
 46. Spencer, S. L. *et al.* The proliferation-quiescence decision is controlled by a bifurcation in CDK2 activity at mitotic exit. *Cell* **155**, 369–383 (2013).
 47. Welcker, M. *et al.* Multisite phosphorylation by Cdk2 and GSK3 controls cyclin E degradation. *Mol. Cell* **12**, 381–392 (2003).
 48. Clurman, B. E., Sheaff, R. J., Thress, K., Groudine, M. & Roberts, J. M. Turnover of cyclin E by the ubiquitin-proteasome pathway is regulated by cdk2 binding and cyclin phosphorylation. *Genes Dev.* **10**, 1979–1990 (1996).
 49. Lachmann, A. & Ma'ayan, A. KEA: kinase enrichment analysis. *Bioinformatics* **25**, 684–686 (2009).
 50. Finn, R. S. *et al.* PD 0332991, a selective cyclin D kinase 4/6 inhibitor, preferentially inhibits proliferation of luminal estrogen receptor-positive human breast cancer cell lines in vitro. *Breast Cancer Research* vol. 11 (2009).
 51. Mulero-Sánchez, A., Pogacar, Z. & Vecchione, L. Importance of genetic screens in precision oncology. *ESMO Open* **4**, e000505 (2019).
 52. Gong, X. *et al.* Genomic Aberrations that Activate D-type Cyclins Are Associated with Enhanced Sensitivity to the CDK4 and CDK6 Inhibitor Abemaciclib. *Cancer Cell* **32**, 761–776.e6 (2017).
 53. Pandey, K. *et al.* Combined CDK2 and CDK4/6 Inhibition Overcomes Palbociclib Resistance in Breast Cancer by Enhancing Senescence. *Cancers* **12**, (2020).
 54. Simoneschi, D. *et al.* CRL4AMBRA1 is a master regulator of D-type cyclins. *Nature* (2021) doi:10.1038/s41586-021-03445-y.
 55. Ruscetti, M. *et al.* Senescence-Induced Vascular Remodeling Creates Therapeutic Vulnerabilities in Pancreas Cancer. *Cell* **181**, 424–441.e21 (2020).
 56. Love, M. I., Huber, W. & Anders, S. Moderated estimation of fold change and dispersion for RNA-seq data with DESeq2. *Genome Biol.* **15**, 550 (2014).
 57. Evers, B. *et al.* CRISPR knockout screening outperforms shRNA and CRISPRi in identifying essential genes. *Nat. Biotechnol.* **34**, 631–633 (2016).
 58. Beijersbergen, R. L., Carlée, L., Kerkhoven, R. M. & Bernards, R. Regulation of the retinoblastoma protein-related p107 by G1 cyclin complexes. *Genes Dev.* **9**, 1340–1353 (1995).
 59. Subramanian, A. *et al.* Gene set enrichment analysis: a knowledge-based approach for interpreting genome-wide expression profiles. *Proc. Natl. Acad. Sci. U. S. A.* **102**, 15545–15550 (2005).
 60. Sturm, M., Schroeder, C. & Bauer, P. SeqPurge: highly-sensitive adapter trimming for paired-end NGS data. *BMC Bioinformatics* **17**, 208 (2016).
 61. Kim, D., Paggi, J. M., Park, C., Bennett, C. & Salzberg, S. L. Graph-based genome alignment and genotyping with HISAT2 and HISAT-genotype. *Nat. Biotechnol.* **37**, 907–915 (2019).
 62. Shen, S. *et al.* rMATS: robust and flexible detection of differential alternative splicing from

- replicate RNA-Seq data. *Proc. Natl. Acad. Sci. U. S. A.* **111**, E5593–601 (2014).
63. Wang, E. *et al.* Targeting an RNA-Binding Protein Network in Acute Myeloid Leukemia. *Cancer Cell* **35**, 369–384.e7 (2019).
 64. Chen, E. Y. *et al.* Enrichr: interactive and collaborative HTML5 gene list enrichment analysis tool. *BMC Bioinformatics* **14**, 128 (2013).
 65. Menegakis, A. *et al.* Resistance of Hypoxic Cells to Ionizing Radiation Is Mediated in Part via Hypoxia-Induced Quiescence. *Cells* **10**, (2021).

SUPPLEMENTARY FILES



Supplemental Figure 1

A Schematic outline of dropout screens. Triple negative breast cancer cell lines CAL-51, CAL-120 and HCC1806 were infected with a shRNA library targeting kinome and cultured in presence or absence of palbociclib. After 8 - 10 population doublings, shRNA sequences were amplified and quantified using next generation sequencing.

B-E CDK2 was knocked down in CAL-51, CAL-120 and HCC1806 using two independent shRNAs.

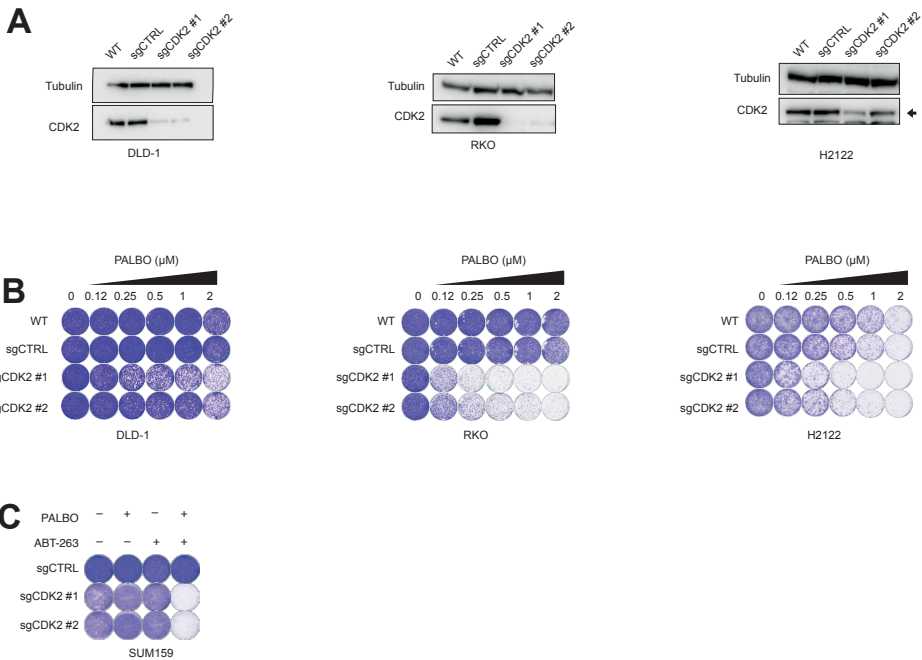
B qPCR analysis of CDK2 normalized against expression of housekeeping gene RPL13. Mean of three technical replicates is shown and error bars indicate standard deviation.

C Long term colony formation assay with palbociclib was performed for 10 days. Representative of three independent experiments is shown (n=3).

D Proliferation assay was performed using 0.5 μM of palbociclib for CAL-51 and CAL-120 and 2 μM for HCC1806. Mean of three technical replicates representative of two independent experiments (n=2) is shown and error bars indicate standard deviation. The end point confluency of all conditions were analysed using two-way ANOVA with Šidák's post-hoc test (** $p < 0.01$, **** $p < 0.0001$)

E SA- β -gal staining in CAL-51, CAL-120 and HCC1806 CDK2 KD and control cells treated for 10 days with 0.5 μM of palbociclib. Scale bar indicates 100 μm . Representative images of two independent experiments are shown (n=2).

F Quantification of SA- β -gal positive cells shown in **E**. CAL-51, CAL-120 and HCC1806 CDK2 KD and control cells treated for 10 days with 0.5 μM of palbociclib. Bars represent mean \pm SD of triplicates. Data was analysed using two-way ANOVA with Šidák's post-hoc test (**** $p < 0.0001$).



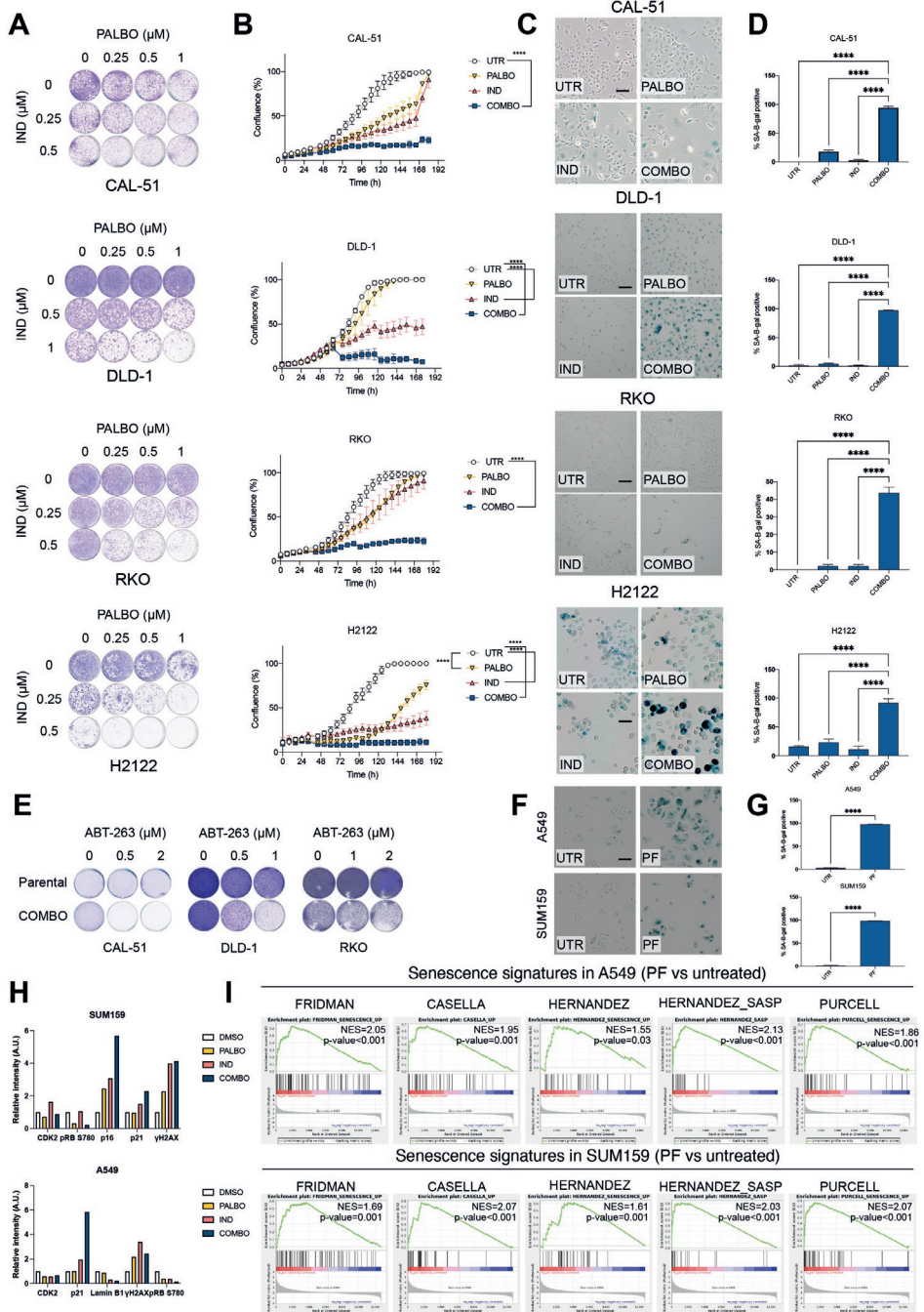
Supplemental Figure 2

A-C CDK2 was knocked out in DLD-1, RKO and H2122 cells using two independent sgRNAs.

A Western blot analysis of CDK2 knock-out DLD-1, RKO and H2122 cells and control cells. Tubulin was used as a loading control. An arrow depicts the CDK2 band in H2122. Representative images of two independent experiments are shown (n=2).

B Long term colony formation assay of DLD-1, RKO and H2122 sgCDK2 and control cells with palbociclib was performed for 10 days. Representative of two independent experiments is shown (n=2).

C Long term colony formation assay of control and SUM159 sgCDK2 cells pre-treated with 2 μM palbociclib for 2 weeks, and then treated with 0.5 μM ABT-263 for 1 week. Representative of two independent experiments is shown (n=2).



Supplemental Figure 3

A Long term colony formation assay of CAL-51, DLD-1, RKO and H2122 cell lines treated with palbociclib, indisulam and the combination for 10 days. Representative of two independent experiments is shown (n=2).

B Proliferation assay of CAL-51, DLD-1, RKO and H2122 cell lines treated with palbociclib, indisulam and

the combination. CAL-51 were treated with 1 μM of palbociclib and 1 μM indisulam, DLD-1 with 0.5 μM of palbociclib and 1 μM indisulam, RKO with 2 μM of palbociclib and 1 μM indisulam and H2122 with 1 μM palbociclib and 0.5 μM indisulam. Mean of three technical replicates representative of two independent experiments (n=2) is shown and error bars indicate standard deviation. The end point confluency of all conditions were analysed using one-way ANOVA with Dunnett's post-hoc test (**** $p < 0.0001$).

C SA- β -gal staining in CAL-51, DLD-1, RKO and H2122 cell lines treated with palbociclib, indisulam and the combination using the same doses as in B. Scale bar indicates 100 μm (n=2).

D Quantification of SA- β -gal positive cells shown in C. CAL-51, DLD-1, RKO and H2122 cell lines treated with palbociclib, indisulam and the combination using the same doses as in B. Bars represent mean \pm SD of triplicates. Data was analysed using one-way ANOVA with Dunnett's post-hoc test (**** $p < 0.0001$).

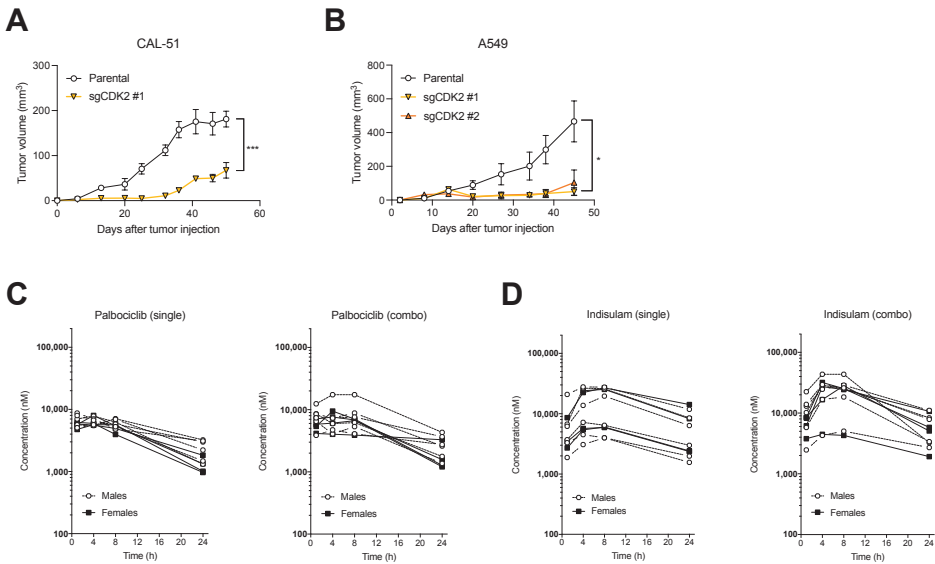
E Long term colony formation assay of CAL-51, DLD-1 and RKO cells pre-treated with palbociclib and indisulam for 2 weeks. CAL-51 were treated with 1 μM of palbociclib and 1 μM of indisulam. DLD-1 were treated with 0,5 μM of palbociclib and 1 μM of indisulam. RKO were treated with 0,25 μM of palbociclib and 0,5 μM of indisulam. Senescent and parental cells were then treated with indicated doses of ABT-263 for 1 week (n=2).

F SA- β -gal staining in A549 and SUM159 cell lines treated with 0.5 μM PF-06873600 for one week. Representative images of two independent experiments are shown (n=2).

G Quantification of SA- β -gal positive cells shown in F. A549 and SUM159 cell lines were treated with 0.5 μM PF-06873600 for one week. Bars represent mean \pm SD of triplicates. Data was analysed using unpaired t-test (**** $p < 0.0001$).

H Quantification of Western blot analysis shown in F. SUM159 cells were treated with 0.5 μM of palbociclib and 2 μM indisulam and A549 with 2 μM palbociclib and 0.5 μM indisulam for 10 days. HSP90, vinculin and tubulin were used as loading controls. Measured intensity of each band was normalized to the corresponding loading control and DMSO treatment. A.U. indicates arbitrary units.

I GSEA of previously published senescence gene sets comparing A549 and SUM159 cells treated with 0.5 μM PF-06873600 for one week with untreated cells. Normalized enrichment score (NES) and p-values of enrichment score are shown. The experiment was performed in duplicates.



Supplemental Figure 4

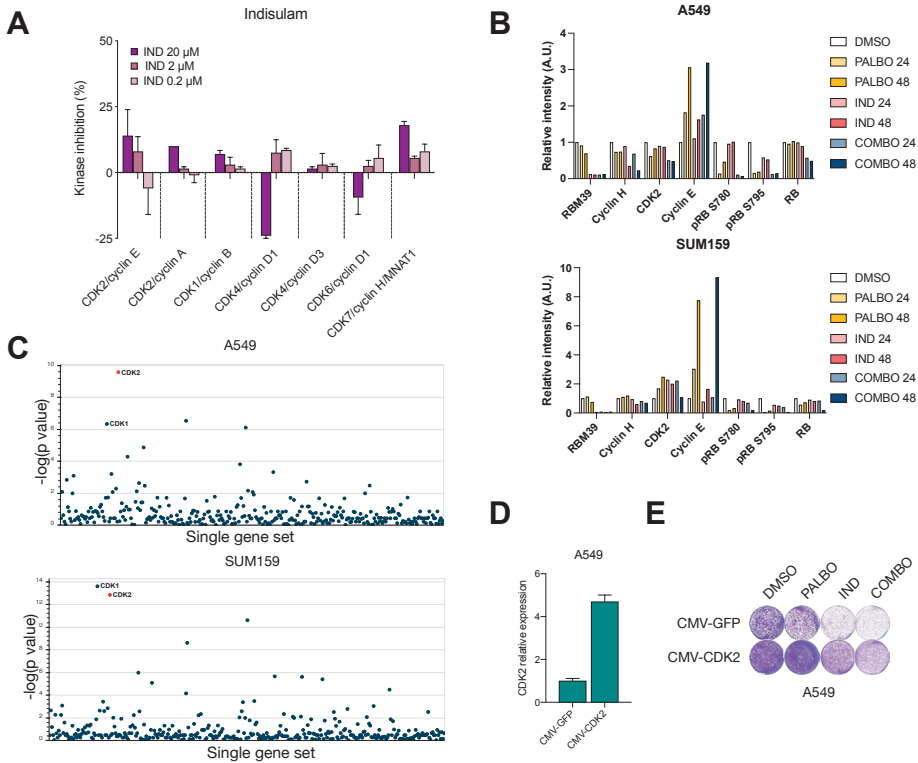
A Tumor growth of CAL-51CDK2 single cell knock-out clone and control xenografts in mice. One million cells were injected orthotopically in the 4th right mammary fat pad of female NMRI nude mice, 5-6 mice per group. Tumor volumes of parental and sgCDK2 tumors at end point were analysed using Welch's t-test (*** $p < 0.001$).

B Tumor growth of two A549 CDK2 single cell knock-out clones and control xenografts in mice. One million cells were injected subcutaneously in the right flank of NMRI nude mice, 5-6 mice per group. Tumor volumes of parental and sgCDK2 tumors at the end point were analysed using one-way ANOVA

with Tukey's post-hoc test (* $p < 0.05$).

C, D Pharmacokinetic studies of palbociclib and indisulam in A549-tumor bearing mice. A549 cells were injected subcutaneously in NMRI nude mice. After tumour establishment (~200 mm³), mice were treated with palbociclib, indisulam or combination. Blood was collected 2, 4, 8 and 24h after drug treatment from 6 male and 6 female mice. The drug concentrations in the blood were determined by mass spectrometry. **C** Palbociclib blood concentration is displayed from every mouse that received the single drug treatment (left) and the combination with indisulam (right).

D indisulam blood concentration is displayed from every mouse that received the single drug treatment (left) and the combination with palbociclib (right).



Supplemental Figure 5

A In vitro kinase inhibition assay of indisulam for CDK/cyclin complexes. IC50 values are shown in triplicates with error bars indicating standard deviation.

B Quantification of Western blot analysis shown in figure 5J. A549 and SUM159 cells were treated with 2 μM palbociclib, 5 μM indisulam and the combination for either 24 or 48 hours. HSP90 was used as a loading control. Measured intensity of each band was normalized to the corresponding loading control and untreated condition. A.U. indicates arbitrary units.

C Kinase enrichment analysis (KEA) on RNA-seq data in A549 and SUM159 cells treated with 3 μM indisulam for 16h compared to untreated. Filtered for adjusted p-value < 0.05. CDK1 and CDK2 are highlighted.

D qPCR analysis of A549 cells transfected with CMV-CDK2 and CMV-GFP vectors. Expression was normalized to the housekeeping gene RPL13. Mean of three technical replicates is shown and error bars indicate standard deviation.

E Long term colony formation assay of A549 cells transfected with CMV-CDK2 and CMV-GFP vectors treated with 0.5 μM palbociclib, 0.5 μM indisulam and the combination for 10 days.

3

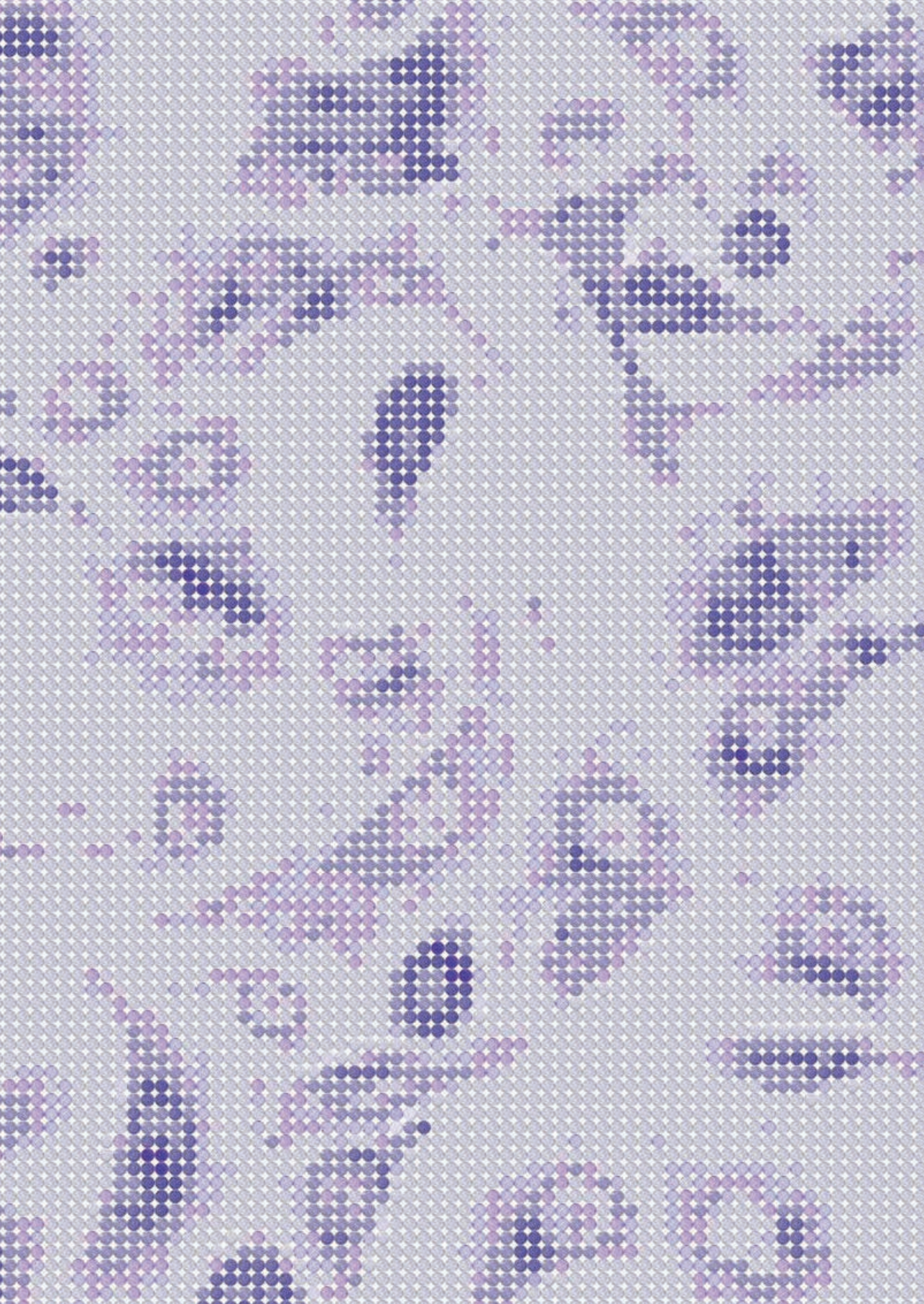
Supplemental Table 1

Casella_UP	PURCELL_UP	HERNANDEZ_SENESCENCE_UP	HERNANDEZ_SASP	FRIDMAN_SENESCENCE_UP
TMEM159	APOL1	GDNF	ICAM1	ALDH1A3
CHPF2	APOL3	PLK3	LEP	C9orf3
SLC9A7	ATF3	SLC16A3	IL1A	CCND1
PLOD1	BATF2	TSPAN13	IL1B	CD44
FAM234B	BIRC3	CCND1	CXCL8	CDKN1A
DHRS7	C3	P4HA2	IGFBP2	CDKN1C
SRPX	C9ORF47	SLC10A3	IL6	CDKN2A
SRPX2	CD163L1	ZBTB7A	IL11	CDKN2B
TNFSF13B	CD82	SCOC	CSF2	CDKN2D
PDLIM1	CLDN1	UFM1	PLAUR	CITED2
ELMOD1	COL17A1	B4GALT7	VEGFA	CLTB
CCND3	CTSS	ACADVL	CXCL1	COL1A2
TMEM30A	CXCL2	POFUT2	IGFBP4	CREG1
STAT1	CYP1A1	TAF13	IGFBP7	CRYAB
RND3	DUSP6	NOL3	FGF2	CTGF
TMEM59	ESPST12	ADPGK	FGF7	CXCL14
SARAF	GBP4	DDA1	IGFBP6	CYP1B1
SLCO2B1	GCA	ZNHIT1	MMP1	EIF2S2
ARRDC4	GMPR	CHMP5	MMP3	ESM1
PAM	GNG11	TOLLIP	MMP10	F3
WDR78	HERC5	KLC1	PGF	FILIP1L
WDR63	ICAM1	TMEM87B	CCL2	FN1
NCSTN	IDO1	BCL2L2	CCL5	GSN
SLC16A14	IFI27	SUSD6	CXCL5	GUK1
GPR155	IFI30	DYNLT3	TIMP2	HBS1L
CLDN1	IL1A	RAI14	TNFRSF10C	HP55
JCAD	IL1B	GBE1	CCL20	HSPA2
BLCAP	IL1RN	FAM214B	AXL	HTATIP2
FILIP1L	IL32	PDLIM4		IFI16
TAP1	ISG20	DGKA		IFNG
TNFRSF10C	ITG53	PLXNA3		IGFBP1
SAMD9L	LCP1	MTCYB		IGFBP2
SMCO3	LGALS9			IGFBP3
POFUT2	MLKL			IGFBP4
KIAA1671	MMP12			IGFBP5
LRP10	MYD88			IGFBP6
DIO2	OASL			IGFBP7
MAP4K3-DT	PLAU			IGSF3
LINC02154	PMAIP1			ING1
TM4SF1-AS1	RSPO3			IRF5
PTCHD4	RTP4			IRF7
H2AJ	TNFAIP3			ISG15
PURPL	TNFAIP6			MAP1LC3B
	TNFRSF18			MAP2K3
				MDM2
				MMP1
				NDN
				NME2
				NRG1
				OPTN
				PEA15
				RAB13

Supplemental Table 1 continued

Casella_UP	PURCELL_UP	HERNANDEZ_SENESENCE_UP	HERNANDEZ_SASP	FRIDMAN_SENESENCE_UP
				RAB31 RAB5B RABGGTA RAC1 RBL2 RGL2 RHOB RRAS S100A11 SERPINB2 SERPINE1 SMPD1 SMURF2 SOD1 SPARC STAT1 TES TFAP2A TGFB111 THBS1 TNFAIP2 TNFAIP3 TP53 TSPYL5 VIM





Chapter 4

Using functional genetic screens to understand cancer immune evasion

Ziva Pogacar¹, Giulia de Conti¹, Lisa Willemsen¹, Liqin Wang¹, Hugo Horlings¹,
Chong Sun², Wouter Scheepers², Jesse Zaretsky⁵, Cor Liefink³,
Roderick Beijersbergen^{1,3,4}, Siwen Hu-Lieskovan⁶, Rene Bernards¹

¹Division of Molecular Carcinogenesis, Oncode Institute. The Netherlands Cancer Institute, Plesmanlaan 121, 1066 CX Amsterdam, The Netherlands.

²Division of Molecular Oncology and Immunology. The Netherlands Cancer Institute, Plesmanlaan 121, 1066 CX Amsterdam, The Netherlands.

³The NKI Robotics and Screening Center, The Netherlands Cancer Institute, Plesmanlaan 121, 1066 CX Amsterdam, The Netherlands.

⁴Genomics core facility, The Netherlands Cancer Institute, Plesmanlaan 121, 1066 CX Amsterdam, The Netherlands.

⁵UCLA Medical center, Departement of Medicine, Los Angeles, CA 90095, United States

⁶Huntsman Cancer Institute, University of Utah, Salt Lake City, UT 84112, United States

ABSTRACT

Even though immune checkpoint blockade has emerged as an effective cancer therapy, there is still a significant number of patients who do not benefit from this treatment. Here, we analyzed DNA sequencing data from biopsies of melanoma patients with acquired resistance to anti PD-1 treatment and compiled a list of candidate genes, which were mutated upon disease progression and might be involved in acquired resistance. Next, we designed a custom CRISPR library consisting of sgRNAs targeting each of the candidate genes. We used the custom library to perform a resistance screen in melanoma cells co-cultured with matched T-cells that recognize and eliminate the melanoma cells. We identified B2M, part of the MHC-I antigen presenting complex, as the top scoring hit of the screen. Additionally, sgRNAs targeting JAK1, APOL2 and SASH1 were also enriched in the screen. Validation experiments confirmed resistance of B2M negative cells, but not JAK1, APOL2 or SASH1. This might be explained by differences between resistance to ICB *in vivo* and to killing by T-cells *in vitro*. Understanding the mechanisms of resistance can help identify new biomarkers and design new rational combination therapies.

INTRODUCTION

Cancer immunotherapy, in particular immune checkpoint blockade (ICB), has become an important pillar of cancer treatment in the past few years. In contrast to other classical cancer treatments, such as radiotherapy or chemotherapy, ICB does not directly target the cancer cells. Instead, it blocks immune checkpoints programmed cell death protein 1 (PD-1), programmed death-ligand 1 (PD-L1) and/or cytotoxic T-lymphocyte-associated protein 4 (CTLA-4) and therefore allows the immune system to eliminate cancer cells. Monoclonal antibodies targeting either PD-1, PDL-1 or CTLA-4 have now been approved for treatment of more than 50 cancer types¹. One of the great advantages of ICB is that the observed responses are usually extremely durable².

Similar to other cancer therapies, resistance is a major limitation of ICB³. The majority of patients treated with ICB do not respond to treatment due to innate resistance. Furthermore, a subset of responders might acquire resistance during therapy, leading to disease progression. Recently, numerous factors that determine response and resistance to ICB have been described⁴. In particular, the response to ICB heavily depends on pre-existing T-cells in the tumor microenvironment. Additional intrinsic factors of the patient, tumor stroma and environment may further influence the response to ICB⁵⁻⁷. However, it has become clear that tumor intrinsic factors are the major players in determining ICB response⁸. Those factors include mutational landscape, interferon signalling and antigen presentation.

Firstly, tumor mutational landscape influences the abundance of neo-antigens on the tumor cells. High mutational burden correlates with response to ICB as demonstrated by microsatellite instable (MSI) tumors which are classified as high responders to ICB^{9,10}. Next, intact interferon- γ (IFN γ) signalling in tumor cells correlates with favorable response to ICB loss of JAK/STAT pathway is associated with resistance to ICB^{11,12}. Loss of IFN γ could also have additional consequences through disruption of bystander effect¹³. Lastly, loss of antigen presentation machinery can lead to immune evasion. For example, loss of β -2-microglobulin (B2M) disrupts MHC I and prevents antigen presentation leading to resistance to ICB^{14,15}. Through understanding the molecular mechanisms of resistance, we can improve patient selection and design rational combination treatments which can improve the response rate to ICB.

One method that allows for an unbiased approach to study resistance to cancer therapies are functional CRISPR screens¹⁶. In recent years, several *in vitro* and *in vivo* CRISPR screens identified players in sensitivity and resistance to ICB, including B2M, IFN γ pathway, PTPN2, SWI/SNF complex and others¹⁷⁻²⁰. However, relevance of these genes to clinical resistance to ICB remains mostly unclear.

Here we curated a list of genes with potential involvement in clinically-acquired resistance to ICB and used a custom built CRISPR immune evasion library to uncover new relevant factors in ICB resistance.

RESULTS

A curated list of candidate ICB resistance gene

To study clinically relevant factors of immune evasion we analyzed DNA sequence data obtained from a cohort of melanoma patients treated with anti PD-1 therapy. We focused on acquired resistance and thus included in our analyses only the subset of patients that initially responded to the therapy, but relapsed later. We compared whole exome sequencing data from biopsies taken at the start of treatment to the biopsies taken upon relapse on treatment. By comparing mutations present at relapse we compiled a list of candidate genes (Supplemental Table 1) with loss of function (LOF) mutations that could be involved in resistance to ICB. We focused on genes that fit one of the following criteria: 1. mutation was present in more than one patient, 2. mutation was present only at relapse and was homozygous or 3. mutation was heterozygous at baseline and homozygous at progression. The list of candidate genes is shown in Supplemental table 1.

Co-culture system of melanoma cells and matched T-cells

Next, we aimed to establish an *in vitro* system for unbiased genetic screening of the candidate genes (Figure 1A). We hypothesized that genes whose LOF mutation led to acquired resistance to ICB in patients would confer resistance to T-cell killing *in vitro* upon knock-out.

We made use of a matched melanoma and T-cell system, where T-cells transduced with MART-1 TCR can recognize and eliminate MART-1 positive melanoma cells²¹. To test the co-culture system, we generated B2M knock-out Mel526 cells as a positive control. As a part of antigen presenting MHC-I complex, loss of B2M impairs antigen presentation and leads to resistance to T-cell killing²². We used CRISPR-Cas9 to knock-out B2M in Mel526 cells and selected a single cell clone which was negative for B2M and MHC-I on flow cytometry (Figure 1B), negative for B2M on IHC (Figure S1A) and showed a deletion in B2M gene (Figure S1B). As expected, B2M KO cells were not sensitive to T-cell killing by MART-1 restricted T-cells (Figure 1C, D). We then generated Cas9-GFP expressing Mel526 cells by sorting high GFP expressing cells twice (Figure 1E, F). We confirmed that the cells expressed Cas9 (Figure 1G). Additionally, we tested editing efficiency of Mel526-Cas9 cells using a GFP reporter pXPR_011 encoding for GFP and sgRNA targeting GFP. A week after transducing parental and Mel526-Cas9 cells with the reporter we observed decrease in GFP signal in Mel-526 cells, but not parental cells (Figure 1H).

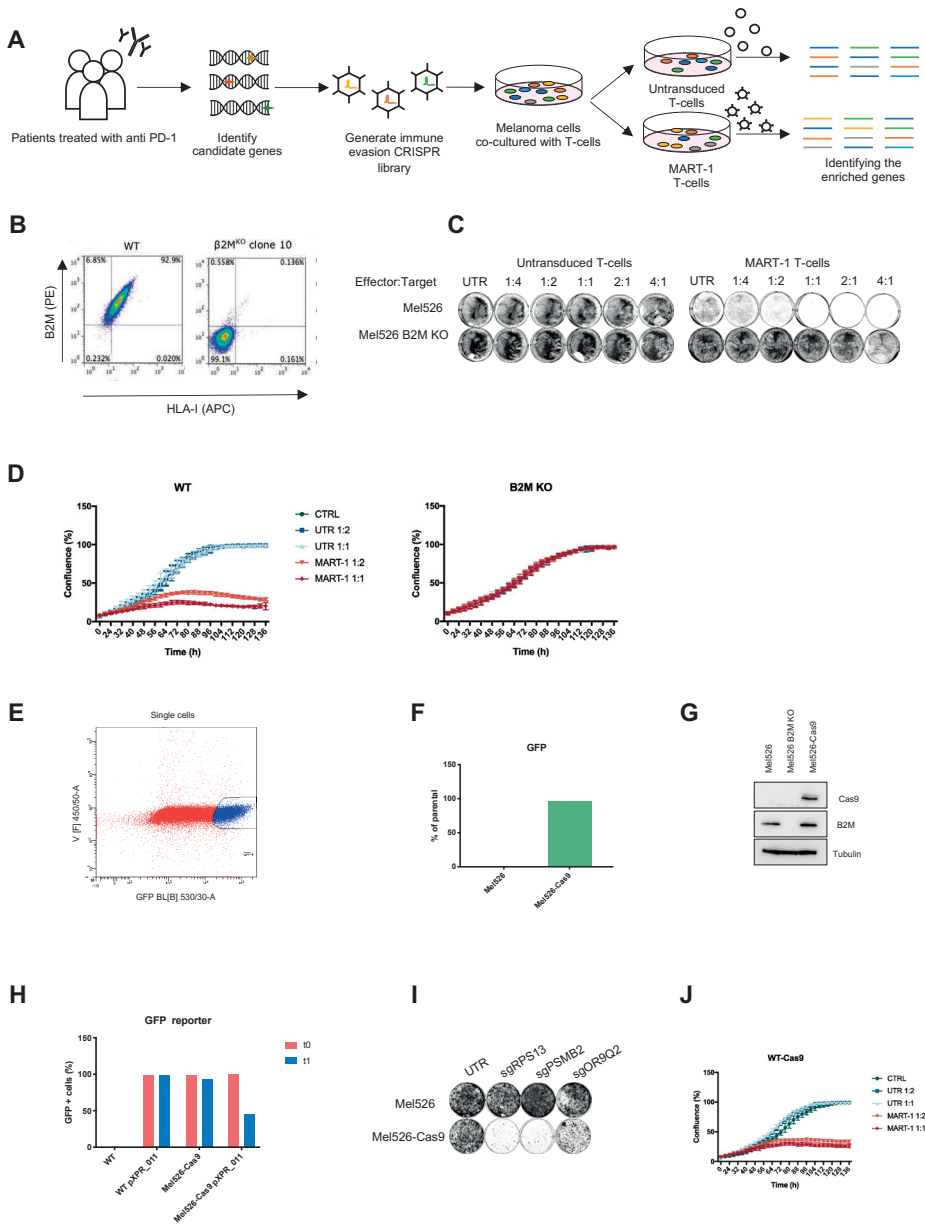


Figure 1: Screening system to identify new immune evasion mechanisms

A Overview of the workflow. First, biopsies of melanoma patients treated with anti PD-1 therapy were evaluated before and after relapse. Comparison of pre- and post-relapse biopsies identified a list of candidate genes potentially involved in resistance to anti PD-1 treatment. Next, CRISPR library of gRNAs targeting the candidate genes was assembled and Cas9 expression melanoma cells were screened in co-culture with matched T-cells. gRNAs enriched in TCR positive T-cell condition compared to control cells were considered for validation.

B Flow cytometry analysis of Mel526 cells and a Mel526 B2M knock-out clone. The cells were stained with B2M and HLA-I antibodies.

C Colony formation assay of Mel526 and Mel526 B2M knock-out cells co-cultured with either untransduced

or MART-1 transduced T-cells in different effector to target ratios for 5 days.

D Proliferation assay of Mel526 cells (left) and Mel526 B2M knock-out cells (right) co-cultured with either untransduced or MART-1 transduced T-cells in different effector to target ratios.

E FACS sorting of Mel526 cells infected with Cas9-GFP vector. The X axis shows GFP and the Y axis shows a spillover channel.

F Flow cytometry analysis of Mel526 parental and Cas9-GFP cells. Increase in GFP is quantified as percent of parental cells.

G Western blot analysis of Mel526 parental, B2M KO and Cas9-GFP cells for Cas9 and B2M. Tubulin was used as a loading control.

H Editing efficiency analysis using a GFP reporter. Parental and Cas9 Mel526 cells were transduced with the reporter and cells were analysed immediately after the selection (t0) and after a week of culture (t1).

I Colony formation assay of Mel526 and Mel526 Cas9 cells. The cells were transduced with sgRNA vectors against two essential genes: RPS13, PSMB2 and a non-essential gene: OR9Q2, selected and cultured for 10 days.

J Proliferation assay of Mel526 Cas9 cells co-cultured with either untransduced or MART-1 transduced T-cells in different effector to target ratios.

It is important to note that Mel526-Cas9 cells already express GFP through the Cas9 vector before transduction with pXPR_011 so editing efficiency indicates knock-out of the reporter as well as background GFP gene. To confirm the editing efficiency at endogenous loci we knocked-out two essential genes: 40S ribosome subunit s13 (RPS13) and proteasome subunit beta type 2 (PSMB2) and a non-essential gene olfactory receptor family 9 (OR9Q2). Upon transduction with gRNAs against the three genes, Mel526-Cas9 cells were sensitive to essential gene knock-out, but not to the non-essential genes indicating good editing efficiency (Figure 1I). Lastly, we confirmed that Cas9 expression does not interfere with T-cell co-culture. We observed similar sensitivity to T-cell killing of Mel526-Cas9 cells as parental cells (Figure 1J, S1C). Taken together, we validated a co-culture system of T-cell killing that can be used for a genetic screen.

Co-culture CRISPR screen using custom immune evasion sgRNA library

To generate a custom CRISPR library we assembled sgRNA sequences targeting candidate genes (Supplemental table 1) as well as positive and negative control sgRNAs. We amplified the oligonucleotide library in a two step PCR (Figure 2A, B) to include overhangs for cloning. After cloning we amplified the sgRNA sequences (Figure 2C) and sequenced them to determine their abundance. We observed that the majority of sgRNAs are present in high numbers and only a minority in lower abundance (Figure 2D).

We then infected Mel526-Cas9 cells with the custom sgRNA library and after selection for sgRNA infected cells co-cultured them with either MART-1 T-cells or control T-cells in 1:1 effector to target ratio for 4 days. After this, cells were harvested, DNA was isolated and sgRNA sequences were amplified (Figure 2E). We then determined the sgRNA abundance in each sample using NGS. Firstly, we observed high correlation between three replicates of each sample (Supplemental Figure 2A) and clustering of control T-cell samples with reference t0 samples (Figure 2F).

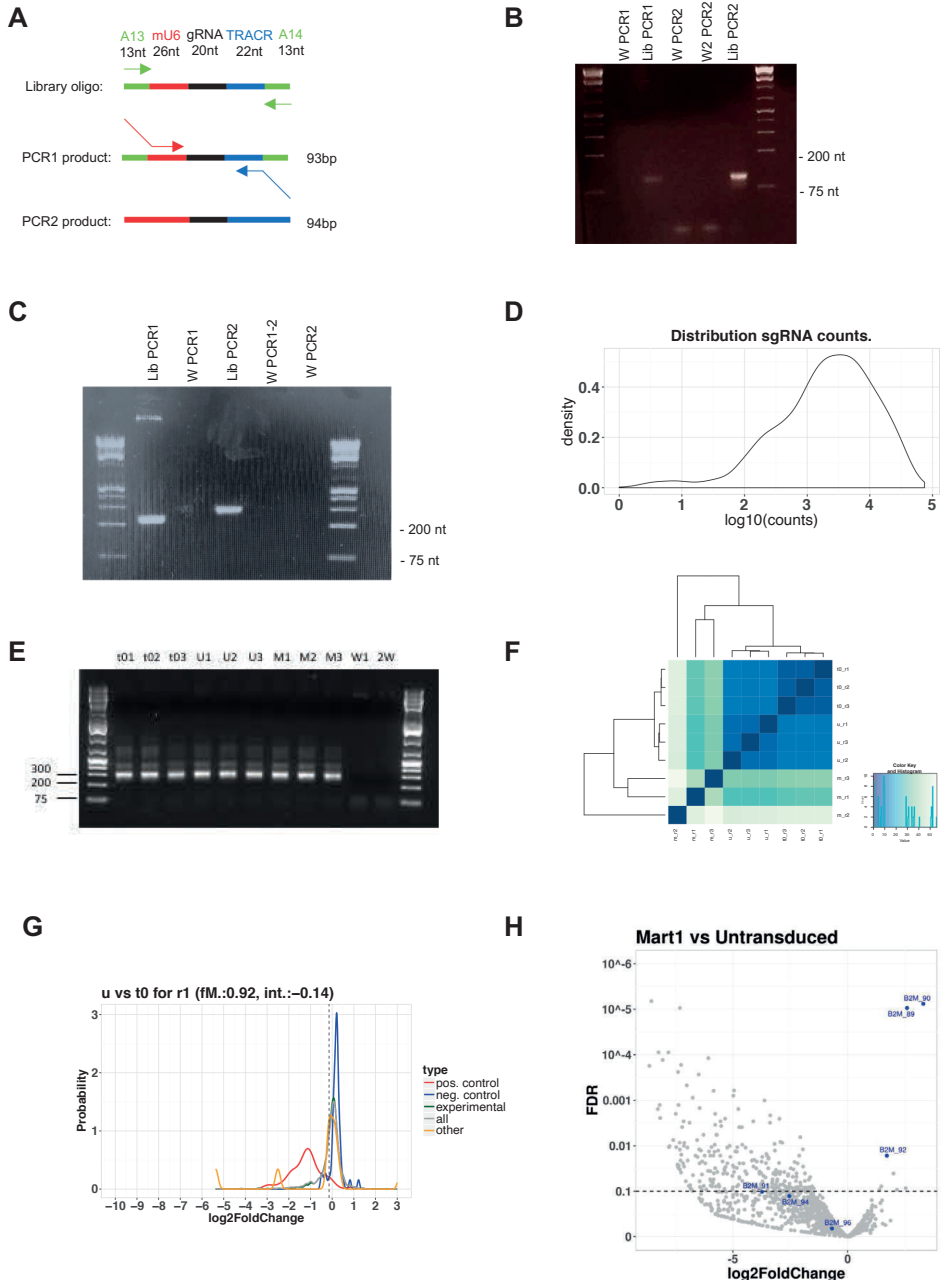


Figure 2: Co-culture CRISPR screen of melanoma cells and T-cells identifies B2M as a hit
A Amplification strategy for library oligonucleotides. Library oligonucleotides were designed to contain A13 sequence, mU6 promoter, variable gRNA region, TRACR sequence and A14 sequence. The library was then prepared for cloning in a two step process - amplification in PCR1 and extending the overhangs in PCR2.
B PCR analysis of the library amplification. Water control of PCR1 (W PCR1), product of PCR1 (Lib PCR1), water control of PCR2 (W PCR2), water control of PCR1 in PCR2 (W2 PCR2) and product of PCR2 (Lib PCR2) were loaded on 2% agarose gel and resolved. Expected product sizes are 93nt for PCR1 and 94nt for PCR2.

C PCR analysis of cloned library. Two step PCR was performed to prepare for sequencing. Water control of PCR1 (W PCR1), product of PCR1 (Lib PCR1), water control of PCR2 (W PCR2), water control of PCR1 in PCR2 (W2 PCR2) and product of PCR2 (Lib PCR2) were loaded on 2% agarose gel and resolved. Expected product sizes are 220nt for PCR1 and 275nt for PCR2.

D Distribution of sgRNA counts in the library prep. Relative number of guides (density) is shown on the y axis and log₁₀ of counts on the x axis.

E PCR analysis of amplified gRNA pools after the screen. Two step PCR was performed to prepare for sequencing. Triplicates of t0, untransduced, MART-1 transduced conditions, water controls for PCR1 and 2 were loaded on 2% agarose gel and resolved. Expected product sizes are 275nt.

F Correlation between different conditions (reference samples t0, untransduced T-cells u and MART-1 T-cells m) and replicates.

G Distribution of log₂ fold changes of sgRNAs targeting positive controls (red), negative controls (blue), experimental sgRNAs (green), all sgRNAs (grey) and others (orange). Samples treated with untransduced T-cells compared to reference samples at time point 0 are shown.

H Resistance screen was performed in Mel526-Cas9 cells co-cultured with either untransduced or MART-1 transduced T-cells. Volcano plot of MART-1 transduced condition compared to untransduced. X axis shows log₂ fold change of normalized read counts and Y axis shows false discovery rate (FDR). Each dot represents an individual gene and B2M is highlighted.

This indicates that samples co-cultured with MART-1 positive T cells were the most different from control and reference samples and shows that selective pressure of MART-1 T-cells was sufficient. Next, we investigated the difference in abundance of positive and negative control sgRNAs. We observed depletion of positive control sgRNAs targeting essential genes when comparing control T-cell samples with reference t0 samples (Figure 2G, Supplemental Figure 2B). Finally, we determined the enrichment of sgRNAs in MART-1 samples compared to control samples (Figure 2H). We observed enrichment of sgRNAs targeting B2M as well as APOL2, SASH1 and JAK1. This indicates that *in vitro* co-culture genetic screens are able to identify previously known factors of immune evasion (B2M¹⁴ and JAK1¹²) as well as novel factors.

Loss of B2M confers resistance to T-cell immunity

Since B2M is part of antigen presentation and JAK1 mediates IFN γ signalling, their loss is expected to result in resistance to *in vitro* T-cell killing. On the other hand, APOL2 and SASH1 are previously unknown factors in resistance to T-cell killing. APOL2 encodes apolipoprotein L2 which influences movements of lipids in the cells. Interestingly, its expression is induced by IFN γ ²³. SASH1 encodes SAM And SH3 Domain Containing 1 protein, which is involved in TLR4 signalling and has recently been described to influence proliferation and apoptosis²⁴.

To validate the hits from the screen, we cloned the individual sgRNAs targeting B2M, APOL2, SASH1 and JAK1 and selected single cell clones. We were able to generate single cell knock-out clones for B2M, JAK1 and APOL2 (Figure 3A), but not for SASH1. This could indicate that complete loss of SASH1 reduces cell fitness or cell viability in Mel526 cells. Knock-out of B2M, but not JAK1 or APOL2 lead to resistance in T-cell killing (Figure 3B,C). Furthermore, when using shRNAs to knock-down SASH1 and B2M, only knock-down of B2M increased resistance to T-cell killing while knock-down of SASH1 did not lead to

meaningful increase in resistance. This indicates that loss of B2M is the only strong hit leading to resistance to T-cell immunity.

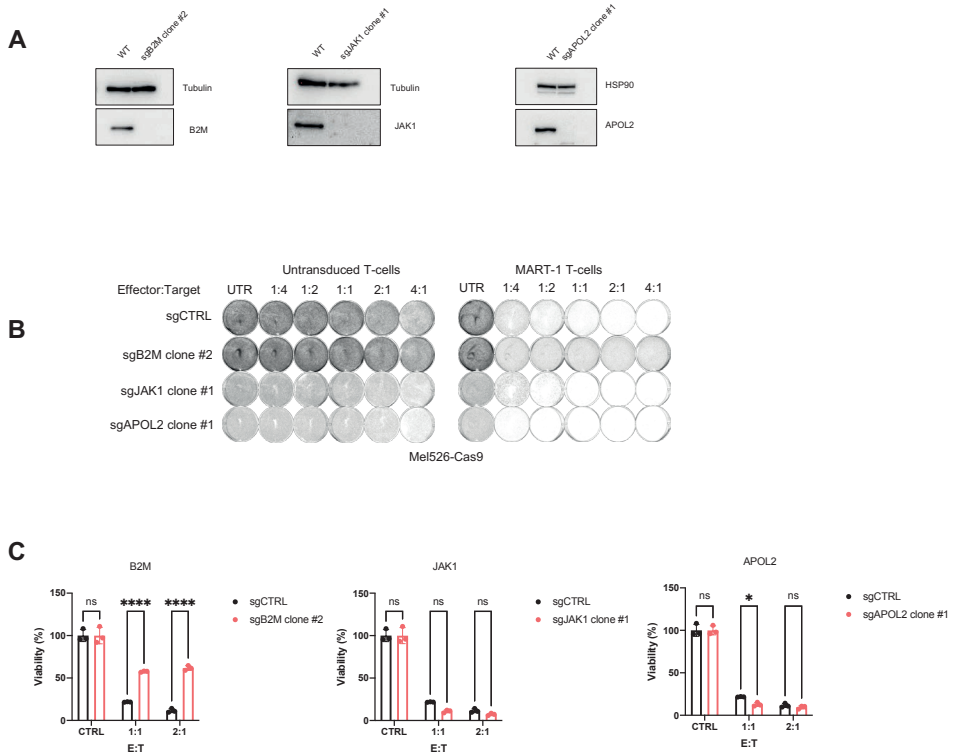


Figure 3: Loss of B2M leads to resistance to T-cell killing

A Western blot analysis of Mel526-Cas9 cells (WT) and single cell clones for B2M, JAK1 and APOL2. Tubulin and HSP90 were used as loading controls.

B Colony formation assay of Mel526-Cas9 cells transduced with sgCTRL and B2M, JAK1 and APOL2 single cell clones co-cultured with either untransduced or MART-1 transduced T-cells in different effector to target ratios for 5 days.

C Viability assay of Mel526-Cas9 cells and single cell knock-out clones for B2M, JAK1 and APOL2 co-cultured with MART-1 positive T cells for 5 days. Effector to target ratios are indicated. Mean of three technical replicates are shown and error bars show standard deviation. Data was analysed using two-way ANOVA with Šidák's post-hoc test (* $p < 0.05$, **** $p < 0.0001$).

DISCUSSION

Immune checkpoint blockade has revolutionized cancer therapy in providing durable responses. However, a majority of the patients still do not benefit from ICB therapy. Here we curated a list of candidate genes involved in acquired resistance to ICB and validated them using a functional genetic screen in an *in vitro* co-culture system. We show that impaired antigen presentation through B2M loss leads to resistance to T-cell killing *in vitro*.

Genetic screens are a valuable tool to understand factors of resistance and sensitivity to various cancer therapies¹⁶. In the past years several CRISPR screens have already uncovered new players in resistance to ICB¹⁷⁻²⁰. A major limitation of such studies is that it remains unclear whether the genes identified in such model systems are relevant to clinically-observed resistance to ICB therapy. We used an alternative approach in which candidate genes associated with clinical resistance to ICB are validated *in vitro*. As we pre-selected candidate genes with clinical relevance this reduces the scale of *in vitro* validation to only include potentially clinically relevant genes. However, the quality of the clinical observation data and choice of validation platform will have a greater impact on the outcome when using this approach. For example, the small size of the patient cohort used here might not represent true variability of the patient population. Here we included pre and on-treatment biopsies from 14 melanoma patients to generate the list of candidate genes. Including a bigger cohort could allow for more rigorous selection criteria of candidate genes. Next, due to a validation system that is based on knocking-out genes by CRISPR we focused on investigating loss of function mutations. Future research might include additional techniques such as CRISPR activation (CRISPRa) to study gain of function mutations and gene upregulations. Lastly, in order to validate the clinical observation *in vitro*, the model system of choice should be able to recapitulate the complexity of the *in vivo* interaction between the tumor and the immune system. Here, we used a co-culture system of MART-1 restricted T-cells and melanoma cells expressing the MART-1 antigen. The advantages of this system are the presence of a strong antigen that allows efficient killing of target cells and suitability to scale the experiment enough to perform a genetic screen. On the other hand, this system is artificial and does not fully resemble the tumor microenvironment *in vivo*. For example, the heterogeneity of antigen expression on the tumor side and heterogeneity of TCRs on the T-cell side are not present. Additionally, resistance to T-cell killing *in vitro* is a proxy for resistance to ICB and other factors involving T-cell activation, expression of immune check-points and the interaction between T-cells and tumor cells might play an important role as well. In this case, the list of candidate genes might also include passenger mutations and not drivers of resistance. Furthermore, a mutation might cause resistance to ICB, but not to T-cell killing through additional immune check-points or interaction with other components of the tumor microenvironment. The development of *in vitro* models that

fully recapitulate the tumor microenvironment and enable high throughput screening will allow for more efficient modelling of resistance and sensitivity to ICB. A recently developed method that includes patient derived tumor and immune cells is the use of ex vivo tumor fragments^{25,26}. Further development of an ex vivo platform that allows for genetic manipulation and screening will be able to accommodate a new generation of ICB research.

Our T-cell resistance screen identified B2M, JAK1, APOL2 and SASH1 as hits. In the initial list of candidate genes B2M was identified as mutated more than once, JAK1 was homozygously mutated at relapse and APOL2 and SASH1 were heterozygous at baseline and homozygous on progression. Loss of antigen presentation through B2M mutation has been previously described as a resistance mechanism to T-cell killing and ICB^{14,15}. It is therefore not surprising that B2M was a hit that validated in our study. Similarly, loss of JAK/STAT pathway has been previously reported to confer resistance to ICB^{11,12}. However, loss of JAK1 did not validate in our co-culture model. This is unexpected, as loss of JAK1 has been reported to confer resistance to ICB and adoptive cell transfer²⁷. However, it has been previously reported that loss of JAK1 and JAK2 does not confer resistance to MART-1 positive T-cell killing *in vitro* due to baseline MHC-I expression allowing for T-cell recognition²⁸. This is also in line with our observation and further underscores the differences in resistance to ICB *in vivo* and T-cell killing *in vitro*. Furthermore, APOL2 and SASH1 were identified as potential novel players of ICB resistance. APOL2 expression is induced upon IFN γ and it was speculated to mediate cell death similarly to APOL1²⁹. Therefore, it might be involved in resistance to T-cell killing through a similar mechanism. However, as knock-down of APOL2 did not influence cell death induced by IFN γ in HeLa cells²³ and knock-out of APOL2 did not prevent T-cell killing, there might be other factors involved in the T-cell mediated cell death. On the other hand, SASH1 has been described as a tumor suppressor gene that opposes cell proliferation³⁰. Loss of SASH1 could therefore increase cell proliferation and lead to resistance. However, our data indicates that SASH1 might be essential in melanoma cells and knock-down of SASH1 does not lead to resistance to T-cell killing. Taken together, APOL2 and SASH1 might be either a passenger mutation or lead to a mild resistance phenotype that is not detectable in the system with strong T-cell killing. Using milder T-cell pressure or polyclonal TCRs might more closely mimic the conditions *in vivo* and allow for validation of milder hits.

Understanding the molecular mechanisms of resistance to ICB can help design new treatment strategies and ICB combination treatments. Since antigen presentation and IFN pathways have been described to lead to ICB resistance, multiple efforts have focused on re-sensitizing resistant tumors to ICB. For example, activating dsRNA sensing through intratumoral BO-112 consisting of polyinosinic:polycytidylic acid (poly I:C) re-sensitized JAK1 negative tumors to ICB^{27,31}. Additionally, using TLR9 agonist SD-101 can

stimulate dendritic cells to produce IFN³² and is effective against resistant tumors²⁸. On the other hand, resistance of tumors with mutations in antigen presenting pathway could be overcome by using CAR-T cells which are not limited by antigen presentation and can directly bind to a surface marker. Additionally, NK cells might be able to target MHC-I negative cells. By understanding the intrinsic and extrinsic factors of ICB resistance we might be able to design biomarkers and combination treatments that will facilitate treatment decisions and further development of precision oncology.

It remains remarkable that even though resistance to ICB therapy can readily be accomplished *in vivo*, most patients that do respond have long term benefit³³. This is in contrast to patients that are treated for advanced disease with small molecule targeted therapies. One possible explanation may be that T cell killing has a bystander effect that can even lead to killing of antigen-negative cells³⁴. This may explain why acquired clinical resistance to ICB is seen less frequently than resistance to targeted therapies. These findings underscore the importance of designing therapies that take advantage of bystander effect, as intra-tumor heterogeneity appears to be the biggest hurdle in treating advanced cancers effectively.

METHODS

Cell lines

Mel526 was a kind gift from Schumacher lab (NKI). The cells were cultured in RPMI (Gibco) supplemented with 10% FBS (Serana) and 1% penicillin-streptomycin (Gibco). HEK293T cells (ATCC) were cultured in DMEM (Gibco) supplemented with 10% FBS (Serana) and 1% penicillin-streptomycin (Gibco). B2M knock-out Mel526 cells were generated by PEI (Sigma Aldrich) transfection using pLV-U6g-EPCG vector and gRNA (Sigma Aldrich). The cells were then analysed by flow cytometry and single cell clones were generated. Mel526-Cas9 cell line was generated by lentiviral transduction of lentiCas9-EGFP (Addgene #63592) and sorted twice for high GFP expression. All cell lines were maintained in a humidified incubator at 37 °C and 5% CO₂.

Antibodies

Antibodies against Cas9 (#14697) and Jak1(#50996) were purchased from Cell Signalling technologies. Antibody against HSP90 was purchased from Santa Cruz (sc-13119). Antibody against Tubulin was purchased from Sigma Aldrich (#T9026). Antibody against B2M was purchased from Abcam (ab75853). Antibody against APOL2 was purchased from Atlas (HPA001078). Secondary anti-rabbit (#170-6515) and anti-mouse (#170-6516) antibodies were purchased from BIO-RAD.

Generation of MART-1 T-cells

T-cells were obtained from buffycoats of healthy donors in collaboration with Sanquin, Amsterdam, the Netherlands. Briefly, peripheral blood mononuclear cells (PBMCs) were isolated using Lymphoprep (Stem Cell Technologies). T-cells were isolated and activated using CD3/CD28 Dynabeads (Thermo Fisher Scientific). Next, T-cells were infected with MART-1 TCR retrovirus on Retronectin-coated (Takara) plates. After 48h T-cells were harvested and MART-1 expression was confirmed by flow cytometry (BD PharMingen, a-mouse TCR b chain). T-cells were cultured in RPMI (Gibco), supplemented with 10% human serum (Sigma Aldrich), 1% penicillin-streptomycin (Gibco), IL-2 and IL-15 at 10ng/ml (both Preprotech).

Flow cytometry

Expression of B2M and HLA-I was analyzed by multicolor flow cytometry using Beckman Coulter CyAn ADP. Cells were stained with PE-conjugated antibodies against HLA-I (#311440, Biolegend) and APC-conjugated antibodies against B2M (#MA5-17683 of Thermo Fisher Scientific). Sorting of Mel526-Cas9 cells was performed on BD FACSDiva 8.0.1 in two steps to ensure high Cas9 expression. Editing efficiency of Mel526-Cas9 cells with GFP reporter was analysed using BDLSRFortessa Cell Analyzer. All data was analyzed using FlowJo.

Analysis of editing efficiency

The editing efficiency of Mel526-Cas9 cells was assessed using the GFP reporter pXPR_011 (Addgene #59702). Wild-type and Cas9 cells were transduced with the reporter plasmid, selected with puromycin and analysed by flow cytometry. Editing efficiency was estimated based on the reduction in GFP signal over time. Additionally, parental and Mel526-Cas9 cells were transduced with 3 gRNAs against two essential genes (RPS13 and PSMB2) and a non-essential gene (OR9Q2). After puromycin selection, the cells were plated for colony formation assay to assess viability and editing efficiency. B2M KO cells were further characterised by PCR using FW: CTCGCTCCGTGGCCTTAG and RV: ATGTCGGATGGATGAAACCC and Sanger sequencing of the amplicon.

Western blot

Cells were seeded and after 24h washed with PBS and lysed using RIPA buffer (25mM Tris-HCL pH 7.6, 150 mM NaCl, 1% NP-40, 1% sodium deoxycholate and 0.1% SDS) containing Complete Protease Inhibitor Cocktail (Roche) and phosphatase inhibitor cocktails I and II (Sigma). Upon protein extraction and normalisation loading buffer and reducing agent (both Thermo Fisher) were added to the samples. Samples were boiled at 95°C and separated on 4-12% polyacrilamide gradient gels (Invitrogen). Next, proteins were transferred to a PVDF membrane, blocked in blocking buffer (5% bovine serum albumin (BSA) in TBS with 0,2% Tween-20 (TBS-T) and incubated with primary antibodies in blocking solution (1:1000). Secondary antibodies were used at 1:10000 dilution.

Chemiluminescence substrate (ECL, Bio-Rad) was then added to the membranes and visualised using ChemiDoc Imaging System (Bio-Rad).

Immunohistochemistry

Staining of B2M KO and control cells was performed on a Discovery Ultra autostainer (Roche) using rabbit polyclonal α - β 2M (Dako) and OmniMap α -Rabbit horseradish peroxidase (HRP) followed by ChromoMap 3,3'-Diaminobenzidine (DAB) detection kit. Nuclei were counterstained with Hematoxylin II and slides were treated with Bluing Reagent (Roche).

Plasmids

The lentiviral shRNA vectors were selected from the arrayed TRC human genome-wide shRNA collection. Control shRNA:

CCTAAGGTTAAGTCGCCCTCGCTCGAGCGAGGGCGACTTAACCTTAGG,

shRNA targeting B2M#1:

CCGGCTGGTCTTTCTATCTCTTGTACTCGAGTACAAGAGATAGAAAGACCAGTTTTTG, shRNA B2M#2:

GTACCGGAGGTTTGAAGATGCCGCATTTCTCGAGAAATGCGGCATCTTCAAACCTTTTTTTTG, shRNA targeting SASH1#1:

CCGGCTGTAGAAAGTCTTCGAGTTCTCGAGAACTGCGAAGACTTCTACAGTTTTTTTG,

shRNA targeting SASH1#2:

CCGGCCACCCTTCTACTGTGCATATCTCGAGATATGCACAGTGAAAGGGTGGTTTTTTTG.

Single gRNAs were cloned into pGINa plasmid in which a mouse U6 promoter drives the sgRNA expression with a modified TRACR sequence as previously described³⁵. After BfuAI (New England Biolabs) digestion Gibson Assembly was performed (New England Biolabs). Control sgRNA: ACGGAGGCTAAGCGTCGCAA, sgRNA targeting B2M:

GCCGAGATGTCTCGCTCC,

sgRNA targeting JAK1: CCTAGACAGCACCGTAAT, sgRNA targeting APOL2:

GCTGGGATTACCTGCAGT, sgRNA targeting OR9Q2: AAGGAAGAACTCCGTCCTA,

sgRNA targeting RPS13: CCAGCGCGCTACTTACAGTG and sgRNA targeting

PSMB2:GAGTACCTCATCGGTATCCA .

Lentiviral transduction

To produce lentivirus, second generation lentivirus packaging system (psPAX2 (Addgene #12260) and pMD2.G (Addgene #12259) was used alongside pCMV-GFP as transfection control (Addgene #11153)). Next, HEK293T cells were transfected with the target vector using PEI. Lentiviral supernatant was filtered and collected. Next, target cells were infected with the lentiviral supernatant using Polybrene (8 μ g/ml) and selected with puromycin (2 μ g/ml).

Custom sgRNA library generation

Upon whole genome sequencing of 14 melanoma patients who relapsed on anti-PD-1 treatment a list of 197 genes was prepared following three criteria: Genes that were mutated more than once (n=28), mutations that were present only at relapse and were homozygous (n=33) and mutations that were heterozygous at baseline and homozygous on progression (n=136). Next, 8 sgRNAs per gene were designed using Toronto³⁶ and Brunello³⁷ libraries and Broad online design tool³⁸. 50 non-targeting gRNAs, 50 gRNAs targeting safe-haven regions and 50 gRNAs targeting essential genes were added as controls. The sgRNA sequences were purchased as a pool (Twist Bioscience) with flanking sequences allowing PCR amplification and cloning. Pool of oligonucleotides was amplified in two-step PCR using FW-TCCCAAGAGCGAA and RV-TGCCTCCATACCA primers for PCR1 and FW- TTTTGAGACTATAAATATCCCTTGAGAAAAGCCTTGTTT and RV-GACT AGCCTTATTTAACTTGCTATTCTAGCTCTTAAAC primers for PCR2. The fragments were then cloned using Gibson Assembly (NEB) into BfuAI digested pGIna vector as described above. The representation of sgRNAs was confirmed using next generation sequencing.

Co-culture colony formation assays

For colony formation assay cells were seeded at a density of 100 000 cells per well. After 24h either MART-1 or control T-cells were added, following indicated effector to target (E:T) ratios. After 5 days of co-culture, cells were fixed with 2% formaldehyde (Milipore) in PBS, stained with 0,1% crystal violet (Sigma) in water and scanned. For proliferation assays, 3500 cells per well were plated in 96 well plates. After 24h either MART-1 or control T-cells were added, following indicated effector to target (E:T) ratios. Plates were incubated at 37°C and images were taken every 4 hours using the IncuCyte live cell imaging system. Confluency was calculated to generate growth curves.

Viability assay

Mel526 cells were co-cultured in 96 well plates as described above. After 5 days of co-culture, wells were washed with PBS and viability was measured using resazurin assay on EnVision plate reader (Perkin Elmer). PAO was used as positive control.

CRISPR screen

Mel526-Cas9 cells were screened using a custom-built gRNA library described above. Mel526-Cas9 cells were infected at multiplicity of infection (MOI) between 0.2 and 0.5 and selected with puromycin. After the selection the reference sample (t=) was collected. Cells were then co-cultured with either MART-1 or control T-cells at effector to target ratio of 1:1 for 4 days while maintaining 2000x coverage of the library. Next, T-cells were removed and remaining cells were recovered for 2 days. gRNA sequences were then recovered, amplified in two-step PCR and sequenced to determine abundance in each condition. To normalize for sequencing depth, a relative total size factor was calculated for each sample by dividing the total counts of each sample by the geometric mean of

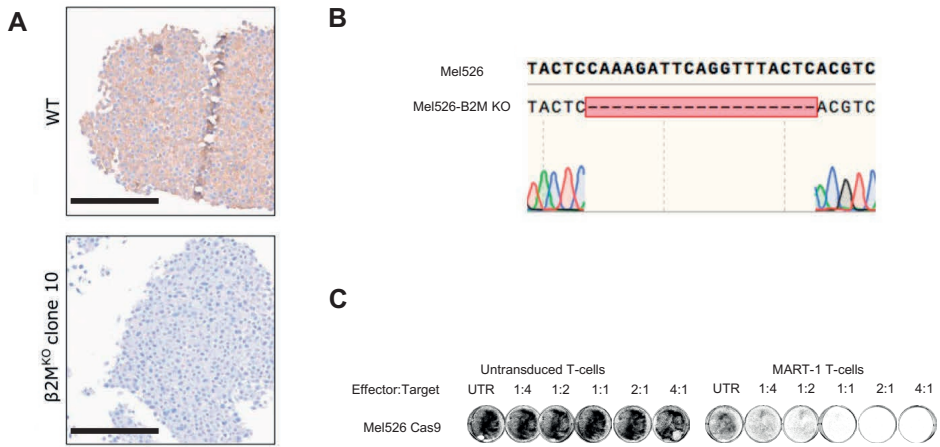
all totals. All values within a sample were then divided by the respective relative total size factor and rounded off to integer values. Hit selection on sgRNA level was performed as differential analysis between MART-1 and control T-cell condition using DESeq2 ³⁹. The results were used as input for gene level analysis using MAGeCK ⁴⁰. Additionally, we calculated median log₂FOLDchange per gene over the sgRNA based on the DESeq2 output.

REFERENCES

1. Xin Yu, J., Hubbard-Lucey, V. M. & Tang, J. Immuno-oncology drug development goes global. *Nat. Rev. Drug Discov.* **18**, 899–900 (2019).
2. Larkin, J. *et al.* Five-Year Survival with Combined Nivolumab and Ipilimumab in Advanced Melanoma. *N. Engl. J. Med.* **381**, 1535–1546 (2019).
3. Jenkins, R. W., Barbie, D. A. & Flaherty, K. T. Mechanisms of resistance to immune checkpoint inhibitors. *Br. J. Cancer* **118**, 9–16 (2018).
4. Barrieto, L. *et al.* Resistance to Checkpoint Inhibition in Cancer Immunotherapy. *Transl. Oncol.* **13**, 100738 (2020).
5. Chowell, D. *et al.* Patient HLA class I genotype influences cancer response to checkpoint blockade immunotherapy. *Science* **359**, 582–587 (2018).
6. Pitt, J. M. *et al.* Resistance Mechanisms to Immune-Checkpoint Blockade in Cancer: Tumor-Intrinsic and -Extrinsic Factors. *Immunity* **44**, 1255–1269 (2016).
7. Fessler, J., Matson, V. & Gajewski, T. F. Exploring the emerging role of the microbiome in cancer immunotherapy. *J Immunother Cancer* **7**, 108 (2019).
8. Kalbasi, A. & Ribas, A. Tumour-intrinsic resistance to immune checkpoint blockade. *Nat. Rev. Immunol.* **20**, 25–39 (2020).
9. Rizvi, N. A. *et al.* Mutational landscape determines sensitivity to PD-1 blockade in non-small cell lung cancer. *Science* **348**, 124–128 (2015).
10. Prasad, V., Kaestner, V. & Mailankody, S. Cancer drugs approved based on biomarkers and not tumor type—FDA approval of pembrolizumab for mismatch repair-deficient solid cancers. *JAMA oncology* (2018).
11. Grasso, C. S. *et al.* Conserved Interferon- γ Signaling Drives Clinical Response to Immune Checkpoint Blockade Therapy in Melanoma. *Cancer Cell* **39**, 122 (2021).
12. Sucker, A. *et al.* Acquired IFN γ resistance impairs anti-tumor immunity and gives rise to T-cell-resistant melanoma lesions. *Nat. Commun.* **8**, 15440 (2017).
13. Hoekstra, M. E. *et al.* Long-distance modulation of bystander tumor cells by CD8 $^{+}$ T cell-secreted IFN γ . *Nat Cancer* **1**, 291–301 (2020).
14. Zaretsky, J. M. *et al.* Mutations Associated with Acquired Resistance to PD-1 Blockade in Melanoma. *N. Engl. J. Med.* **375**, 819–829 (2016).
15. Sade-Feldman, M. *et al.* Resistance to checkpoint blockade therapy through inactivation of antigen presentation. *Nat. Commun.* **8**, 1136 (2017).
16. Mulero-Sánchez, A., Pogacar, Z. & Vecchione, L. Importance of genetic screens in precision oncology. *ESMO Open* **4**, e000505 (2019).
17. Vredevogd, D. W. *et al.* Augmenting Immunotherapy Impact by Lowering Tumor TNF Cytotoxicity Threshold. *Cell* **180**, 404–405 (2020).
18. Manguso, R. T. *et al.* In vivo CRISPR screening identifies Ptpn2 as a cancer immunotherapy target. *Nature* **547**, 413–418 (2017).
19. Patel, S. J. *et al.* Identification of essential genes for cancer immunotherapy. *Nature* **548**, 537–542 (2017).
20. Pan, D. *et al.* A major chromatin regulator determines resistance of tumor cells to T cell-mediated killing. *Science* **359**, 770–775 (2018).
21. Gomez-Eerland, R. *et al.* Manufacture of gene-modified human T-cells with a memory stem/central memory phenotype. *Hum. Gene Ther. Methods* **25**, 277–287 (2014).
22. Marincola, F. M., Jaffee, E. M., Hicklin, D. J. & Ferrone, S. Escape of Human Solid Tumors from T-Cell Recognition: Molecular Mechanisms and Functional Significance. in *Advances in Immunology* (ed. Dixon, F. J.) vol. 74 181–273 (Academic Press, 1999).
23. Galindo-Moreno, J. *et al.* Apolipoprotein L2 contains a BH3-like domain but it does not behave as a BH3-only protein. *Cell Death Dis.* **5**, e1275 (2014).
24. Burgess, J. T. *et al.* SASH1 is a prognostic indicator and potential therapeutic target in non-small cell lung cancer. *Sci. Rep.* **10**, 18605 (2020).
25. Kaptein, P. *et al.* Addition of interleukin-2 overcomes resistance to neoadjuvant CTLA4 and PD1 blockade in ex vivo patient tumors. *Sci. Transl. Med.* **14**, eabj9779 (2022).
26. Voabil, P. *et al.* An ex vivo tumor fragment platform to dissect response to PD-1 blockade in cancer. *Nat. Med.* **27**, 1250–1261 (2021).
27. Kalbasi, A. *et al.* Uncoupling interferon signaling and antigen presentation to overcome immunotherapy resistance due to JAK1 loss in melanoma. *Sci. Transl. Med.* **12**, (2020).
28. Torrejon, D. Y. *et al.* Overcoming genetically based resistance mechanisms to PD-1 blockade. *Cancer Discov.* **10**, 1140–1157 (2020).
29. Wan, G. *et al.* Apolipoprotein L1, a novel Bcl-2 homology domain 3-only lipid-binding protein, induces autophagic cell death. *J. Biol. Chem.* **283**, 21540–21549 (2008).
30. Chen, E.-G., Chen, Y., Dong, L.-L. & Zhang, J.-S. Effects of SASH1 on lung cancer cell proliferation, apoptosis, and invasion in vitro. *Tumour Biol.* **33**, 1393–1401 (2012).
31. Márquez-Rodas, I. *et al.* Intratumoral nanoplexed poly I:C BO-112 in combination with systemic anti-PD-1 for patients with anti-PD-1-refractory tumors. *Science Translational Medicine* vol. 12 (2020).
32. Ribas, A. *et al.* SD-101 in Combination with

- Pembrolizumab in Advanced Melanoma: Results of a Phase Ib, Multicenter Study. *Cancer Discov.* 8, 1250–1257 (2018).
33. Schadendorf, D. *et al.* Pooled Analysis of Long-Term Survival Data From Phase II and Phase III Trials of Ipilimumab in Unresectable or Metastatic Melanoma. *Journal of Clinical Oncology* vol. 33 1889–1894 (2015).
 34. Hoekstra, M. E. *et al.* Publisher Correction: Long-distance modulation of bystander tumor cells by CD8⁺ T-cell-secreted IFN- γ . *Nat Cancer* 1, 749 (2020).
 35. Evers, B. *et al.* CRISPR knockout screening outperforms shRNA and CRISPRi in identifying essential genes. *Nat. Biotechnol.* **34**, 631–633 (2016).
 36. Hart, T. *et al.* Evaluation and Design of Genome-Wide CRISPR/SpCas9 Knockout Screens. *G3* 7, 2719–2727 (2017).
 37. Doench, J. G. *et al.* Optimized sgRNA design to maximize activity and minimize off-target effects of CRISPR-Cas9. *Nat. Biotechnol.* **34**, 184–191 (2016).
 38. Joung, J. *et al.* Genome-scale CRISPR-Cas9 knockout and transcriptional activation screening. *Nat. Protoc.* **12**, 828–863 (2017).
 39. Love, M. I., Huber, W. & Anders, S. Moderated estimation of fold change and dispersion for RNA-seq data with DESeq2. *Genome Biol.* **15**, 550 (2014).
 40. Li, W. *et al.* MAGeCK enables robust identification of essential genes from genome-scale CRISPR/Cas9 knockout screens. *Genome Biol.* **15**, 554 (2014).

SUPPLEMENTARY FILES



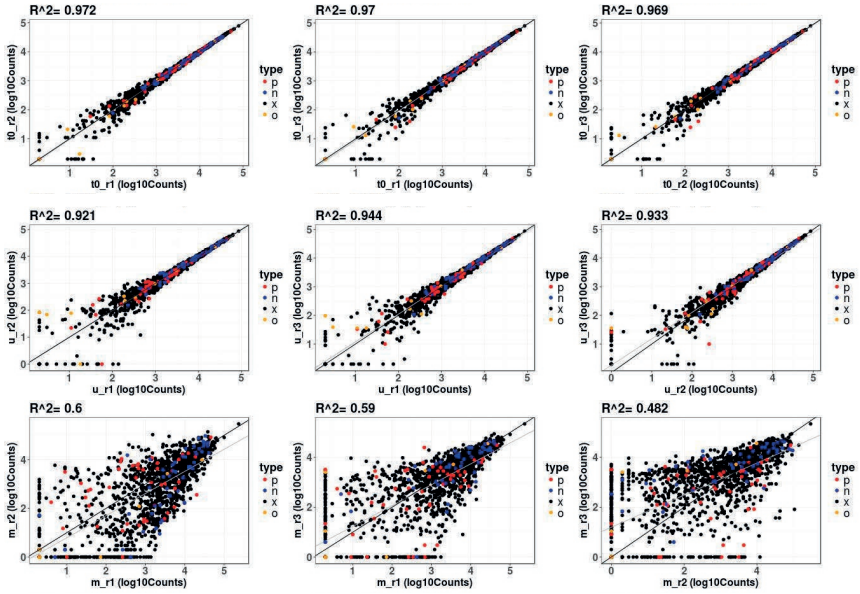
Supplemental Figure 1

A Immunohistochemistry analysis of Mel526 parental cells and Mel526 B2M knock-out cells stained with anti B2M antibody. Scale bar indicates 100 μ m.

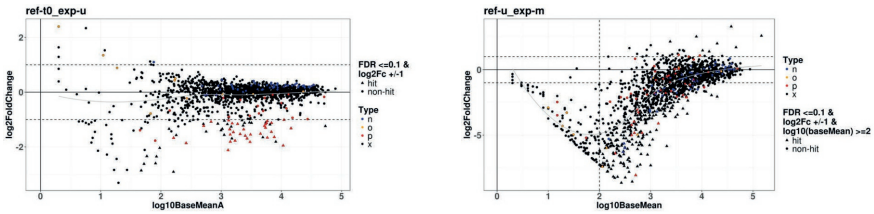
B Sanger sequencing of B2M gene in Mel526 parental and B2M knock-out cells. Codons 74-92 are shown and the 19bp deletion is shown in red.

C Colony formation assay of Mel526 Cas9 cells co-cultured with either untransduced or MART-1 transduced T-cells in different effector to target ratios for 5 days.

A



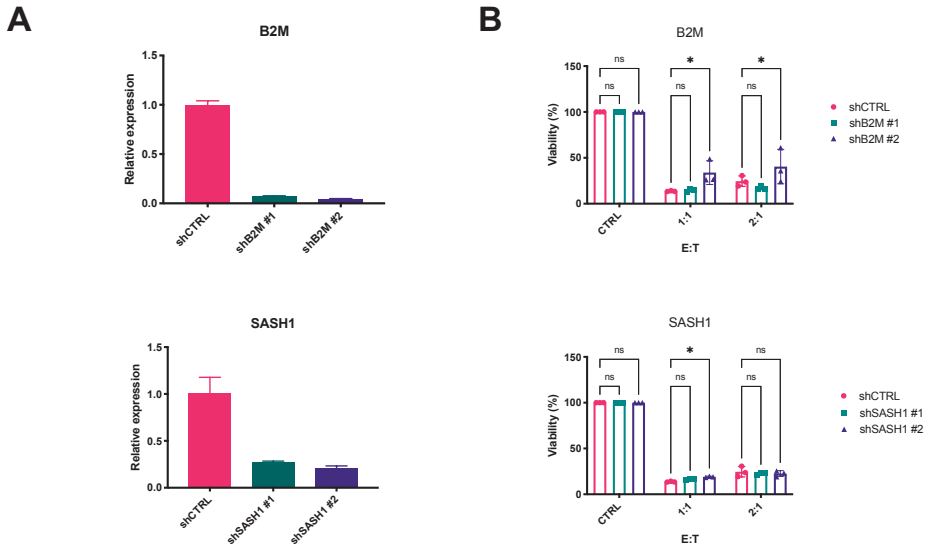
B



Supplemental Figure 2

A Correlation between replicates for reference samples (top), untransduced condition (middle) and MART-1 condition (bottom). Each dot represents a sgRNA, sgRNAs targeting positive controls are marked in red, negative controls in blue, experimental sgRNAs in black, and others in orange. Correlation coefficient for each comparison is shown.

B MA plots comparing reference condition to untransduced (left) and untransduced to MART-1 (right). The y axis shows \log_2 fold change and the x axis shows \log_{10} base mean. Each dot represents a sgRNA, sgRNAs targeting positive controls are marked in red, negative controls in blue, experimental sgRNAs in black, and others in orange. Dotted line denotes the cutoff of significance for hit calling.



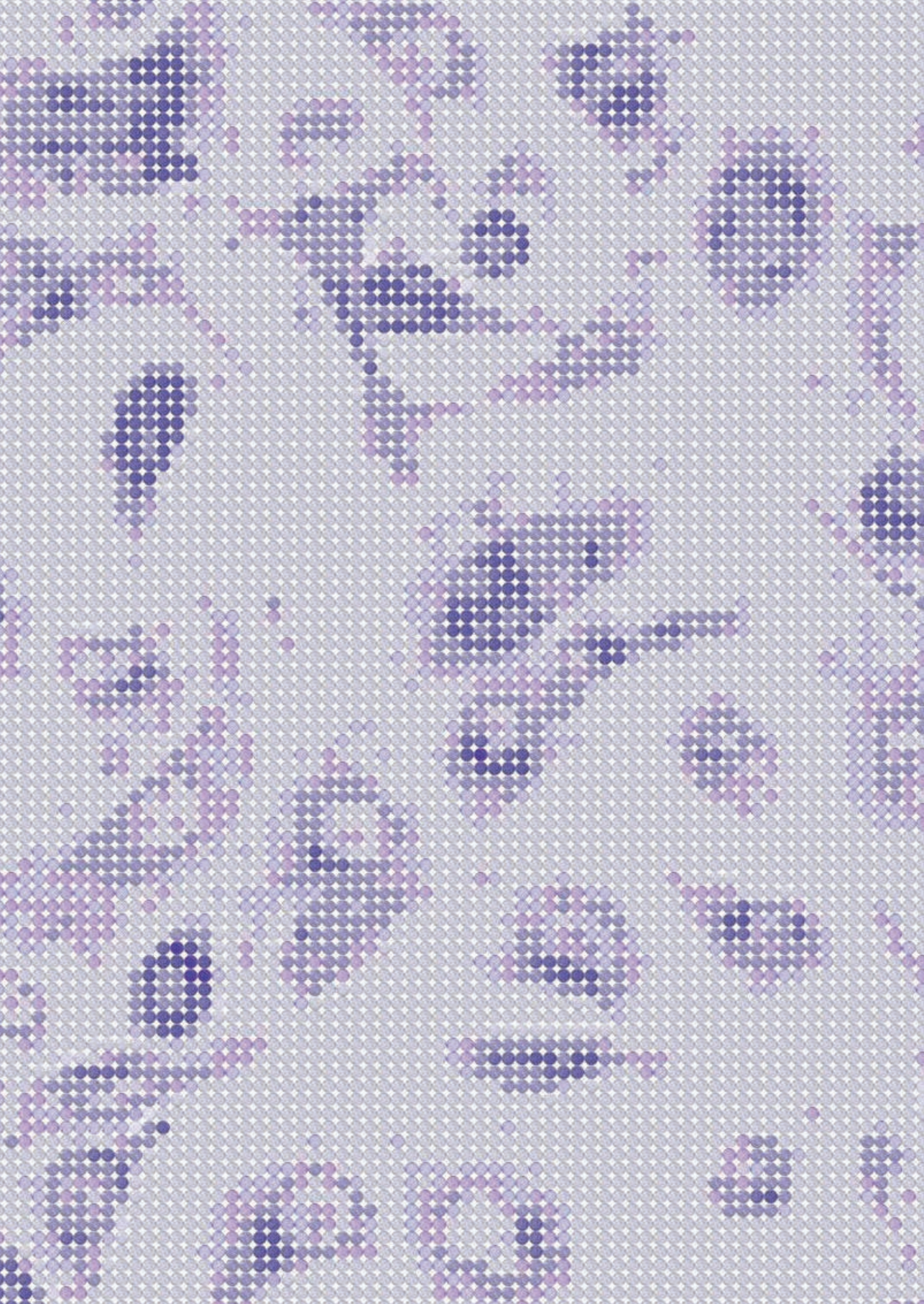
Supplemental Figure 3

A qPCR analysis of B2M and SASH1 normalized against expression of housekeeping gene GAPDH. Mean of three technical replicates is shown and error bars indicate standard deviation.

B Viability assay of Mel526 cells, shB2M, shSASH1 cells. Two independent shRNAs were used to knock down B2M and SASH1. Cells were co-cultured with MART-1 positive T cells for 5 days. Effector to target ratios are indicated. Mean of three technical replicates are shown and error bars show standard deviation. Data was analysed using two-way ANOVA with Šidák's post-hoc test (* p < 0.05).

Supplemental Table 1

Priority 1	Priority 2	Priority 3				
ANKRD62	FBXO22	ACSM2A	TTC22	TULP1	BPIFB6	PROP1
ANKS1B	FBXW4	AK5	UBR4	ULK4	BTN1A1	RCOR1
ANO4	RPRD1B	BPIFB4	VIM	ZFHX2	CD163L1	SPAG8
B2M	ANKRD62	BRCA2	WDFY4	CDH20	CHMP3	ZNF862
BIRC6	ANKS1B	C1orf168	YTHDF2	PIEZO2	DNAH6	
C1orf168	BCL2L1	C1orf168	ZNF500	SETBP1	DSC2	
CD163L1	MKI67	C1orf50	ZNF728	CDKAL1	E2F3	
DCLRE1C	OTP	CLUAP1	FAM166A	CFHR5	FAM188A	
DGKI	PTGS1	CSMD2	FBP2	DENND4A	FOXJ2	
DNAH5	QRICH1	DEPDC1	OLFM1	FOXA3	FSHR	
DNAH6	RFXANK	FAM151A	OR13D1	MUC16	IRX3	
DNM1	SASH1	FGGY	TAF1L	MYO1F	LZTR1	
EIF3A	SIGLEC1	FRY	WNK2	PPAN	MFSD2B	
GPR98	SPEM1	GATSL3	AFF4	RDH8	MUC16	
KCNV2	SPTBN5	GIPC2	BTNL9	SLC12A3	MUC16	
KRT2	C22orf46	HSD3B2	DHRS4-AS1	WIZ	MUC19	
MGAM	GFOD1	LACTBL1	EIF5	ZNF66	MYH4	
MUC16	HIST1H1E	LRIG2	ELP6	ZNF765	NDUFAF7	
PHF3	JAK1	MACF1	FAM83B	ZNF98	OGFR	
PKHD1L1	EYA1	MYBPHL	FAT2	ADRA1D	OLAH	
PPIL1	SAMD15	NBEA	NFKBIE	HPN	PKHD1L1	
SAMD15	STARD9	NGF	OR5AU1	CDH18	PPIL1	
SENP1	ZFHX4	PKD1	PAPLN	DCBLD2	SALL1	
SIGLEC1	KIAA1107	PODN	PGK2	DEFB131	SAMD14	
TTN	PRKAR1A	RAB11FIP3	POP1	NLRP14	SGTA	
WDR52	SPATA31A1	RBFOX1	PREX2	SEC24B	SH3BP2	
ZFHX4	SPATA31E1	RND1	RP1	TMEM200A	SPDYE4	
ZNF765	LOXL4	SLC44A5	SLC22A13	VWA3B	VPRBP	
	MAGEA10	SLC5A9	SYNE2	ANK3	WASF1	
	WDR16	SPON2	TACC1	APOL2	MGAM	
	CILP2	SYCP1	TCTE1	ARHGAP15	NUTM2F	
	JAK2	TIGD7	TMEM63B	ART1	OR1S1	
	B2M	TSC2	TMEM89	BIRC6	OR5D16	



Chapter 5

General Discussion

Even though chemotherapy has been an important pillar of cancer therapy, many approved and widely used chemotherapeutics do not have a clear mechanism of action^{1,2}. The advancements in sequencing technology allowed for a new understanding of cancer as a genetic disease that depends on mutations of driver genes. Efforts to target the mutated drivers led to development of targeted therapy. In contrast to chemotherapy, the exact mechanism of action of targeted therapies is usually known. Known targets, mechanism of action and biochemical effects of the treatment can help understanding which other factors are involved in resistance and sensitivity. For example, EGFR inhibitor cetuximab is not effective in colorectal cancer patients harboring mutations in KRAS which activates downstream signaling of MAPK pathway³. In this way, understanding mechanisms of action can help stratify patients and increase response. Curiously, responses to targeted therapy have been vastly disappointing due to resistance and lack of predictive biomarkers. In an effort to overcome resistance, different combinations of targeted therapies have been tested in numerous clinical trials. However, these trials often fail or show limited response and reasons behind lack of response are rarely investigated. Therefore, improving precision oncology relies not only on knowledge of drugs' mechanisms of action but also understanding of factors mediating sensitivity and resistance. Only then can we design rational approaches to cancer therapy that are biomarker driven supported by effective combination treatment. A useful tool to achieve these objectives is through the use of functional genetic screens. This unbiased approach allows for individual perturbation of every gene in the genome and is therefore not limited to existing knowledge. Recently, knowledge generated from genetic screens has shown the potential to change clinical practice. A genetic screen in colorectal cancer cells treated with BRAF inhibitor vemurafenib revealed EGFR as synthetic lethal interaction⁴. After extensive pre-clinical and clinical validation, EGFR inhibitors are now approved as a combination treatment with BRAF inhibition in colorectal cancer⁵. Using new technologies to improve genetic screens, new libraries and new models of disease can help us uncover even more rational combination therapies for cancer.

RATIONAL REUSE OF ABANDONED DRUGS

In **chapter 2** we performed resistance and synthetic lethality screens in cancer cells treated with indisulam. Indisulam has been shown to be well tolerated in patients but showed limited clinical response and was thus abandoned. The limited clinical response might be due to lack of patient selection, as subpopulation with a specific mutation might benefit more from the treatment. Furthermore, there might be a tumor type that would be more responsive to indisulam. For example, recent study showed that neuroblastoma might be highly responsive to indisulam⁶.

Indisulam has since its discovery as a sulfonamide chemotherapeutic agent been re-

classified as a molecular glue that specifically degrades splicing factor RBM39. Molecular glues and proteolysis targeting chimeras (PROTACs) are interesting new additions to targeted therapy as they allow for targeted degradation of undruggable targets. PROTACs consist of two protein binding domains that connect an E3 ubiquitin ligase and a target protein, thereby allowing proteasomal degradation of the target protein. On the other hand, molecular glues are small molecules that allow direct protein-protein interaction of proteins that would otherwise not interact⁷. Identification of novel molecular glues has so far been serendipitous, but recent approaches of performing compound screens in hypo-neddylated cells can enable systematic identification of new molecular glues⁸. Since indisulam has a favorable clinical profile and known mechanism of action it is a good candidate for rational reuse in the clinic. However, it is clear that the reuse has to be driven by biomarkers and new combination therapies. It has been shown that high DCAF15 expression and copy number correlates with indisulam sensitivity in hematopoietic and lymphoid cancers⁹, but not in other cancer types. Similarly, MYC amplification correlated with indisulam response in neuroblastoma⁶. This could be due to increased transcription levels in MYC amplified tumors and therefore higher reliance on splicing or due to other MYC-driven changes of cell metabolism which sensitize the cells to indisulam⁶. Furthermore, it is important to note that biomarkers for indisulam sensitivity or resistance might be context dependent. We identified SRPK1 loss as synthetic lethal with indisulam treatment. Our data thus indicate that SRPK1 levels could predict responses to indisulam. As mutations in SRPK1 are rare, transcriptional downregulation of SRPK1 could be used to potentially predict response to indisulam. Furthermore, we described that loss of CAND1 leads to resistance to indisulam. Interestingly, most mechanisms of resistance, including CAND1 loss, DCAF15 loss and RBM39 point mutations, lead to reduced RBM39 degradation. Similarly, it has been shown that reduced RBM39 protein levels on treatment correlated with indisulam sensitivity in myeloid leukemia¹⁰. However, as only degradation of RBM39 on indisulam treatment correlates with response this limits the application of RBM39 as a predictive biomarker of indisulam response. Additionally, Panc10.05 cells that acquired resistance to indisulam but still degrade RBM39 indicate that RBM39 degradation is not a universal marker of response and that additional factors might play a role as well. Future research could include genetic screens in indisulam resistant Panc10.05 cells treated with indisulam to uncover other factors of resistance.

In addition to developing biomarkers of response, finding effective combination strategies can help re-introduction of indisulam into clinical studies. We identified SRPK1 as a possible target for combination therapy. As SRPK1 is another factor involved in splicing, this synthetic lethal interaction is especially interesting as it might indicate that combining other splicing inhibitors with indisulam might be a promising therapeutic strategy. This is further indicated by an increase in splicing errors in cells treated with a combination of indisulam and SRPK1 inhibitor. Using a different compound that

would increase splicing errors might lead to a similar outcome. Interestingly, we did not identify other splicing factors in the dropout screen. As the screen was performed using a library targeting human kinome many splicing factors might not be present in the library. It would be interesting to test a custom splicing library in a similar screen. Even though SRPK1 inhibitor SPHINX31 was active *in vitro* and combination of SPHINX31 and indisulam induced apoptosis and prevented acquired resistance to indisulam, the compound was not stable enough *in vivo*. It was therefore not suitable for validation in animal experiments. Future experiments might include additional SRPK1 inhibitors such as SRPKIN-1¹¹ to test *in vitro* and *in vivo* and facilitate the translation to the clinic. Furthermore, we showed that cancer cells readily acquire resistance to indisulam upon long exposure, which may be prevented by using combination treatments with SRPK1 inhibitor or BCL-xL inhibitors. Further understanding of the acquired resistance to indisulam and acquired vulnerability to BCL-xL inhibitors will determine the scope of this finding. For example, a dropout screen in indisulam resistant Panc10.05 cells could help identify the mechanism of resistance. Another exciting opportunity for combination with indisulam is immune checkpoint blockade (ICB). Indisulam induced splicing errors can generate neo-antigens which enables a favorable inflamed tumor microenvironment and response to ICB. This has been tested *in vivo* recently, and showed better response in mice treated with indisulam and anti-PD-1 than either of the single treatments¹². Interestingly, this finding shows that generation of neo-antigen can happen downstream of DNA mutations. Other splicing modulators, such as PRMT inhibitor MS-023 showed similar effect as indisulam¹². Expanding the toolbox of neo-antigen generation from DNA to RNA allows more opportunities for combination treatments with ICB. Additionally, other cellular processes downstream of DNA might be considered to generate neo-antigens. For example, ribosomal frameshifting might generate novel peptides that act as neo-antigens and improve immune recognition¹³. Combining indisulam with other neo-antigen inducers might allow for robust neo-antigen generation especially in tumors with low mutational burden.

In addition to indisulam induced splicing errors it is important to note that indisulam was first described as a CDK2 inhibitor¹⁴. Indisulam could therefore also be combined with CDK4/6 inhibitors as we discuss in **chapter 3**.

The success of re-introduction of indisulam in the clinic now depends on additional preclinical validations of combination treatments. Future clinical studies could include validation of potential biomarkers in the clinical samples. It will be interesting to see if biomarker-driven indisulam clinical trials will show more success than in the past and if combination treatments can further improve it.

IMPROVING SENEESCENCE INDUCTION FOR CANCER THERAPY

In **chapter 3** we performed genetic screens to find enhancers of CDK4/6 inhibitor palbociclib in triple negative breast cancer cells. Palbociclib and other CDK4/6 inhibitors such as ribociclib and abemaciclib have been shown to induce cellular senescence in various cancer types¹⁵⁻¹⁹. Senescence induction has become a new option for cancer treatment, as it stops cell proliferation and recruits immune cells through SASP. Although many factors that prevent senescence induction have been identified²⁰⁻²³, factors that facilitate senescence induction have been largely unknown. Many senescence inducers, such as etoposide (topoisomerase II inhibitor) and alisertib (aurora kinase A inhibitor) are very efficient at inducing senescence *in vitro*²⁴. On the other hand, palbociclib is a weak senescence inducer in cancer cells. As the number of available senescence inducers is limited it would be interesting to test other weak senescence inducers in a genetic screen for combinations that improve senescence induction. We identified that loss of *CDK2* increased senescence induction in cells treated with palbociclib in multiple cancer cell lines. It would be interesting to check if patients with low CDK2 activity, for example due to *CCNH* mutation, would respond better to palbociclib. In this case, reduction of CDK2 activity could be a biomarker for palbociclib treatment. Improved understanding of senescence induction could help using senescence inducers in the clinic.

One of the hurdles of using senescence inducers *in vivo* is heterogeneity of senescence induction due to differences in drug concentration within a tumor, tumor heterogeneity and potential reversibility of senescence. Interestingly, combination therapy has been shown to improve senescence induction *in vivo*. For example, combining palbociclib with MEK inhibitor trametinib led to an increase of SA-Bgal positive tumor area in preclinical mouse models^{25,26}. Similarly, we show that the combination of palbociclib and indisulam improved senescence induction *in vitro*. Our data suggests that palbociclib and indisulam induce senescence across cancer cell lines of different tissue type and genotype. Future research using additional mouse models will confirm if this combination is comparable to palbociclib and trametinib *in vivo*. Additionally, future studies can assess how homogeneous palbociclib and indisulam induced senescence is *in vivo*. It would also be interesting to perform a genetic screen to study bypass of senescence induction in cells treated with palbociclib and indisulam or CDK2 knock-out cells treated with palbociclib. Furthermore, as indisulam is an indirect CDK2 inhibitor that modulates the activation of CDK2 it would be interesting to compare it to a direct CDK2 inhibitor as it becomes available. Interestingly, another CDK4/6 inhibitor abemaciclib has been shown to also target CDK2 which could be the reason it is more effective in the clinic compared to palbociclib²⁷. Furthermore, it would be interesting to test abemaciclib as well as the triple inhibitor of CDK2/4/6 combined with a senolytic in a clinical study.

Another hurdle to using senescence inducers as cancer therapy is that senescent cells can lead to tumor promoting microenvironment. This is one of the reasons that senolytic therapies, which kill senescent cells, have been developed. For example, we showed that cells treated with the combination of palbociclib and indisulam respond to the senolytic agent ABT-263. It would be interesting to perform a similar experiment *in vivo* as well. Finally, as indisulam degrades RBM39 and leads to accumulation of splicing errors leading to neo-antigen generation, immune cells can recognize and eliminate them¹². The treatment of palbociclib and indisulam could be followed by ICB therapy to increase the activity of T-cells. As senescent cells already attract the immune system through SASP, combination of senescence inducers with ICB could improve the outcome (reviewed in ²⁸). If senescent cells also harbor neo-antigens due to indisulam treatment this could further improve the response.

To use senescence inducers as cancer treatment we have to understand the factors mediating senescence induction and bypass in cancer cells as well as develop potent senolytic strategies.

ACQUIRED RESISTANCE TO CHECKPOINT BLOCKADE

Recent advancements in immunotherapy, especially success of immune checkpoint blockade (ICB) have transformed cancer treatment. Initial success of ICB led to numerous clinical trials testing combinations of ICB and other targeted treatments, chemotherapeutic agents and other experimental compounds. As many of these combinations were not based on preclinical data or a rational hypothesis it is not surprising that the outcomes of many of these trials were disappointing. Therefore, the need for new combination therapies that improve the efficacy of ICB is still present. In addition, intrinsic and acquired resistance to ICB can limit the effect of ICB treatment or combination treatment. Understanding the factors of resistance, discovering predictive biomarkers and testing rational combinations will improve the clinical use of ICB.

In **chapter 4** we describe an unconventional approach to study acquired resistance to ICB. Generally, genetic screens are performed and validated *in vitro* followed by assessment of clinical relevance of the finding. It is therefore not uncommon that the findings have little clinical importance (for example, the candidate gene turns out to be not relevant in causing the studied phenotype in patients) which limits the translational value of the discovery. We therefore used a reverse approach, where clinical data is used to generate a list of candidate genes used to assemble a custom CRISPR library that can be used for screening in an *in vitro* model of the disease. It would be of high interest to create multiple custom sgRNA libraries using patient data of a specific disease

and treatment. Custom libraries are usually smaller and thus easier to handle, allowing higher complexities for screening. Additionally, this approach could also include CRISPR activation (CRISPRa) technology to study gain of function mutations and transcriptional activation. Interestingly, a recent study performed a CRISPRa screen in melanoma cells co-cultured with T-cells which shows the potential of such an approach²⁹.

Next, success of *in vitro* validation of a clinical observation depends on the choice of model. One of the biggest hurdles of studying ICB is a lack of suitable *in vitro* models that adequately recapitulate the complexities of tumor microenvironment. In particular, the heterogeneity of T-cells and tumor cells is challenging to model *in vitro*. One interesting approach cultures tumor organoids co-cultured with T-cells from the same patient's peripheral blood^{30,31}. As this system more closely resembles tumor microenvironment it would be valuable to adapt it for genetic screens. Other options include *in vivo* screens in immunocompetent mouse models or using a simpler T-cells co-culture system *in vitro*. In this case using T-cell killing as a readout is simpler but it overlooks the complexity of ICB. Most notably, as we do not use ICB in this model it offers only a limited representation of resistance. For example, other immune checkpoints such as TIM-3 and LAG-3 have been described and it might be involved in response to ICB, but not detectable *in vitro*³². Furthermore, in MART-1 system cancer cells all express a strong antigen leading to very efficient T-cell killing, which might not be the case *in vivo*. Therefore, we might miss weak hits that lead to mild resistance, which still might be relevant *in vivo*. For example, loss of JAK1 has been described to be involved in resistance to ICB, but it did not validate using the MART-1 system. This is most likely due to background MHC-I expression and strong T-cell pressure. On the other hand, loss of B2M leads to strong resistance phenotype and B2M was the only validated hit in our screen.

Loss of antigen presentation due to B2M loss has been extensively studied as a mechanism of immune evasion and resistance to ICB. However, there are also reports of patients with B2M negative tumors that still benefit from ICB³³. This could be for example due to clearance by other immune cells such as NK-cells or $\gamma\delta$ T-cells³⁴. It is becoming increasingly clear that any biomarkers of response to ICB will need to include tumor intrinsic as well as tumor extrinsic factors together. For example, the cancer immunogram combines different aspects of the tumor and tumor microenvironment to determine therapeutic strategy for each patient³⁵.

Lastly, even though we focused on acquired resistance to ICB it is unclear if factors involved in innate and acquired resistance are very different. Due to immunosurveillance tumors develop under constant pressure of the immune system, which can lead to innate resistance.

Blocking the immune checkpoints can lead to new pressure from the immune system

leading to acquired resistance. It would be interesting to include patients that do not respond to ICB and compare the candidate genes to those who respond and later relapse.

One of the unique strengths of ICB are the long term benefits of the responding patients³⁶. The reasons for the long-lasting effects might be presence of memory T-cells³⁷ and bystander effect of T-cell killing³⁸ which can ensure killing of antigen-negative neighboring cells. Exploiting the bystander effect to design better treatment strategies might allow treatment of heterogeneous tumors and prevent resistance to ICB.

CONCLUSIONS AND FUTURE PERSPECTIVES

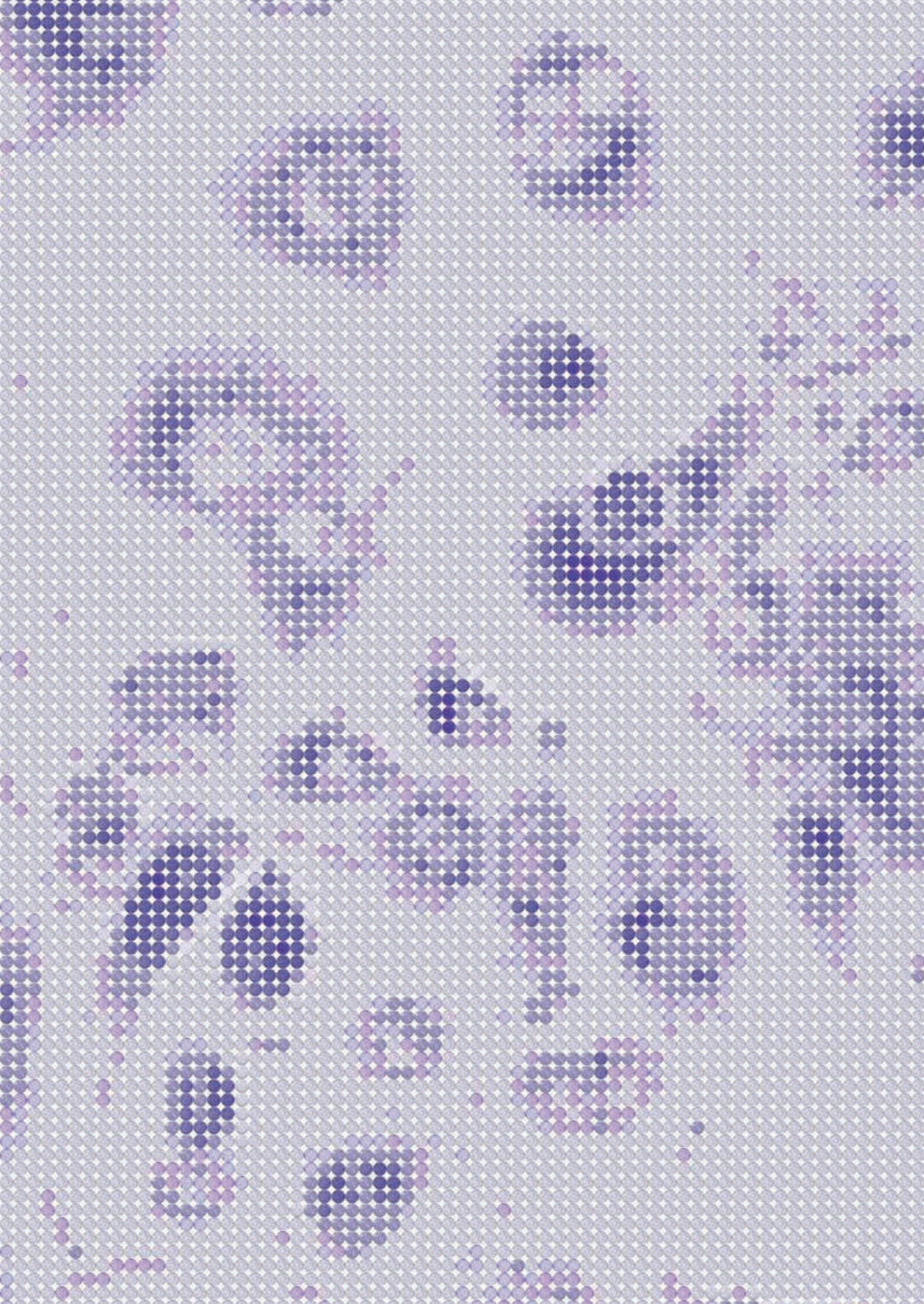
In the past decade genetic screens have allowed for discovery of novel genes that act in cancer-relevant signaling cascades. For example, multiple genetic screens led to discovery of novel factors of resistance and sensitivity to cancer treatment as also described in this thesis. However, it seems that most straightforward resistance and sensitivity genetic screens using most common anti-cancer compounds have now already been done. It would be interesting to see how the power of genetic screens can be used to answer more complex biological questions in the next few years. Genetic screens still offer a great unbiased opportunity to identify new players in cancer-relevant processes. Combining screening technology with different read-outs such as single cell RNA-sequencing³⁹ will offer an additional layer of knowledge. Additionally, development of combinatorial screens will allow probing for genetic interactions⁴⁰. Using various fluorescence-based reporters can enable the identification of new genes in complex biological processes. Taken together, genetic screens performed in an appropriate biological model with suitable read-out still have a potential to discover new biology. The new generation of screens will be able to answer more complex questions and provide knowledge for the next developments in precision oncology.

REFERENCES

1. Lee, M. J. et al. Sequential application of anticancer drugs enhances cell death by rewiring apoptotic signaling networks. *Cell* 149, 780–794 (2012).
2. Moffat, J. G., Vincent, F., Lee, J. A., Eder, J. & Prunotto, M. Opportunities and challenges in phenotypic drug discovery: an industry perspective. *Nat. Rev. Drug Discov.* 16, 531–543 (2017).
3. De Rooij, W. et al. KRAS wild-type state predicts survival and is associated to early radiological response in metastatic colorectal cancer treated with cetuximab. *Ann. Oncol.* 19, 508–515 (2008).
4. Prahallad, A. et al. Unresponsiveness of colon cancer to BRAF(V600E) inhibition through feedback activation of EGFR. *Nature* 483, 100–103 (2012).
5. Taberero, J. et al. Encorafenib Plus Cetuximab as a New Standard of Care for Previously Treated BRAF V600E-Mutant Metastatic Colorectal Cancer: Updated Survival Results and Subgroup Analyses from the BEACON Study. *J. Clin. Oncol.* 39, 273–284 (2021).
6. Nijhuis, A. et al. Indisulam targets RNA splicing and metabolism to serve as a therapeutic strategy for high-risk neuroblastoma. *Nat. Commun.* 13, 1380 (2022).
7. Kozicka, Z. & Thomä, N. H. Haven't got a glue: Protein surface variation for the design of molecular glue degraders. *Cell Chem Biol* 28, 1032–1047 (2021).
8. Mayor-Ruiz, C. et al. Rational discovery of molecular glue degraders via scalable chemical profiling. *Nat. Chem. Biol.* 16, 1199–1207 (2020).
9. Han, T. et al. Anticancer sulfonamides target splicing by inducing RBM39 degradation via recruitment to DCAF15. *Science* 356, (2017).
10. Hsiehchen, D., Goralski, M., Kim, J., Xie, Y. & Nijhawan, D. Biomarkers for RBM39 degradation in acute myeloid leukemia. *Leukemia* 34, 1924–1928 (2020).
11. Hatcher, J. M. et al. SRPKIN-1: A Covalent SRPK1/2 Inhibitor that Potently Converts VEGF from Pro-angiogenic to Anti-angiogenic Isoform. *Cell Chem Biol* 25, 460–470.e6 (2018).
12. Lu, S. X. et al. Pharmacologic modulation of RNA splicing enhances anti-tumor immunity. *Cell* (2021) doi:10.1016/j.cell.2021.05.038.
13. Bartok, O. et al. Anti-tumour immunity induces aberrant peptide presentation in melanoma. *Nature* 590, 332–337 (2021).
14. Fukuoka, K. et al. Mechanisms of action of the novel sulfonamide anticancer agent E7070 on cell cycle progression in human non-small cell lung cancer cells. *Invest. New Drugs* 19, 219–227 (2001).
15. Guan, X. et al. Stromal Senescence By Prolonged CDK4/6 Inhibition Potentiates Tumor Growth. *Mol. Cancer Res.* 15, 237–249 (2017).
16. Muñoz-Espín, D. et al. A versatile drug delivery system targeting senescent cells. *EMBO Mol. Med.* 10, (2018).
17. Miettinen, T. P. et al. Thermal proteome profiling of breast cancer cells reveals proteasomal activation by CDK4/6 inhibitor palbociclib. *EMBO J.* 37, (2018).
18. Torres-Guzmán, R. et al. Preclinical characterization of abemaciclib in hormone receptor positive breast cancer. *Oncotarget* 8, 69493–69507 (2017).
19. Iyengar, M. et al. CDK4/6 inhibition as maintenance and combination therapy for high grade serous ovarian cancer. *Oncotarget* 9, 15658–15672 (2018).
20. Berns, K. et al. A large-scale RNAi screen in human cells identifies new components of the p53 pathway. *Nature* 428, 431–437 (2004).
21. Brummelkamp, T. R. et al. TBX-3, the gene mutated in Ulnar-Mammary Syndrome, is a negative regulator of p19ARF and inhibits senescence. *J. Biol. Chem.* 277, 6567–6572 (2002).
22. Peeper, D. S. et al. A functional screen identifies hDRIL1 as an oncogene that rescues RAS-induced senescence. *Nat. Cell Biol.* 4, 148–153 (2002).
23. Shvarts, A. et al. A senescence rescue screen identifies BCL6 as an inhibitor of anti-proliferative p19ARF–p53 signaling. *Genes Dev.* 16, 681–686 (2002).
24. Jochems, F. et al. The Cancer SENESCopedia: A delineation of cancer cell senescence. *Cell Rep.* 36, 109441 (2021).
25. Lee, M. S. et al. Efficacy of the combination of MEK and CDK4/6 inhibitors in vitro and in vivo in KRAS mutant colorectal cancer models. *Oncotarget* 7, 39595–39608 (2016).
26. Ruscetti, M., Leibold, J., Bott, M. J. & Fennell, M. NK cell-mediated cytotoxicity contributes to tumor control by a cytostatic drug combination. (2018).
27. Hafner, M. et al. Multiomics Profiling Establishes the Polypharmacology of FDA-Approved CDK4/6 Inhibitors and the Potential for Differential Clinical Activity. *Cell Chem Biol* 26, 1067–1080.e8 (2019).
28. Wang, L., Lankhorst, L. & Bernards, R. Exploiting senescence for the treatment of cancer. *Nat. Rev. Cancer* 22, 340–355 (2022).
29. Joung, J. et al. CRISPR activation screen identifies BCL-2 proteins and B3GNT2 as drivers of cancer resistance to T cell-mediated cytotoxicity. *Nat. Commun.* 13, 1606 (2022).
30. Dijkstra, K. K. et al. Generation of Tumor-Reactive T Cells by Co-culture of Peripheral Blood Lymphocytes and Tumor Organoids. *Cell* 174, 1586–1598.e12 (2018).

31. Cattaneo, C. M. et al. Tumor organoid-T-cell coculture systems. *Nat. Protoc.* 15, 15–39 (2019).
32. Qin, S. et al. Novel immune checkpoint targets: moving beyond PD-1 and CTLA-4. *Mol. Cancer* 18, 155 (2019).
33. Middha, S. et al. Majority of B2M-Mutant and -Deficient Colorectal Carcinomas Achieve Clinical Benefit From Immune Checkpoint Inhibitor Therapy and Are Microsatellite Instability-High. *JCO Precision Oncology* 1–14 (2019) doi:10.1200/po.18.00321.
34. de Vries, N. L. et al. $\gamma\delta$ T cells are effectors of immune checkpoint blockade in mismatch repair-deficient colon cancers with antigen presentation defects. *bioRxiv* 2021.10.14.464229 (2021) doi:10.1101/2021.10.14.464229.
35. Blank, C. U., Haanen, J. B., Ribas, A. & Schumacher, T. N. The ‘cancer immunogram’. *Science* 352, 658–660 (2016).
36. Schadendorf, D. et al. Pooled Analysis of Long-Term Survival Data From Phase II and Phase III Trials of Ipilimumab in Unresectable or Metastatic Melanoma. *Journal of Clinical Oncology* vol. 33 1889–1894 (2015).
37. Principe, N. et al. Tumor Infiltrating Effector Memory Antigen-Specific CD8+ T Cells Predict Response to Immune Checkpoint Therapy. *Front. Immunol.* 11, 584423 (2020).
38. Hoekstra, M. E. et al. Publisher Correction: Long-distance modulation of bystander tumor cells by CD8+ T-cell-secreted IFN- γ . *Nat. Cancer* 1, 749 (2020).
39. Dixit, A. et al. Perturb-Seq: Dissecting Molecular Circuits with Scalable Single-Cell RNA Profiling of Pooled Genetic Screens. *Cell* 167, 1853–1866. e17 (2016).
40. Boettcher, M. et al. Dual gene activation and knockout screen reveals directional dependencies in genetic networks. *Nat. Biotechnol.* 36, 170–178 (2018).





Appendix

Nederlandse samenvatting
Povzetek v slovenščini
Curriculum Vitae
Publications
Acknowledgements

NEDERLANDSE SAMENVATTING

Om kankertherapie te verbeteren is er gedetailleerd inzicht vereist in de factoren die de (on)gevoeligheid voor een behandeling verklaren. Als een specifieke mutatie bijvoorbeeld leidt tot resistentie, kunnen we deze mutatie gebruiken als biomarker om de reactie op de medicatie te voorspellen. Op deze manier kunnen we patiënten selecteren voor specifieke behandelingen. Voor het identificeren van nieuwe biomarkers en combinatiebehandeling strategieën kunnen functionele genetische screens worden toegepast, welke het mogelijk maken om elk gen in het genoom gelijktijdig te onderzoeken op veranderingen in gevoeligheid voor een kankergeneesmiddel. In dit proefschrift gebruiken we functionele genetische screens om de gevoeligheid en resistentie van kankercellen voor verschillende 'small molecule' kankergeneesmiddelen en immuuntherapie te bestuderen.

In **hoofdstuk 2** hebben we het kandidaatgeneesmiddel indisulam onderzocht, een geneesmiddel dat eerder in klinische onderzoeken is getest, maar vanwege de lage effectiviteit niet verder is ontwikkeld. Indisulam werkt als een 'moleculaire lijm', waardoor RNA splicing factor RBM39 wordt afgebroken. We laten zien dat verlies van SRPK1 kankercellen gevoelig maakt voor indisulam doordat RNA splicingfouten accumuleren. Daarbij laten we zien dat verlies van CAND1 voorkomt dat RBM39 wordt afgebroken en leidt tot resistentie tegen indisulam. Kankercellijnen kunnen resistentie verwerven tegen indisulam, hetgeen kan worden voorkomen door indisulam te combineren met BCL-xL-remmers. Factoren zoals SRPK1 en CAND1 kunnen potentieel worden gebruikt als biomarkers voor de stratificatie van patiënten voor de behandeling met indisulam. Bovendien zou de combinatie van SRPK1- en BCL-xL-remmer een nieuwe behandeling strategie kunnen zijn.

In **hoofdstuk 3** hebben we indisulam gecombineerd met CDK4/6 remmer palbociclib om kankercellen in een slaapstand te brengen die senescence wordt genoemd). We voerden genetische screens uit om genen te vinden die, indien geremd, het effect van palbociclib versterken. Hieruit kwam CDK2 naar voren als beste gen. CDK2-knock-outcellen die zijn behandeld met palbociclib vertonen kenmerken van senescence. We gebruiken vervolgens indisulam als een indirecte CDK2-remmer en laten inductie van senescence zien in cellen die zijn behandeld met palbociclib en indisulam. Bij het testen van de combinatie van palbociclib en indisulam in muizen was een afname zichtbaar van de tumorgroei ten opzichte van de individuele behandelingen. We toonden aan dat indisulam voorkomt dat CDK2 wordt geactiveerd dankzij CCNH-'downregulatie'. Onze onderzoeksgroep heeft laten zien dat het senescent maken van kankercellen potentieel een nieuwe strategie kan zijn voor de behandeling van kanker, aangezien senescente cellen kwetsbaarheden vertonen waarop kan worden ingespeeld met medicatie. En inderdaad, kankercellen die senescent zijn gemaakt door een combinatie van palbociclib

en indisulam zijn gevoelig voor ABT-263, welke BCL-2, BCL-xL en BCL-W-remt. Tot slot kunnen we concluderen dat we senescence inductie met palbociclib kunnen verbeteren door deze te combineren met indisulam.

In **hoofdstuk 4** hebben we factoren onderzocht die leiden tot verworven resistentie tegen immuuntherapie. Checkpointremmers hebben veel aandacht gekregen doordat deze langdurige respons teweegbrengen in patiënten met melanoom. Een deel van deze patiënten heeft echter geen baat heeft bij deze behandeling. We onderzochten een cohort van patiënten met melanoom die behandeld werden met PD1-remmers en vergeleken DNA-sequenties van biopten van patiënten vóór behandeling en na terugkeer van de tumor. Vervolgens hebben we een lijst samengesteld met kandidaatgenen die mogelijk betrokken zijn bij resistentie tegen checkpointremmers. Vervolgens voerden we een genetische screen uit met een 'library' gericht tegen deze kandidaatgenen in melanoomcellen die in de aanwezigheid van T-lymphocyten waren gekweekt. Hierbij lieten we zien dat verlies van antigeenpresentatie door verlies van B2M leidt tot resistentie tegen T-celdoding. Om de interactie van tumorcellen en het immuunsysteem beter te begrijpen zijn nieuwe modellen nodig.

Het is eerder aangetoond dat genetische screens kunnen leiden tot nieuwe ontdekkingen die impact hebben op de behandeling van kankerpatiënten. In dit proefschrift laten we meer voorbeelden zien van genetische screens die nieuwe factoren van gevoeligheid en resistentie aan het licht hebben gebracht voor verschillende typen kankerbehandelingen. Deze kennis kan leiden tot potentiële biomarkers en combinatiebehandelingsstrategieën die doelgerichte therapieën kunnen verbeteren. Toekomstig onderzoek kan genetische screens combineren met andere technologieën, zoals RNA-sequencing, om nog complexere vragen over kankerbiologie te beantwoorden.

POVZETEK V SLOVENŠČINI

Izboljšanje zdravljenja raka zahteva podrobno razumevanje dejavnikov, ki so pomembni za občutljivost in odpornost na zdravljenje. Če specifična mutacija vodi v odpornost, jo lahko uporabimo kot biološki označevalec za napoved odziva na zdravljenje. S tem znanjem lahko oblikujemo nove kombinacije zdravil, ki preprečijo pojav odpornosti. Da bi našli nove biološke označevalce in kombinacije zdravil, lahko uporabimo funkcionalne genetske preglede (ang. genetic screens), ki nam omogočajo, da na nepristranski način hkrati testiramo vsak gen v genomu. V tej doktorski disertaciji smo z genetskimi pregledi raziskovali občutljivost in odpornost rakavih celic na tarčna zdravila in imunoterapijo.

V drugem poglavju smo raziskovali indisulam, zdravilo, ki je bilo testirano v kliničnih študijah in kasneje opuščeno zaradi nizkih stopenj odziva na zdravljenje. Indisulam deluje kot 'molekularno lepilo', ki razgradi faktor izrezovanja (ang. splicing factor) RBM39. Naši rezultati kažejo, da izguba SRPK1 vodi do večje občutljivosti rakavih celic na indisulam zaradi kopičenja napak pri izrezovanju. Po drugi strani, izguba CAND1 preprečuje razgradnjo RBM39 in vodi v odpornost na indisulam. Rakave celice lahko pridobijo odpornost na indisulam, ki jo lahko preprečimo, če indisulam kombiniramo z inhibitorji BCL-xL. Faktorje, kot sta SRPK1 in CAND1, lahko uporabimo kot biološke označevalce za napoved odziva na zdravljenje z indisulamom. Poleg tega bi lahko kombinacije indisulama z inhibitorji SRPK1 ali BCL-xL predstavljale novo možnost zdravljenja.

V tretjem poglavju smo s kombinacijo indisulama in inhibitorjem CDK4/6 palbocicliba sprožili senescenco rakavih celic. Z genetskim pregledom smo iskali ojačevalce odziva na palbociclib in potrdili CDK2 kot kandidatni gen. Celice z izbitim CDK2 in zdravljene s palbociclibom so pokazale znake senescence. Nato smo uporabili indisulam kot indirektni inhibitor CDK2 in potrdili, da celice, zdravljene s kombinacijo palbocicliba in indisulama, kažejo znake senescence. Ko smo kombinacijo palbocicliba in indisulama testirali na miših, smo opazili zmanjšanje rasti tumorja v primerjavi z zdravljenjem s posamičnim zdravilom. Pokazali smo, da indisulam prepreči aktivacijo CDK2 preko znižanja CCNH. Naša raziskovalna skupina je predlagala nov način zdravljenja raka, ki najprej sproži senescenco in nato z drugim zdravljenjem cilja na pridobljeno ranljivost senescentnih celic. Na primer, rakave celice, pri katerih smo s kombinacijo palbocicliba in indisulama sprožili senescenco, postanejo občutljive na inhibitor proteinov BCL-2, BCL-xL in BCL-W ABT-263. S tem smo pokazali, da lahko sprožitev senescence s palbociclibom izboljšamo z dodatkom indisulama.

V četrtem poglavju smo raziskovali dejavnike, ki so povezani s pridobljeno odpornostjo na imunoterapijo. Zaviralci kontrolnih točk (ZKT) veljajo za obetaven način zdravljenja, saj vodijo do dolgoročnih odzivov pri pacientih z melanomom. Na žalost pa se številni pacienti ne odzovejo na ta tip zdravljenja. Raziskovali smo kohorto pacientov z melanomom, ki so bili zdravljeni z zaviralcem anti-PD-1. Primerjali smo DNA zaporedje v

rakavih celicah iz biopsij pred zdravljenjem in ob ponovitvi bolezni ter pripravili seznam kandidatnih genov za odpornost na ZKT. Nato smo pripravili po meri narejeno knjižnico vodilnih RNK, ki ciljajo kandidatne gene za genetski pregled v celicah melanoma gojenih skupaj z limfociti T. Pokazali smo, da izguba predstavljanja antigenov preko izgube B2M vodi do odpornosti rakavih celic na ubijanje z limfociti T. Da bi nadalje izboljšali razumevanje interakcij med rakavimi celicami in imunskim sistemom potrebujemo nove, bolj kompleksne modele.

Nekatera odkritja dosežena z genetskimi pregledi so že spremenila klinično prakso. V tej disertaciji smo uporabili genetske preglede, da bi odkrili nove dejavnike občutljivosti in odpornosti na različne tipe zdravljenje raka. S tem znanjem lahko razvijemo nove biološke označevalce in kombinacije zdravil, ki pripomorejo k izboljšanju natančne onkologije. Prihodnje raziskave se lahko osredotočijo na bolj kompleksna vprašanja biologije raka z uporabo kombinacije genetskih pregledov in drugih tehnologij, kot je na primer RNK sekvenciranje.

CURRICULUM VITAE

Živa Pogačar was born on the 2nd of January 1992 in Ljubljana, Slovenia. She graduated from high school Gimnazija Vič, Ljubljana in 2010. She was awarded a Zois scholarship for gifted students for her high school and university studies. In 2010, she started her studies of Biotechnology at University of Ljubljana where she obtained a BSc degree in 2013 with a thesis about long non-coding RNA in cancer. She also performed an internship at the Oncology institute in Ljubljana under the mentorship of Prof. Maja Čemažar studying electroporation for cancer treatment. She then enrolled in a master program of Molecular and Functional biology at University of Ljubljana. In 2014, she was awarded an Erasmus+ grant for an exchange program at University of Amsterdam where she also completed an internship in the lab of Prof. René Bernards at the Netherlands Cancer Institute studying resistance to MTH1 inhibitors in cancer. In 2015, she completed her MSc degree and started her PhD in the lab of Prof. René Bernards, where she used genetic screens to understand resistance and sensitivity to cancer treatments. The results of her work are presented in this thesis.

PUBLICATIONS

Pogacar Z*, Groot K*, Jochems F, Dos Santos Dias M, Mulero-Sánchez A, Morris B, Roosen M, Wardak L, De Conti G, Velds A, Liefink C, Thijssen B, Beijersbergen RL, Bernardis R#, Leite de Oliveira R#. (*shared first authors, #shared corresponding authors)
Genetic and compound screens uncover factors modulating cancer cell response to indisulam
Life Science Alliance (2022) doi: 10.26508/lsa.202101348

Pogacar Z, Johnson JL, Krenning L, De Conti G, Jochems F, Liefink C, Velds A, Wardak L, Groot K, Schepers A, Wang L, Song JY, van de Ven M, van Tellinghen O, Medema RH, Beijersbergen RL, Bernardis R*, Leite de Oliveira R* (*shared corresponding authors)
Indisulam synergizes with palbociclib to induce senescence through inhibition of CDK2 kinase activity
PLOS ONE (2022) doi: 10.1371/journal.pone.0273182

Jochems F*, Thijssen B*, De Conti G, Jansen R, **Pogacar Z**, Groot K, Wang L, Schepers A, Wang C, Jin H, Beijersbergen RL, Leite de Oliveira R, Wessels LFA, Bernardis R. (*shared first author)
The cancer SENESCopedia: A delineation of cancer cell senescence.
Cell Reports (2021) doi: 10.1016/j.celrep.2021.109441

Schepers A, Jochems F, Liefink C, Wang L, **Pogacar Z**, Leite de Oliveira R, De Conti G, Beijersbergen RL, Bernardis R.
Identification of autophagy-related genes as targets for senescence induction using a customizable CRISPR-based suicide switch screen
Molecular Cancer Research (2021) doi: 10.1158/1541-7786.MCR-21-0146

Mulero-Sánchez A*, **Pogacar Z***, Vecchione L. (*shared first author)
Importance of genetic screens in precision oncology
ESMO Open (2019) doi: 10.1136/esmoopen-2019-000505

Kunej T, Obsteter J, **Pogacar Z**, Horvat S, Calin GA.
The decalog of long non-coding RNA involvement in cancer diagnosis and monitoring.
Critical Reviews in Clinical Laboratory Sciences (2014) doi: 10.3109/10408363.2014.944299

Bosnjak M, Lorente BC, **Pogacar Z**, Makovsek V, Cemazar M.
Different incubation times of cells after gene electrotransfer in fetal bovine serum affect cell viability, but not transfection efficiency.
Journal of Membrane Biology (2014) doi: 10.1007/s00232-014-9649-9

ACKNOWLEDGEMENTS

My road to the end of PhD was long and sometimes difficult. It would not be possible without the support, love and friendship of many of you. I am deeply grateful we got to share a part of the journey!

Firstly, thank you **René** for providing a great microenvironment for young scientists. Your 'big picture' thinking, scientific storytelling magic and endless optimism are inspiring to me. Thank you for believing in my abilities to finish my PhD even when I doubted it.

Dear **Rodrigo**, I have learned so much from you. You adopted me half-way through my PhD and we shared the joys and sorrows of science ever since. Your dedication to being a good mentor is exceptional and your ability to demand better is your superpower. Thank you for your enthusiastic support and being the best co-promotor I could wish for!

I would like to thank my reading committee: **Thijn Brummelkamp**, **Boudewijn Burgering**, **Madelon Maurice**, **Onno Kranenburg** and **Daniel Peeper** for your time and effort in assessing this thesis. I am also grateful to my PhD committee: **Thijn Brummelkamp**, **Lodewyk Wessels** and **Fred van Leeuwen** for all the helpful comments and discussions about my PhD projects throughout the years.

My dear paranympths, I feel grateful and privileged that I have you by my side at this exciting time. **Fleur**, through the years of sharing the office we became true science sisters! I'm so grateful we got to sit side by side through this crazy journey. You are determined to make me see the sunny side of every situation and are an endless source of support. The memories of our adventures in Boston and New York hold a special place in my heart. I admire your ability to laugh at yourself and how you are always striving to do better. I will miss our office chats about everything and nothing!

Mariana, we for sure have the same genotype. It has been an honor to learn alongside you how to use our powers in a kind and constructive way. You are caring and dedicated, which makes you completely unstoppable! I admire your honesty and scientific determination. I can't wait to see who gets to benefit from your skills next and I'm looking forward to making more memories in Barcelona (and Slovenia)!

My PhD journey has been greatly influenced by all the lab members with whom we shared both the frustrations and happiness. Being surrounded by honest, caring and determined people has impacted me greatly.

Dear **Antonio**, you shine so bright. I don't know anyone else that comes close to the

amount of positivity and energy you bring with you. Thank you for being by my side through all the challenges and being such a good friend. Our moments of singing and dancing in the lab are some of my most cherished PhD memories (blot, blot, Western, baby, Figure 1 will be amazing!). I'm so proud of you and your PhD journey!

Liqin, look, I finally made it! I always admired your ability to see a bigger picture of projects and to make smart scientific decisions. I had a lot of fun sharing the office with you for all these years and seeing you evolve into a proper panda daddy!

Jeroen, I was so happy when you joined the lab. Your creativity and humor make you a great friend in the lab and on the climbing wall. It's really great that we get to finish our PhDs together and I'm so curious to see what amazing things you will do next!

Giulia, from your first lab visit I knew you would fit right in. Your enthusiasm to join every project (or party) is infectious. I had a lot of fun isolating T-cells together and convincing them to do their only job. It's been very sweet to see you start your new position as mama and I'm excited to see how industry life works out for you!

Matheus, there is no-one like you. Your optimism and love for science are inspiring. I really enjoyed our long discussions about science and everything else. I can't wait to see you build your paradoxical science empire!

Robin, your enthusiasm will serve you well in and out of science. Thank you for taking my spot at the PhD council and as a new M2K4 enthusiast! Good luck and don't forget to have fun! **Roderick**, thank you for your contributions to my projects. I always enjoyed discussing science with you. Your care and dedication are extremely valuable. **Cor**, thank you for your bioinformatics magic in all my screen analyses! **Kathy, Sara, Annemiek and Katrien**, you bring some stability to the ever changing world of B7. Your scientific wisdom and kindness had a big impact on me. Thank you for so generously sharing your knowledge! **Astrid & Marielle**, keeping this lab running is not an easy task, especially during the pandemic. Thank you for all your care, effort and positive energy! **Patty**, thank you for your endless support and positivity. You go above and beyond and I so appreciate you! **Michiel, Haojie, Mengnuo, Silvana, Mani, Johan, Marieke** and **Elke** thank you for making B7 a great place to work at.

A big thank you also to all the previous lab members who contributed to my PhD journey. Thank you **Diede**, I learned so much from you during the time we shared in the lab! **Bastiaan**, you helped me turn my science enthusiasm from spark into a flame and I'll always be grateful for that. **Kristan**, you are always up for a good time. It's been great to catch up once in a while and see your mini dragons grow! **Wouter**, both your humor and your dedication to improvement have made the days in the lab better. Thanks for

all your support! **Arnout**, it was such a pleasure to work with you. Equal parts science sharpness and always being up to no good. I greatly enjoyed your sinterklaas poems, valentine and christmas cards, deep science discussions and borrels. **João**, we shared a lot of our PhD journeys. I'm glad to see your family grow and wish you all the best in sunny Portugal! **Finn**, you brought some fresh energy to the lab when we really needed it. You made long hours in TC during revision months much more fun! Let's go climbing again soon! **Sander**, it feels special that we got to share our PhD journeys. Thank you for all the yoga lessons and your friendship! **Ben, Tonći, Lorenzo, Begoña, Isabel M., Zheng, Jeroen H., Martin, Loredana, Cun, Jackie, Chong** thank you for sharing the lab and good times!

During my PhD I was lucky to supervise multiple student internships. Thank you **Janna, Dirk-Jan, Leyma** and **Kelvin** for working with me and contributing to my projects. **Kelvin**, your determination and dedication amazed me every day. I'm grateful we got to work together!

Henri, you know things before they even happen and are still always in a good mood. Thank you for all your support throughout the years!

For the majority of my PhD I served as department representative of NKI PhD council, where I learned important lessons in advocacy and team-work. **Iris**, thank you for your leadership and determination! It was such a privilege to have you by my side to advocate for support for PhD students. **Claire**, you're a fantastic leader and I can't wait to see what you will do after your PhD! **Mees**, it was a relief when you joined the mental health task-force. Keep up the good work!

My PhD life would not be the same if it wasn't for the NKI Mafia. The community and friendship was invaluable to me during all these years. From countless parties, trips, dinners and game-nights we developed strong friendships, which are a highlight of my life.

My dear Space **Anna**, what would I do without you?! During our endless sporty plans we somehow became inseparable. Thank you for always pushing and pulling me out of my comfort zone and showing me the beauty of being brave. I admire your resilience, endless energy and true scientific mind. I know you can do whatever you set your mind to. I'm so looking forward to all the adventures still ahead of us.

Ale, if you say something 17 times it becomes true and it's true we will be friends forever. You always ask the right questions and are fiercely supportive of all your people. It has been amazing to see you find your joy. Your openness and bravery to face the challenges are unique. If being cool would be a job, you would be the richest in the world, but until

then maybe opening a bakery will have to do.

Isa, you came into my life unexpectedly then stayed for good. I love your enthusiasm and dedication and your commitment to be your best self. Your growth has been inspiring and I'm sure you're not even done yet. It makes me so happy to see you living your best life. All the memories that we shared during the years for sure bound us together forever.

Louise, you care deeply and that's beautiful. I have always been amazed at your determination to work hard and have a good time at the same time. I'm grateful to have you in my life and I'm super excited for all the memories we will still make together!

Eric, our overthinking often works in similar ways. I admire your methodical and thorough way of life and I don't know anyone else who would approach challenges so bravely. You are courageous in picking your paths and I sure hope they lead you somewhere spectacular.

Jeremy, I admire your dedication to living a good life. I learned a lot from climbing with you about overcoming fear, setting scary high goals and not giving up before it's time. Thank you for entertaining Space for me until we resume random trips!

Migurk, there is a part of our brain that vibrates with the same frequency. Your creativity, humor and endless list of interests are an inspiration to me.

Mathias, I was so happy when you came back for a PhD! I'm often jealous of your down to earth attitude to life and science. It's been great to be your friend.

Ronak, it was very special to witness your growth from a baby scientist to a scientifically confident almost Dr. We made so many memories together, especially during long days of lockdown and playing with Kiwi. I'm sure your determination will serve you well whatever you choose to do next!

Dear **Simon** (or Sealmon?!), I'm glad we got to share our PhD journeys, especially during all the parties that help express your true phenotype. Thank you for being a friend!

Bruno, Angela, Alberto and Clara, Xabi, Mar, Stefan, Soufiane, Marjon, Lisa, Ruben, Alberto G.J., Julia, Dario you made my time at NKI more colorful and I'm very grateful for that!

Rui, you were the first one to give me a reality-check about the PhD experience which made me feel less alone. Thanks for all the science jokes and gossip!

Nina & Clement, when you guys moved to Switzerland that just gave me a perfect excuse to come visit for some hiking adventures. You both showed me what it means to live life fully. Our days of exploring were a perfect antidote to PhD stress. Let's continue the tradition in the Slovenian mountains!

A big special thanks also to **Wieger** for both your expertise in Dutch tax system and consulting with the Dutch translation of the thesis summary!

Dragi moji Vičani: **Nina N., Barbi, Sara, Nina L., Miha** in **Nejc**! Leta od mature nam bežijo, ampak z vami je še vedno vse kot je bilo na hodnikih GimVič. Hvala vam za vso podporo, (čast in) tortice, in vsa vprašanja o tem kdaj bom zaključila PhD. Zaradi vas je vsak obisk doma še slajši!

Edo, Vita, Zupi, Ana, Martin in **Anja**: Dvomim da bi se sploh kdaj lotila doktorata, če ne bi bilo vas! Že od faksa dalje sem se od vas naučila kako najti izzive, ki bodo kos našim sposobnostim, se učiti dovolj (ampak ne preveč) in hkrati žurat brez omejitev. Hvala vam, da mi še vedno kažete kaj pomeni bit uspešen. Če kdo ma to, pol mi mamó to!

Neja, ko sva pred 15 leti na morju obsedeno brali Harryja si verjetno ne bi mogli predstavljati kakšno bo najino življenje čez eno desetletje. Od vseh pisem med gimnazijo do epskega vikenda v Londonu - res je kul videti kako se vse spreminja, hkrati sva pa še vedno isti. Res občudujem tvojo odločnost in predanost, da si najboljša mami svojima puncama. Se že veselim naslednjih 15 let!

Dragi moji **Mami, Oči, Maj** in **Anže**, vaša neverjetna podpora mi je pomagala pri vsakem PhD izzivu. Hvala vam za vse zgodnje ure prevozov iz in na Brnik, hribovske izlete vsakič ko pridem domov izčrpana od ravnine, ure in ure namiznih iger in vse videoklice. Hvala da ste poskrbeli, da sem imela doma vedno zatočišče pred stresom in da sem se od doma vedno vračala spočita in polna energije.

In the end, all thanks to **Hadi**. You experienced the last, and probably most challenging part of my PhD with me. Your constant encouragement, honesty and humor have made a huge difference in my life. I'm inspired by your insatiable curiosity every day. I'm both extremely grateful and excited for our future adventures!

Lots of love,

Živa

